Cranfield University

Maud Seraffon

Low Temperature ITO Thin Film Deposition For Solar Cells

School of Applied Sciences

MSc Advanced Materials

Cranfield University

School of Applied Sciences

MSc Individual Project Report

2008

Maud Seraffon

Low Temperature ITO Thin Film Deposition For Solar Cells

Supervisors:
Dr. Sue Impey
Mr. Ken Lawson
Dr. Jeff Rao

Academic Year 2007 to 2008

This individual project report is submitted in fulfilment of the requirements for the degree of MSc Advanced Materials

Abstract

The electrical and optical properties as well as the microstructure of indium tin oxide thin films deposited on glass and flexible substrates is demonstrated in this project report. This project is a part of an MSc in Advanced Materials at Cranfield University.

The understanding and improvement of indium tin oxide coatings deposited by magnetron sputtering on both glass and polymer substrates has been an area of extensive research in the last decade. This technology appears to be very interesting in terms of money saving and efficiency in the solar cell domains where the coatings are used in thin film solar cells.

Research into the thin film solar cells mechanism, the sputtering process and ITO coatings is reported, along with detailed consideration of the best results obtained in the past in terms of ITO films' electrical and optical properties.

ITO thin films were deposited on glass and different sputtering parameters were changed in order to investigate their influence on the coatings properties: film thickness, chamber pressure, rotation, oxygen amount and sputtering power. A decision was made to establish the best sputtering parameters. These parameters were set to deposit ITO on polyethylene terephthalate (flexible substrate). The samples were also annealed at 150°C and 370°C.

An ITO thin film with a resistivity of $1x10^{-4}$ Ωcm and a 90% transmissivity was obtained.

An Energy Dispersive Spectrometry analysis was finally made on samples showing a substoichiometric composition of the ITO films.

Key Words: Magnetron Sputtering, Indium Tin Oxide, Thin Film, Solar Cells, Flexible Substrates, Annealing, Substoichiometry

Acknowledgements

I would like to extend grateful thanks to all at Cranfield University that have helped and advised in the undertaking of this project. In particular:

- Dr. Sue Impey for her supervision, advice and help as a facilitator throughout the course of the project.
- Mr. Ken Lawson for his supervision, advice and help throughout the course of the project.
- Dr. Jeff Rao for his advice and extensive assistance with the sputtering machine.
- Mr. Andrew Dyer for his assistance and advice regarding optical microscopy.
- Dr. Matthew Kershaw for his facilitation of the use of the Scanning Electron Microscope and the X-Ray Diffraction machine and advice / guidance on the interpretation of the results.
- Dr. Diego Gallardo for his facilitation of the use of the Spectrophotometer.
- Ms. Christine Kimpton for her help using the Atomic Force Microscope
- Dr. Christopher Shaw for his advice on the use of the Dektak.

I would also like to thank my family and friends, especially Pauline Bouin, for their support all along this project.

Table of Tables

Table of Figures

Table of Content

1. Introduction

In the solar cell industry, the development of thin film technologies is extremely important in order to enhance light absorbing properties, energy conversion efficiency and to reduce costs. Highly conductive transparent conducting oxides are commonly used for this application as contact layers and among them Indium Tin Oxide (ITO) exhibits the best optical and electrical properties.

The quality of solar cells depends on the quality of the ITO thin films, which have to show high transparency and high electrical conductivity. An adequate surface texture is also necessary to produce light scattering and light trapping to improve the current generation. Sputter deposition is an easy and efficient method to deposit ITO on different substrates. In the past, much research has focused on the deposition of ITO on glass. This demonstrated that films are very sensitive to the deposition parameters such as the substrate temperature, the sputtering power or the amount of oxygen in the chamber for example.

Due to this dependence, it is nowadays relatively easy to obtain high quality films on glass substrates. However, such parameters found for those films on glass may not be applied when ITO is deposited on flexible substrates. Poor quality films are generally created because of low temperature processes or stresses induced on the polymer substrates.

The focus of this project was the deposition of high quality indium tin oxides on glass and polymer substrates and the enhancement of their electrical and optical properties.

2. Aim and Objectives

2.1. Aim

- To deposit high quality ITO films on glass and flexible substrates by direct current magnetron sputtering.

2.2. Objectives

- To deposit ITO coatings on glass substrates with a resistivity below 2×10^{-4} Ωcm.
- To deposit ITO coatings on glass substrates with a transmissivity above 90%.
- To find the best sputtering parameters and deposit high quality ITO thin films on flexible substrates.
- To investigate the relation between the ITO microstructure and its properties.
- To explain the sudden brownish aspect of some coatings and its effect on the electrical and optical properties.

3. Literature Review

3.1. Thin film solar cells

A solar cell consists of a device which converts solar energy into electricity by the photovoltaic effect. Photovoltaics are described as the field of technology and research related to the application of solar cells as solar energy. The term solar cell is sometimes kept for devices intended to capture energy from sunlight, while the term photovoltaic cell is used when the source is unspecified.

Nowadays, solar cells are used for many applications. Individual cells can power small devices such as electronic calculators. Photovoltaic arrays create a form of renewable electricity, critical in situations where electrical power from power stations is unavailable such as in earth-orbiting satellites, remote radio telephones and water pumping applications. Photovoltaic electricity is also increasingly deployed in grid-tied electrical systems (Luque & Hegedus, 2005).

3.1.1. Theory

The general mechanism of a solar cell is divided in three parts. First, photons present in sunlight hit the solar panel and are absorbed by semi conducting materials, such as silicon. When this photon is absorbed, its energy is associated with an electron in the crystal lattice.

The energy absorbed by the photon excites an electron into the conduction band, where it is free to move within the semiconductor. The covalent bond originally associated with now mobile electron has one less electron. This is called a hole. This missing covalent bond allows bound electrons of close atoms to move into the hole, leaving another void behind, and in this way a hole can move through the lattice. That's why, it is said that photons absorbed in the semiconductor create mobile electron-hole pairs. This phenomenon produces the charge carriers essential for the generation of electricity.

Finally, a p-n junction made from silicon allows the charge carrier separation and therefore, the creation of a current. Indeed, when a piece of p-type silicon is placed in intimate contact with a piece of n-type silicon, diffusion of electrons occurs from the region of high electron concentration (the n-type side of the junction) into the region of low electron concentration (p-type side of the junction). The electric field established across the p-n junction creates a diode that promotes current to flow in only one direction across the junction. (U.S. department of energy, 2007)

The first generation of photovoltaic cells uses a single layer p-n junction diode in order to convert sunlight into usable electrical energy. These cells are typically made using a diffusion process with silicon wafers. They represent 86% of the terrestrial solar cell market. A scheme of a silicon based solar cell is showed in Figure 3-1.

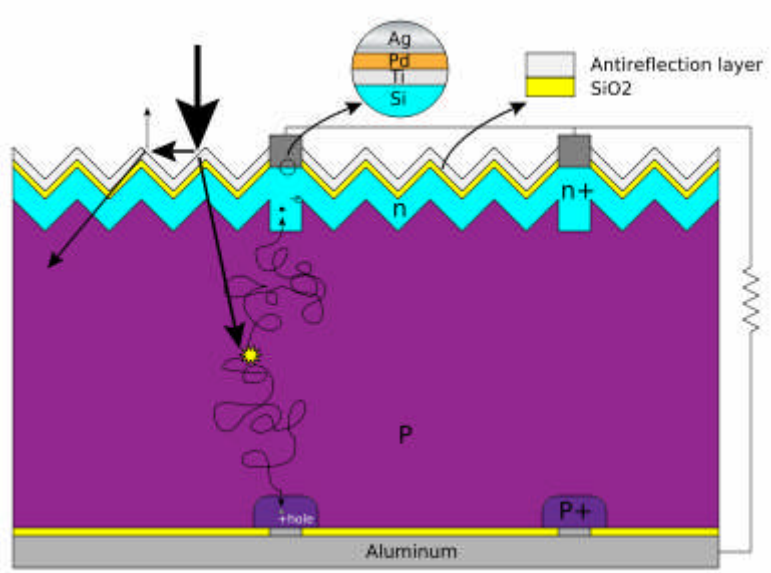

Figure 3-1: Scheme of a silicon based solar cell (Wikipedia)

Because of the high cost of silicon wafers, industry has begun to look at cheaper materials to make solar cells. The selected materials are strong light absorbers and need to be around 1micron thick only. In this way, material costs are significantly reduced. The most commonly used materials are amorphous silicon (a-Si, a different form of silicon), or polycrystalline materials such as cadmium telluride (CdTe) and copper indium (gallium) diselenide (CIS or CIGS).

The semiconductor junction is formed either as a p-i-n device in amorphous silicon, or as a hetero-junction for CdTe and CIS. A transparent conducting oxide layer (such as tin oxide) forms the front electrical contact of the cell, and a metal layer forms the rear contact. (Solarbuzz, 2008)

To choose a proper transparent conducting oxide, several criteria said to be critical by Beyer et al., in 2007:

- High transparency in the range of solar spectrum,
- High conductivity,
- High carrier mobility,
- A good refractive index for the absorption of light into the silicon wafer,
- A rough surface texture for optimum light scattering,
- Non toxic, chemically stable and sustainable materials
- Low cost.

The usual materials used for this purpose are: ZnO, TiO_2, SiO_2 or ITO.

3.2. General properties of ITO

3.2.1. ITO Microstructure

The properties of ITO come from its structure and composition. Indium oxide has a cubic structure which is shown in Figure 3-2. One unit cell is formed of 16 units of In_2O_3. That's why there are 80 atoms in one unit cell for defect free In_2O_3 crystal. The lattice constant is reported by Elfallal et al in 1993 to be 10.118Å. The theoretical density of In_2O_3 is 7.12g/cm^3. Two kinds of non-equivalent indium sites can be found in In_2O_3 crystal structure which are shown in Figure 3-3(a). In Figure 3-3(b), the separation between indium and oxygen atoms is 2.18Å, and the oxygen atoms are positioned at the corners of the cube with two body-diagonally opposite corners unoccupied. The In-O separations are 2.13, 2.19 and 2.23Å, where the oxygen atoms occupy positions at the corner of the cube with two face-diagonally opposite corners unoccupied (Zhou, 2005).

Based on the description above, both indium sites can be considered as an incomplete body centred cubic structure with an indium atom located at the centre and oxygen atoms at the corners. To increase the material electrical and optical properties, In_2O_3 can be extrinsically doped with tin. When tin atoms substitute for indium atoms, it creates either SnO or SnO_2. The material keeps its cubic structure. However, the tin atoms may enter interstitially and distort the lattice structure if the doping level is too high. Like a polycrystalline structure, the ITO crystal grain size depends on various processing parameters such as substrate temperature and deposition rate (Zhou, 2005).

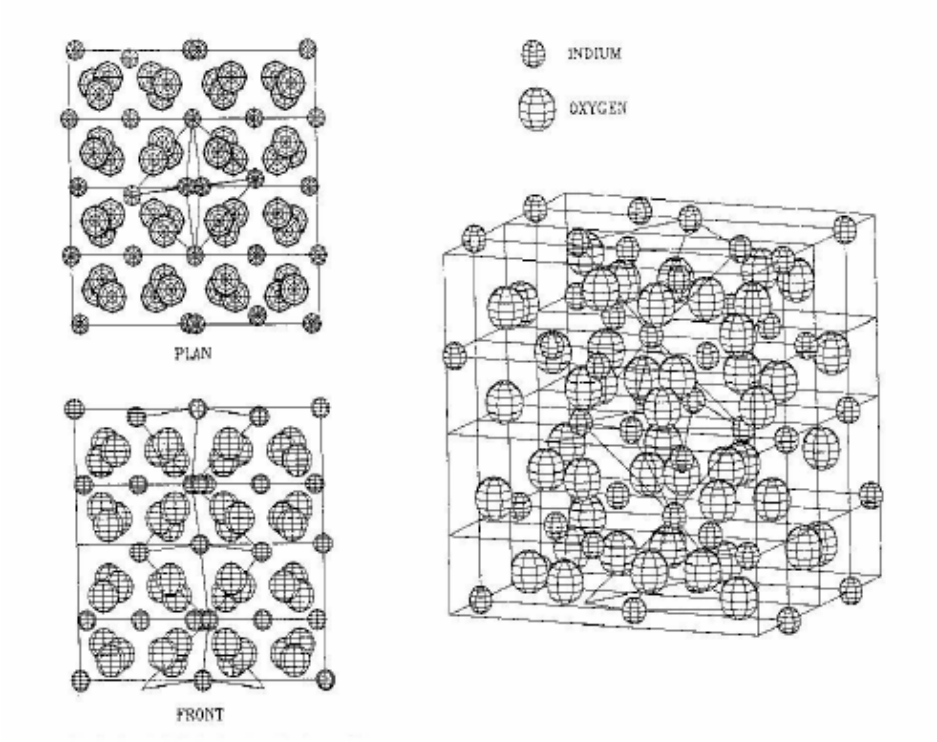

Figure 3-2: In_2O_3 crystal structure (Elfallal et al., 1993)

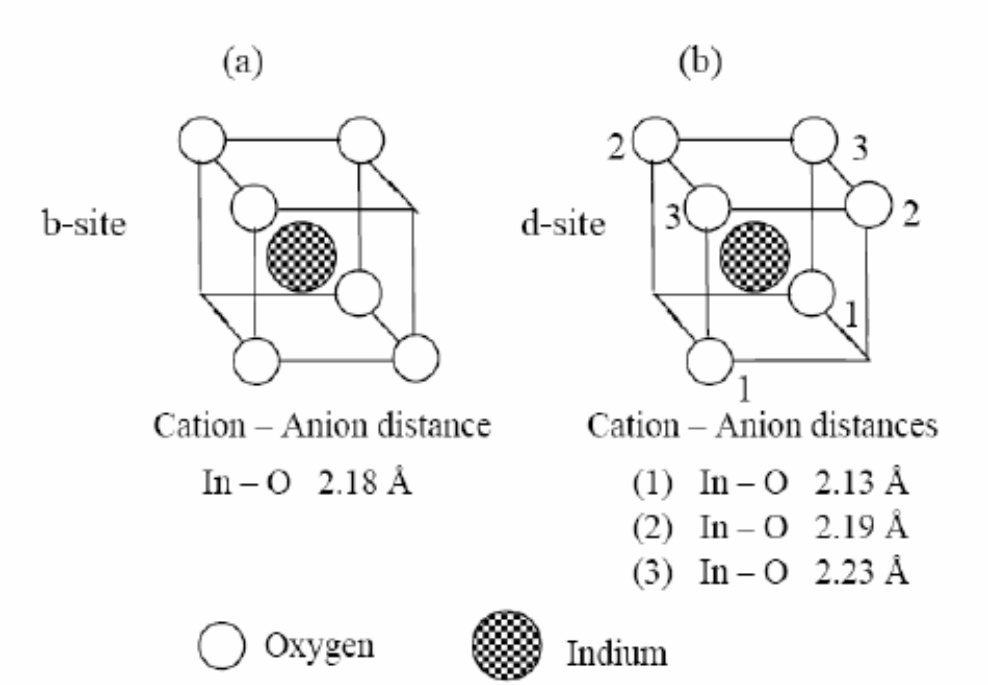

Figure 3-3: Two indium sites of ITO films (Ederth, 2003)

3.2.2. Electrical properties of ITO

Indium oxide is a wide gap semiconductor. The band gap of In_2O_3 was reported by Gupta et al. in 1989 to be 3.75eV. Generally, because oxygen vacancies are present, In_2O_3 crystal structure is not ideal. The detailed formula of indium oxide should take in account those oxygen vacancies. Oxygen vacancies dominate the conduction mechanism of In_2O_3 and the free charge carrier concentration has been reported to be in the range 10^{19} - $10^{20}cm^{-3}$.

Extrinsic doping can change the electrical properties of indium oxide a lot. If In_2O_3 is doped with tin atoms, the latter will replace indium atoms and form tin oxide in either SnO or SnO_2 depending on the valence. If SnO is created, tin acts as an acceptor as it accepts an electron. Otherwise, when SnO_2 is formed, it acts as donor since it gives off an electron. Usually, more SnO_2 molecules are formed. In this latter case, tin atoms act as donors. Thus, both tin and oxygen vacancies contribute to the conductivity of ITO.

The doping level is critical for electrical properties. As the tin concentration increases, the carrier concentration increases until a saturation level is reached. An enhancement of the tin concentration above the saturation level causes a fall of the free carrier concentration. This is caused by an increased probability of the occupation of adjacent cation positions by tin atoms, which can reduce the active tin concentration (Zhou, 2005).

3.3. Deposition method - Magnetron Sputtering

The most common forms of physical vapour deposition are evaporation, e-beam evaporation, plasma spray deposition and sputtering.

Sputtering is an interesting process because of a lot of advantages:

- A high deposition rate
- The possibility to deposit and maintain complex alloy compositions
- The capability to deposit at low temperature
- Achieving uniform films
- The capability to clean before depositing metal (Chang & Sze, 1996)

3.3.1. Fundamentals of the sputtering process

Basically, the sputtering process needs plasma of argon gas. This plasma is generated by a glow discharge (Figure 3-4). A glow discharge can be built up of different dark and glowing regions. Close to the cathode is a very thin layer of ion space charge generally named the cathode glow. It is followed by a gap, the Crookes dark space, where the potential between the anode and the cathode drops. A negative glow (the glow discharge) is located next to this gap and a negative dark space, the Faraday dark space, comes after it (Chang & Sze, 1996).

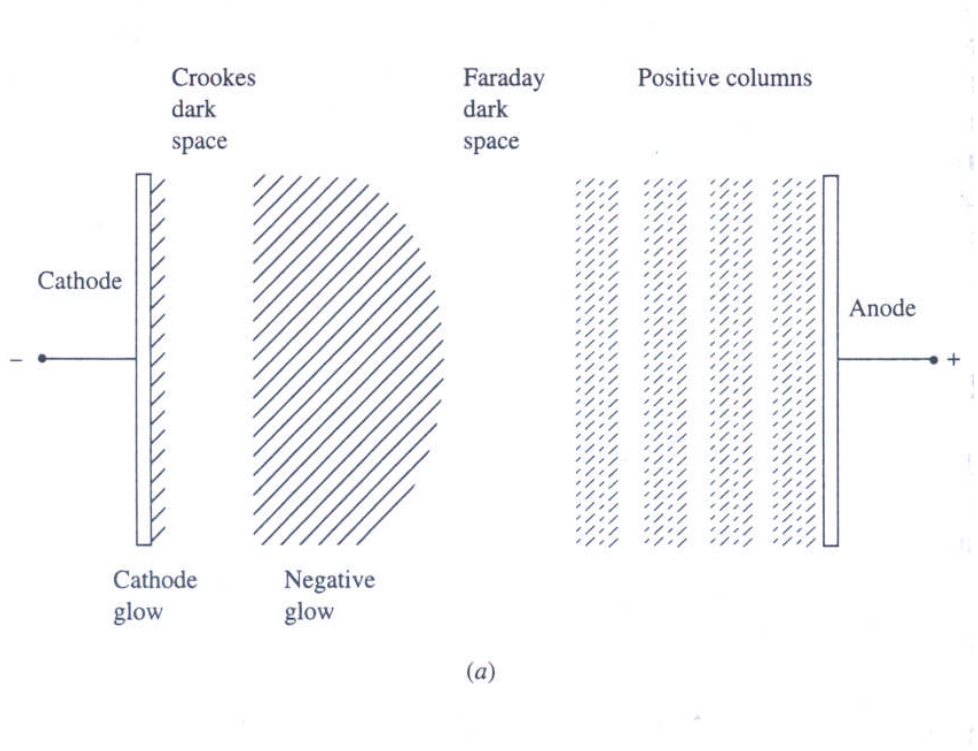

Figure 3-4: Description of a glow discharge (Chang & Sze, 1996)

Secondary electrons generated from the ion bombardment of the cathode, accelerate away from the cathode, getting the full energy of the imposed potential across the electrodes when passing through the Crookes dark space, and collide with an argon atom in the glow discharge region and excite it. This is how the plasma is created and sustained.

The mechanism of sputtering consists of an ejection of atoms from a target (cathode) which land on the substrates. To be more accurate, the charged ions in the argon plasma diffuse into the Crookes dark zone and acquire practically all the energy from the voltage drop. Then, they hit the target's surface with a momentum that is immediately transferred to the cathode's material. Neutral atoms are therefore ejected from the surface, fly through the plasma and are deposited on the wafer.

The most important concern in sputter deposition is to enhance the ion bombardment rate on the cathode so that a good deposition rate can be achieved. That is why means to increase the secondary electron production are designed to improve the

sputtering rate. The invention of magnetron sputtering where the use of an electromagnetic field improves the trapping of electrons greatly assisted the deposition rate and made sputtering the leading technique of physical vapour deposition (Chang & Sze, 1996). See Figure 3-5.

The electrons are confined close to the cathode which they normally tend to drive away from, making it much easier to sustain an electrical discharge at low pressure. Consequently, the required residual gas pressure can be reduced allowing the transfer of sputtering material without many collisions. A better deposition rate is reported to be obtained as well as a good quality coating (Danson & Safi, 1997).

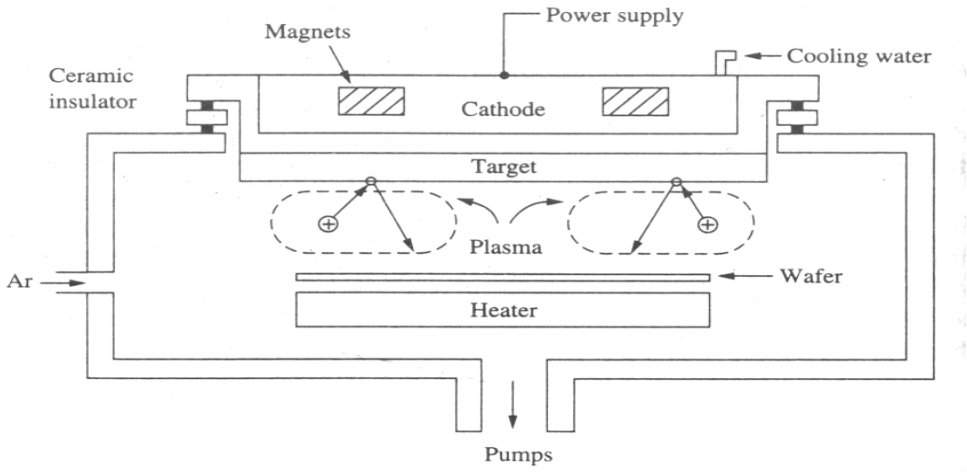

Figure 3-5: A dc-magnetron sputtering system (Chang & Sze, 1996)

Instead of applying a direct current (dc) field to create the plasma, a radio frequency (rf) field can be used to achieve sputtering. In the latter case, only electrons can respond to the alternating current whereas the ions act as if the field was dc. The advantage of rf sputtering is that no charge accumulates at the target since the electrons are oscillating with the field. The rf technique is mostly used for deposition on insulating or semi-conducting materials (Chang & Sze, 1996).

Another way to raise the deposition rate is to provide an additional amount of power to the argon plasma. Most of this power is absorbed by the target which needs to be water-cooled.

Knowing the basics of sputtering mechanics, let's now focus on the films obtained from this technique.

3.3.2. ITO film properties

In magnetron sputtering, the film properties depend on a lot of parameters. The substrate temperature is the most important of them. One can also influence the coating's quality by changing the sputtering pressure, the film's thickness, the target's or the substrate's bias voltage, the oxygen flow rate or the sputtering power. As part of this project, the fluctuation of the electrical and optical properties of the ITO will be highlighted.

3.3.2.1. Effect of the substrate temperature :

When the films are deposited at higher temperatures, surface diffusion occurs during the sputtering resulting in films with good physical properties. The coatings are columnar at this stage because the grains grow unidirectionally. The grain size gets bigger with higher temperatures because of lower density of nucleation with increasing temperature (Chang & Sze, 1996).

The film resistivity also varies with the substrate temperature. This dependence is illustrated in Figure 3-6 (Calnan et al., 2007).

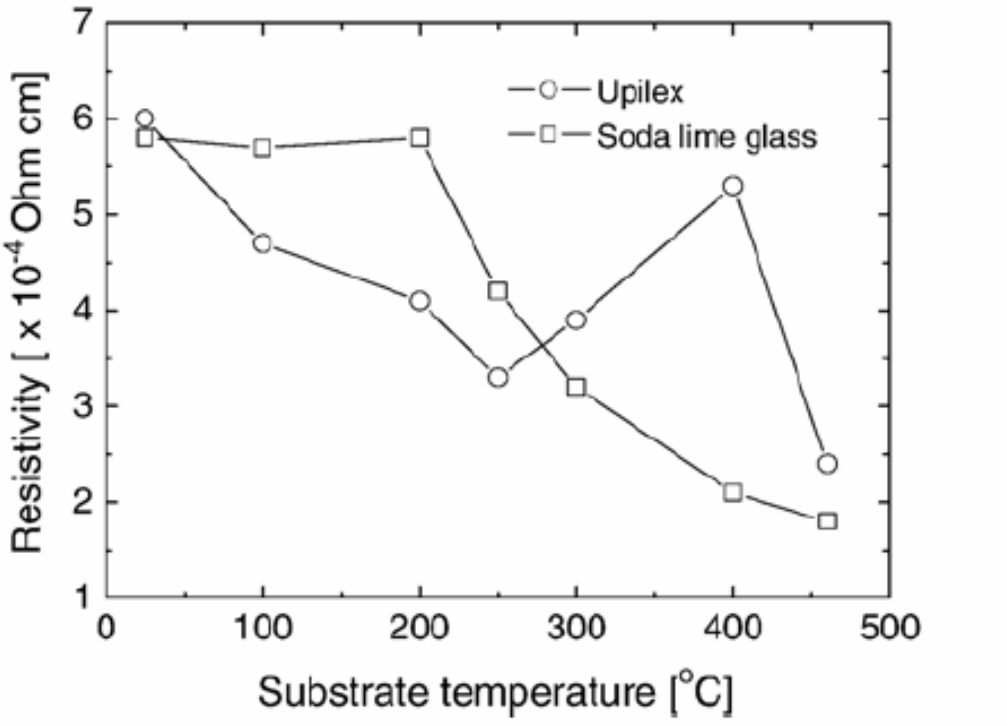

Figure 3-6: Resistivity of ITO films on glass and Upilex (polymer) as a function of substrate temperature (Calnan et al., 2007)

The decrease of resistivity with increasing temperature coincides with an increase in grain sizes of the indium tin oxide films. Larger grains formed this way reduce the recombination and the scattering of charge carriers at the grain boundaries. Consequently a higher carrier mobility in those ITO films results in higher conductivities (Calnan & Upadhyaya, 2007). Carriers are created both by substituted Sn^{4+} ions and by oxygen vacancies in polycrystalline ITO (Cho et al, 2007).

Grains with columnar structure were observed in films deposited at 70°C (Figure 3-7). Indeed, even though an amorphous layer was formed at the initial stage of deposition, thanks to moderate heating, polycrystalline ITO can be obtained (Kim et al, 2006).

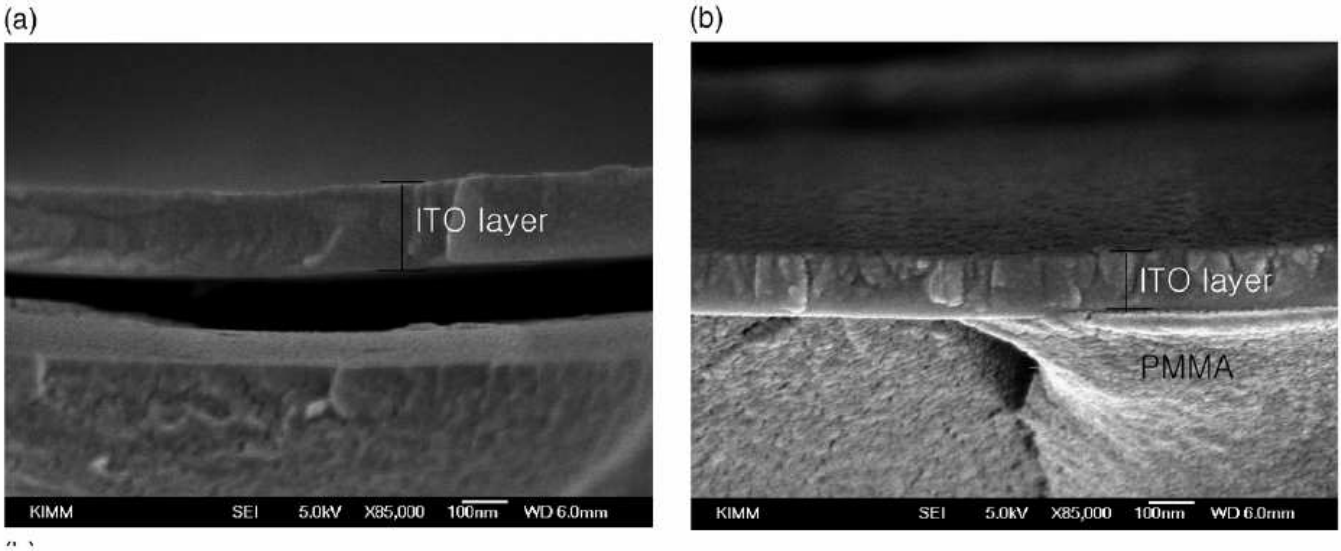

Figure 3-7: FESEM images of the cross section of ITO films (a) deposited without intentional heating (b) deposited at 70°C (Kim et al, 2006)

At low temperature, the sputtered ions coming from the target cannot gain enough heat energy to adjust the bond direction and length to obtain good bonding to adjacent atoms. This leads to bad adherence to the substrate and to low carrier mobility. The grain boundaries contribute to the scattering of the charge carriers resulting in a high resistivity (Lee et al, 2007).

3.3.2.2. Effect of the sputtering pressure :

The effect of the deposition pressure is controversial.

On one hand Tohsophon et al. have found that the resistivity of ITO coatings decreases with increasing deposition pressure (Figure 3-8).

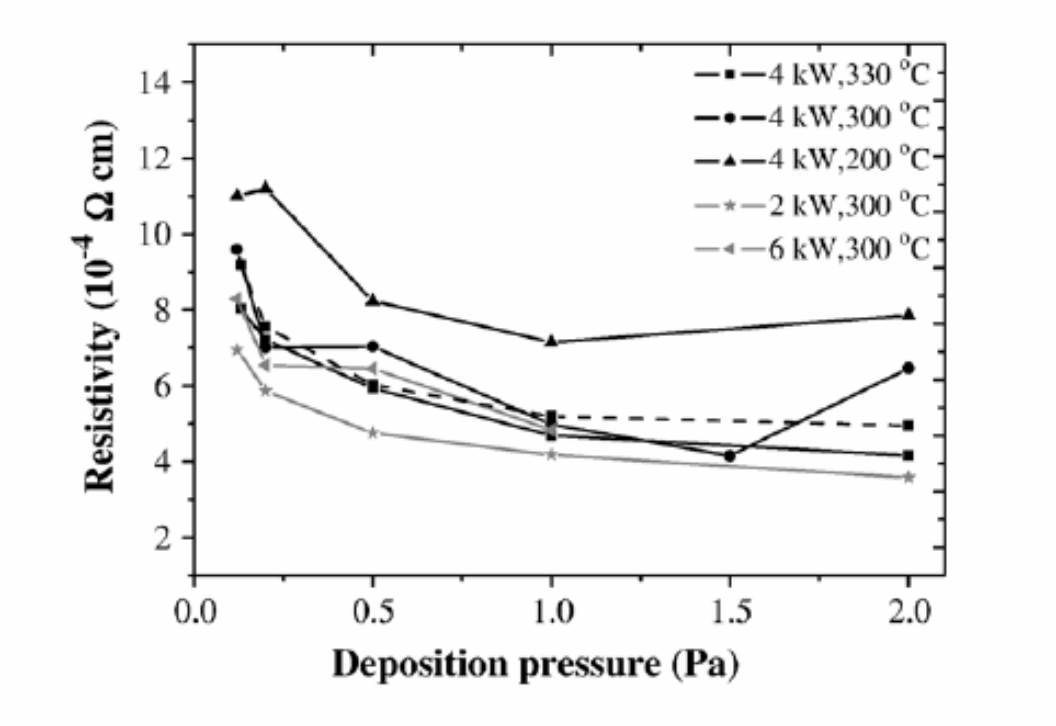

Figure 3-8: Electrical properties of films as a function of deposition pressure prepared at various substrate temperature and power (Tohsophon et al., 2007)

On the other hand Lin et al. observed that thin film resistivity increased with increasing work pressure (Figure 3-9).

However, with Lin's data, between 1 and 5 mtorr, as deposition pressure increases, the resistivity decreases. Outside of this range, there is an overall increase of the resistivity. Tohsophon may also see this trend if the data beyond 2 Pa could be available.

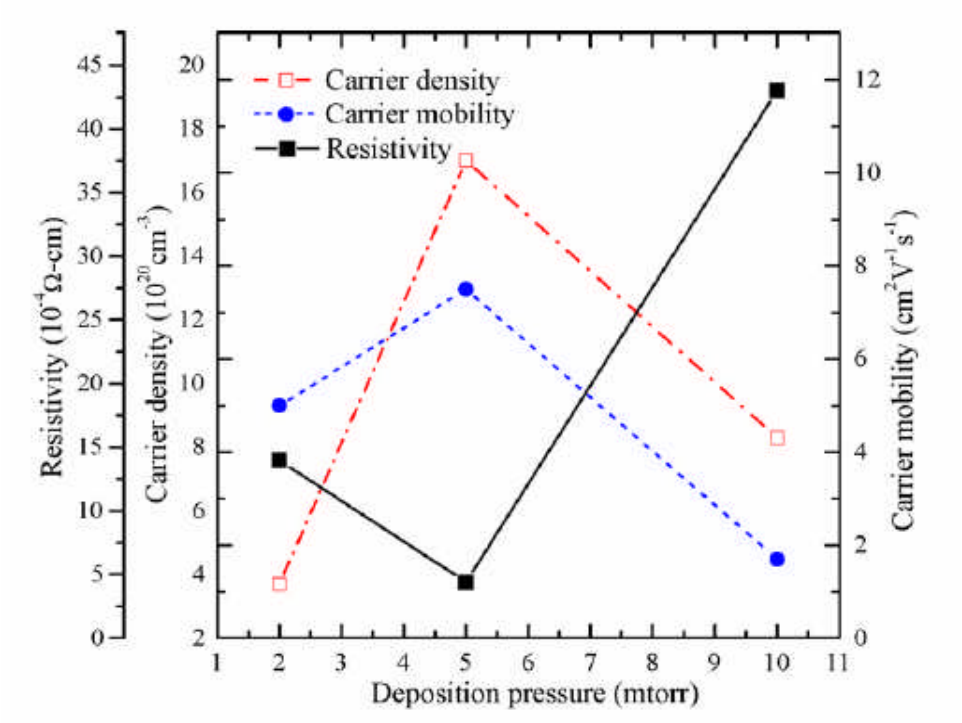

Figure 3-9: ITO films resistivity as a function of the deposition pressure. (Lin et al., 2007)

Low sputtering pressures causes the elongation of the electron mean free path. This improves the thin film structure and therefore optimises the carrier mobility reducing the resistivity. However, if the pressure is too low, the bombardment energy will become excessively strong causing the thin film defects to increase, thus reducing the electrical properties.

A longer mean free path also permits better deposition rates.

3.3.2.3. Effect of the film thickness:

The coatings thickness has significant effect on the properties. It has been shown by Kim et al. in 2006, that the resistivity of ITO films decreased with an increase in ITO thickness from 0 to 300 nm (Figure 3-10). Guillén & Herrero in 2008 have investigated the change in specific resistivity with the thickness by determination of the carrier concentration and mobility. They have discovered that the carrier concentration increased with the film thickness. Thus, the variations in the resistivity are mainly related to changes in the carrier concentrations.

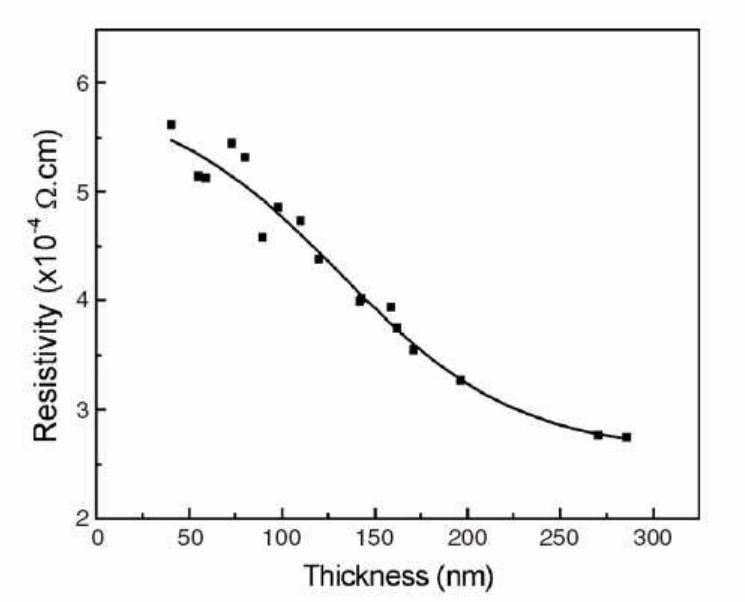

Figure 3-10: Electrical resistivity of ITO films with various thicknesses. (Kim et al., 2006)

The change in the properties with increasing thickness can also be explained by a modification of the film's microstructure (Figure 3-11). Thin coatings tend to be amorphous whereas thick ones are more crystalline. Yang et al. in 2007 show that the ITO film is amorphous to 250 nm, thereafter at 450 nm the film is a mixture of crystalline and amorphous.

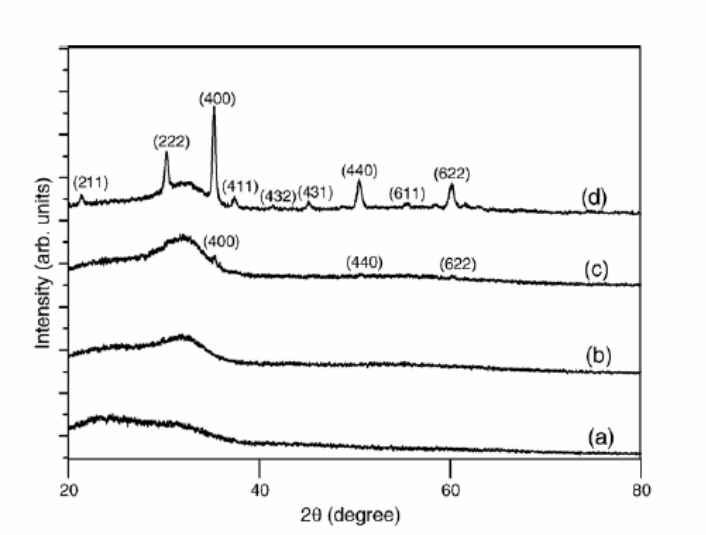

Figure 3-11: XRD diffraction patterns for ITO films deposited on glass substrate at various film thickness (a) 50 nm (b) 150 nm (c) 250 nm (d) 450 nm. (Yang et al., 2007)

3.3.2.4. Effect of the target bias voltage:

The target bias voltage is set by adding some power to the cathode of the sputtering system.

Calnan et al. show in 2007 that increasing the voltage raises the ITO film conductivity, (Figure 3-12) which is indicated by a reduction of the resistivity values. This phenomenon can be explained by an increase in both the carrier concentration and carrier mobility. Yet, it is reported to cause a decrease of the optical properties which showed poor transmittance in the near infra red region. It is said to be due not only to high free carrier absorption but also to a shift in the optic band gap to the lower wavelengths. It can be noticed too from Figure 3-12 that the ITO films on polyimide are slightly higher in resistivity the ITO films on glass. However the trends are very similar.

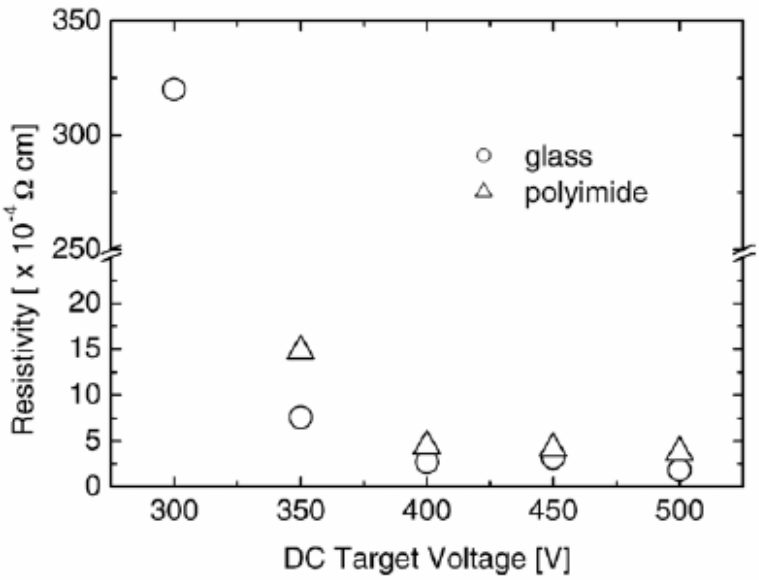

Figure 3-12: Resistivity of ITO films on glass and polyimide as a function of DC target voltage (Calnan et al, 2007)

It is thought that lowering the target voltage results in lower ion energies during the process. This causes a reduction of the deposition rate and thus a reduction of the film growth. (Figure 3-13) (Calnan et al, 2007)

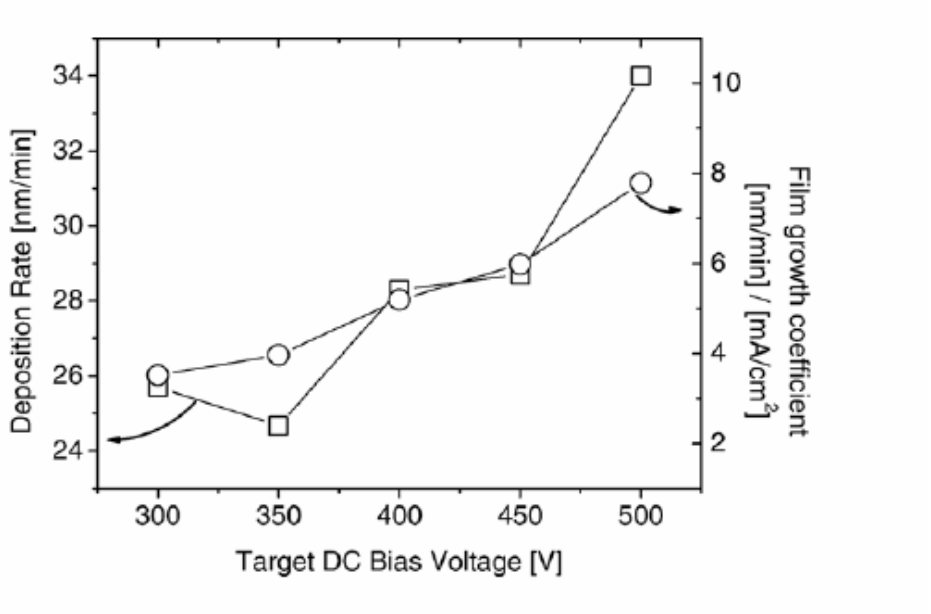

Figure 3-13: Deposition rate and film growth coefficient as a function of DC bias voltage applied to the target (Calnan et al, 2007)

3.3.2.5. Effect of the substrate bias voltage:

ITO deposited at low substrate temperature is not favourable for depositing good quality films. To compensate for this problem, a bias can be applied to the substrate. It attracts cations from the plasma to bombard the growing film giving an additional energy to the molecules and peel off the ones with weak bonding from the film. It enhances the film crystallinity and can replace the energy provided to high temperature substrates. (Jaehyeong et al, 2004)

Lee at al. in 2004 report that, increasing the substrate bias makes the deposition rate decrease, as shown in Figure 3-14. This effect can be explained by the enhancement of the number of molecules removed from the surface during the bombardment leading to a slower deposition rate.

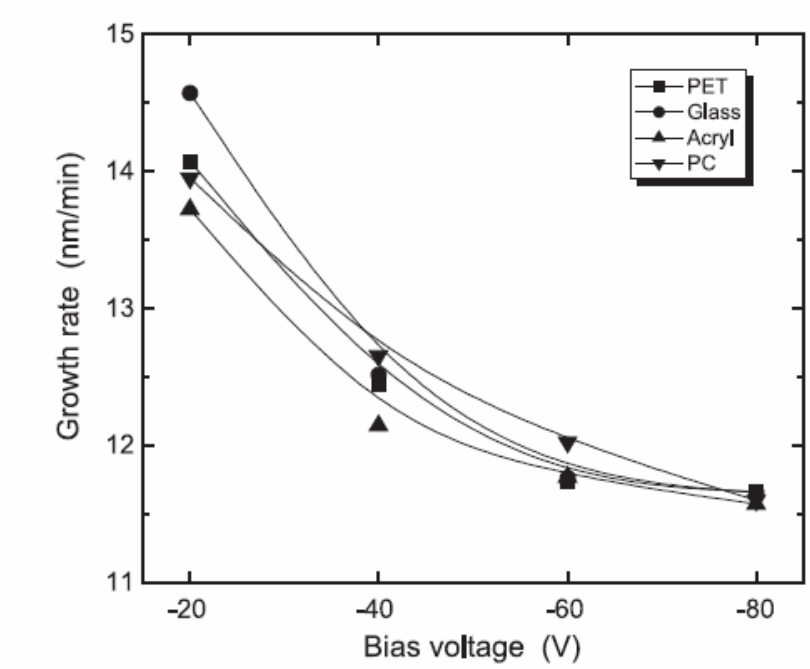

Figure 3-14: Deposition rate of ITO films deposited at different bias voltage (Lee et al, 2004)

It has been observed by Lee et al. in 2004 that the film becomes more non stoichiometric when the bias increases. It is thought that the number of oxygen vacancies also rises.

Regarding the resistivity, it has been shown that it decreases with increasing the bias voltage (Figure 3-15). This is said to be due to the presence of more impurity donors, which improves the carrier density of the films. Interestingly, it is noted by the author of this report that the substrate does not appear to have a significant effect.

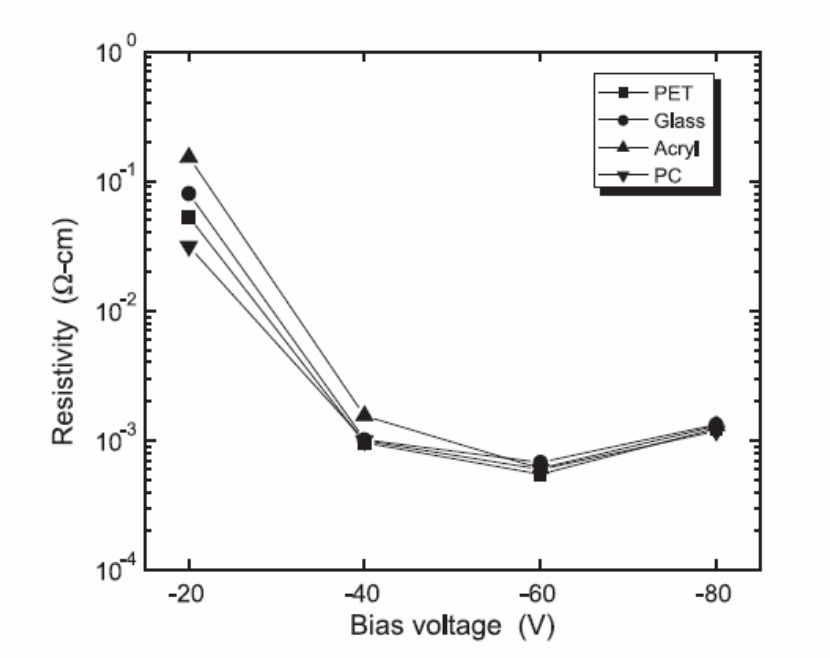

Figure 3-15: Dependence of electrical resistivity of ITO films on bias voltage. (Lee et al, 2004)

Concerning the optical properties, in the visible region, the transmissivity improves with increasing the bias voltage as shown in Figure 3-16.

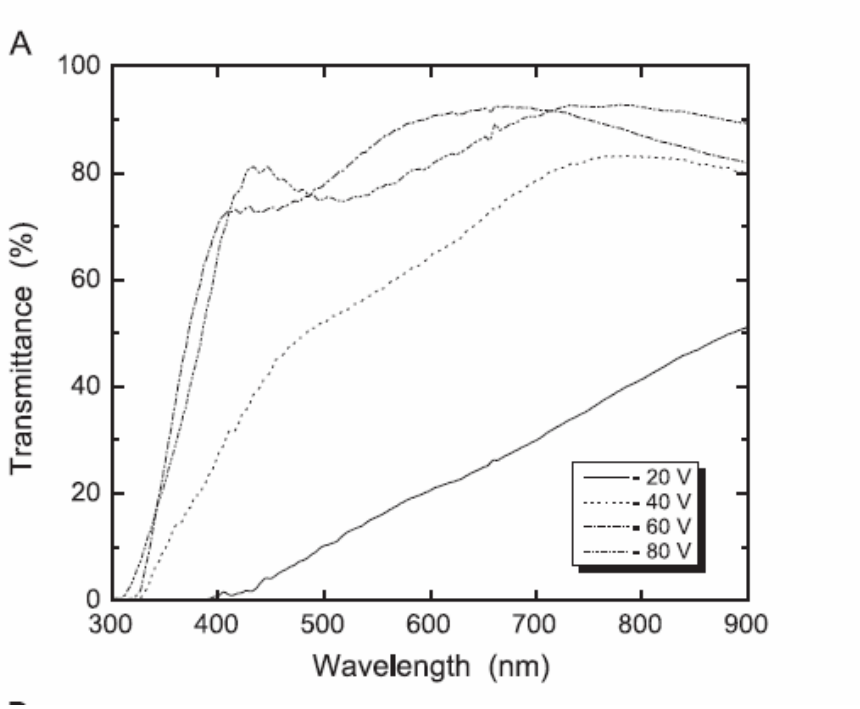

Figure 3-16: Optical transmittance spectra of ITO films deposited at different bias voltages. (Lee et al, 2004)

In summary, although the growth rate of films decreases with increasing bias voltage, the increased bias voltage is an advantage for enhanced conductivity and high optical transmittance.

3.3.2.6. Effect of the oxygen flow rate:

It has been confirmed by Cho et al in 2007 that there is an optimum O_2 addition to obtain the lowest resistivity. Indeed, the resistivity decreased within an optimum O_2 addition, and then resistivity increased with a further increase of O_2. In this case, the best conductivity, coinciding with the lowest resistivity, was obtained with a ratio of 0.5% oxygen.

Kim et al., have observed that even though the film is not greatly affected by a small amount of additional oxygen, the values extend exponentially with the increase of O_2 flow rate as shown in Figure 3-17. This can be explained by a decrease of the carrier concentration which results from the reduction of the oxygen vacancies of the ITO.

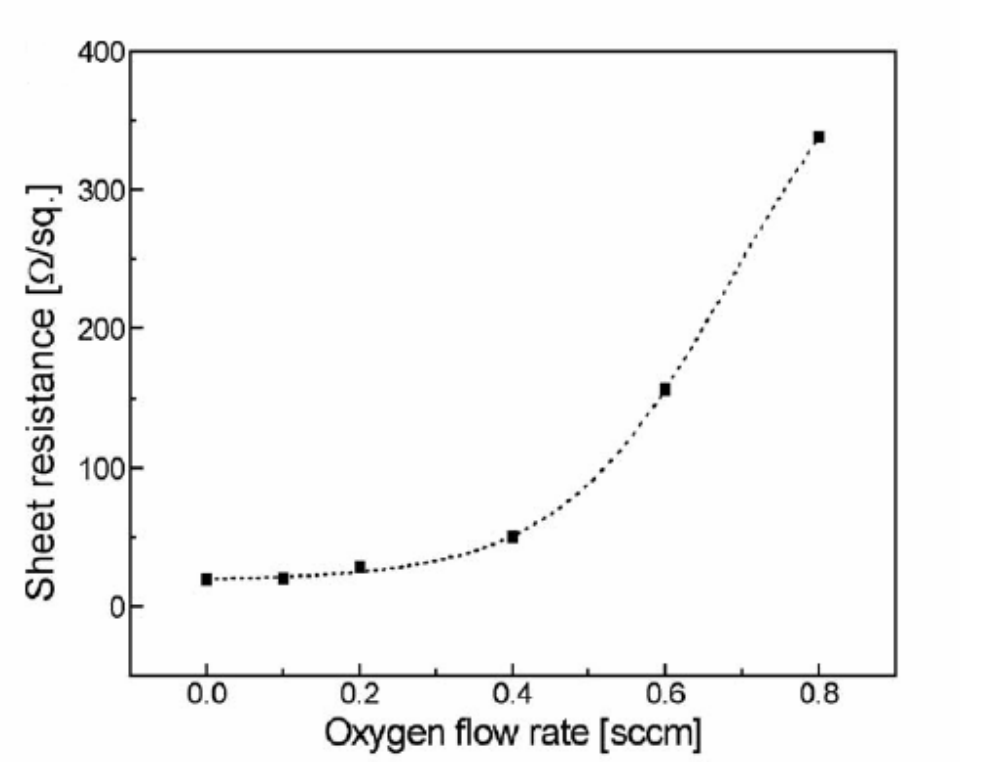

Figure 3-17: Effect of the oxygen flow rate on electrical properties of ITO films. (Kim et al, 2006)

Concerning the transmittance of ITO film, Figure 3-18 shows that the transmittance increases in the near infra-red region with increasing O_2 addition ratio. This behaviour is explained by Cho et al. in 2007, by a reflection of the electromagnetic wave due to the plasma oscillation of free carrier. It has been confirmed that increasing transmittance with increasing O_2 in the near infra red region could be attributed to the reduction of the carrier density, which correlates with the behaviour observed for the electrical properties.

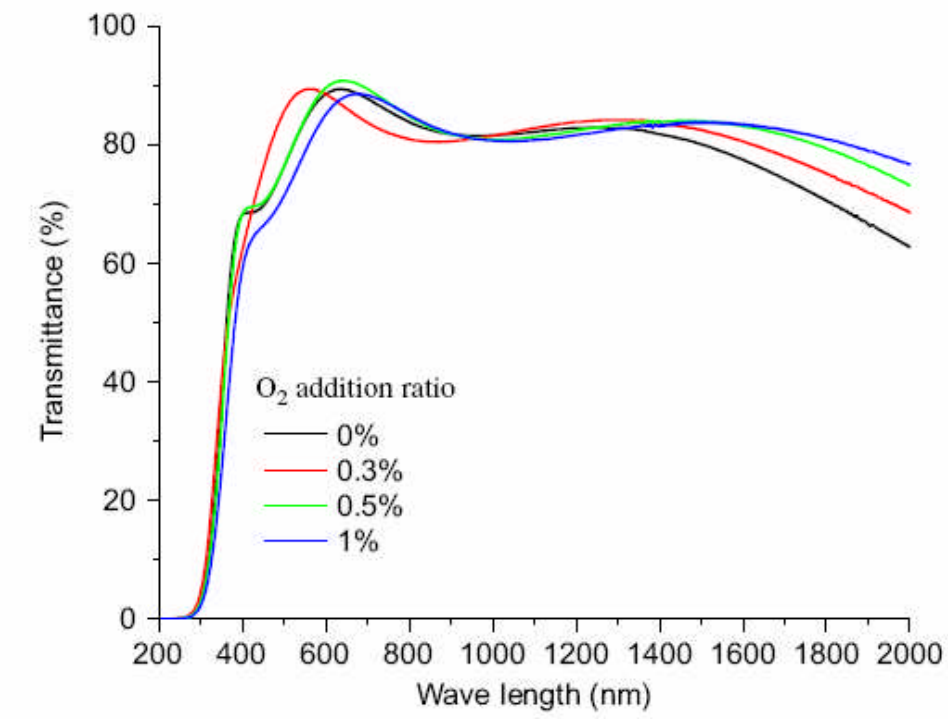

Figure 3-18: Transmittance of ITO films deposited with various ITO targets under different O_2 ratios (Cho et al, 2007)

3.3.2.7. Effect of the sputtering power :

Modification in the sputtering power initially affects the ZnO:Al (behaviour similar to ITO) film's growth rate. Lee et al. have written that a linear increase in the growth rate was seen as the power increased (Figure 3-19). This enhancement indicates that the number of particles sputtered from the target is proportional to the power. With higher sputtering powers, the atoms have higher energy that contributes to the film growth. These high energy species have high surface mobility and therefore greater growing process takes place at the surface.

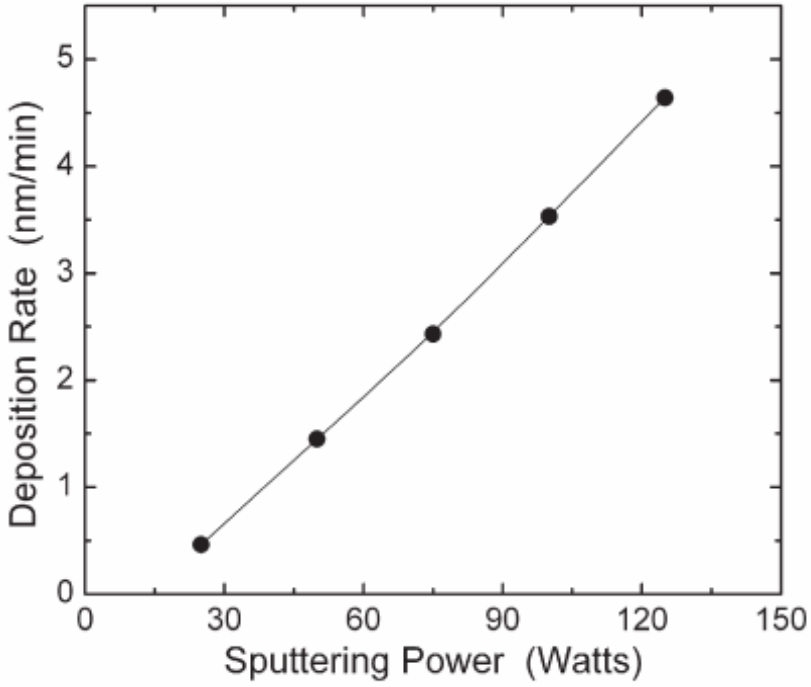

Figure 3-19: Influence of sputtering power on the deposition rate of ZnO:Al films on glass substrate (Lee et al., 2007)

The electrical properties are also affected by a change in the sputtering power. Indeed, the resistivity decreases with increasing deposition power and is shown in Figure 3-20. When the sputtering power increases, the carrier concentration goes up slightly and the carrier mobility increases significantly. It is said by Lee et al. to have the effect of increasing the crystallite size and thus, reduces charge carriers scattering due to grain boundaries. The mobility is therefore enhanced. It reduces the resistivity of the films (Lee et al., 2007). Interestingly, Figure 3-20 also shows that only films on glass respond to deposition power in this way. ZnO:Al films on polycarbonate do not show the same trend of reduced resistivity with increasing sputtering power but show the inverse behaviour. Indeed, at high sputtering pressures, the high energetic ion bombardment leads to damage of the polymer substrate. It as an effect on the properties of the film and diminishes its quality . (Lee et al., 2007)

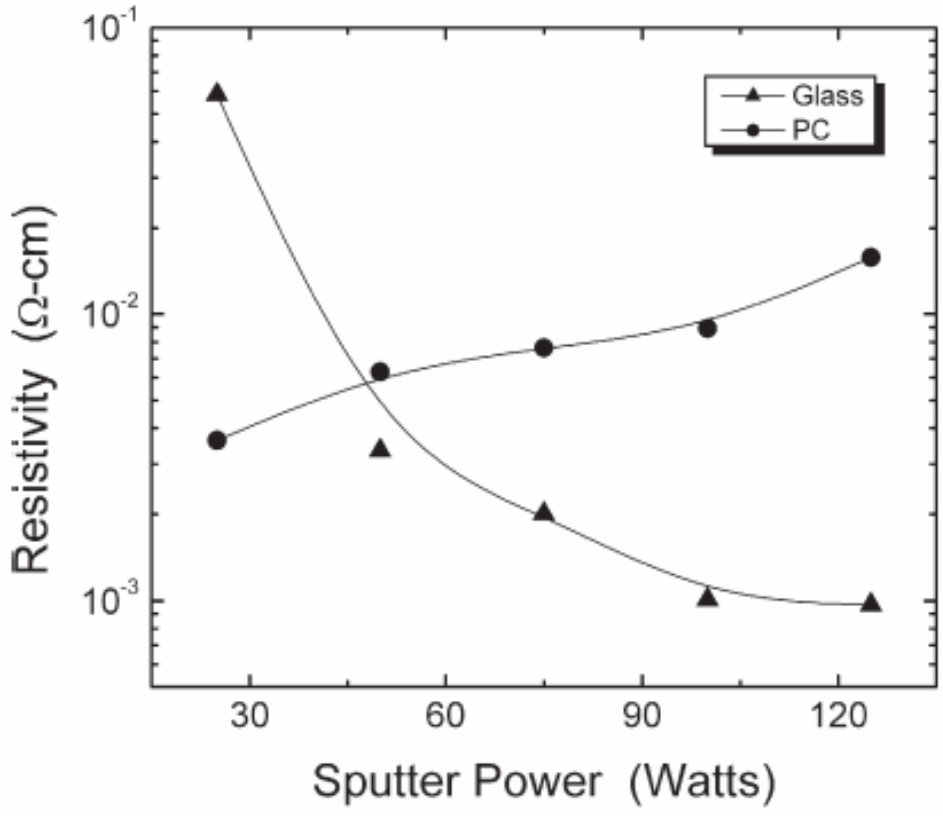

Figure 3-20: Dependence of electrical properties of ZnO:Al films on sputtering power (Lee et al., 2007)

In summary, the literature review has shown a range of work on ITO on glass. Effects including increase of substrate temperature have been shown to reduce the resistivity. An increase in ITO film thickness, in DC target voltage and substrate bias voltage lead also to an enhancement of the film conductivity. An increase of the O_2 flow rate makes the resistivity increase but enhance the optical properties unlike the other parameters. The effect of deposition pressure initially decreases the resistivity then after 5mtorr increases it.

Reported secondary effects of consequences in microstructure which reduce the resistivity appear to be an increase in grain size and crystallinity.

The review has also indentified that most sputtered ITO films on polymer respond in a similar way to ITO films on glass to sputtering parameters. However, the following section of the review looks at polymer substrates in more details.

3.4. Polymers substrates

The purpose of coating deposition on polymer is to replace the rigid glass substrates by flexible ones. Indeed, it gives advantages such as lighter weight and higher shock resistance than glass. However, some constraints such as poor thermal endurance and reduced hardness also appear.

For this research work, the data needed is the type of polymers commonly used for the sputtering deposition and the influence of the substrate on the electrical and optical properties of the film.

3.4.1. Polymers commonly used for magnetron sputtering.

The main characteristics that the polymer must fulfil are high thermal resistance, in order to withstand the deposition temperature and high optical transparency so that the best transmissivity can be expected. Moreover, the material must possess good physical properties like acceptable tensile strength and elongation.

The most commonly used polymers with all these desired properties are polyethylene terephthalate (PET), polycarbonate (PC), cyclo-olefin copolymers (COC) and polyether sulphone (PES). (Lin et al., 2007 –Yang et al., 2007 – Boehme & Charton, 2005 – Lee et al., 2007 – Guillén & Herrero, 2008) The properties of these polymers have been gathered in the following table (Table 3-1):

	PET	**PC**	**COC**	**PES**
Working Temperature (°C)	115 - 170	~ 70	60 - 150	150 - 200
Transparency	Yes	Yes	Yes	Yes
Refractive Index	1,58 - 1,64	1,58	1,45 - 1,53	1,65
Tensile Strength (Mpa)	80	55 - 80	70	80 - 105
Elongation (%)	30 - 300	80	03-oct	50 - 100

Table 3-1: Properties of PET, PC,COC and PES (Yang et al., 2007 – Tangram Technology ltd.)

Among those four polymers, the polyethylene terephthalate is usually used often because of is low cost compared to the others.

3.4.2. The influence of the polymer substrates on the film properties

3.4.2.1. ITO thin film residual stress

As the substrate is not as rigid as glass slides, the films are easily subjected to residual stress. As long as the sputtering operation goes on, the surface accumulated energy increases causing the enhancement of residual stress. Figure 3-21 shows an example form Lin et al., ITO films showing development of flexural behaviour linked to the development of residual stress.

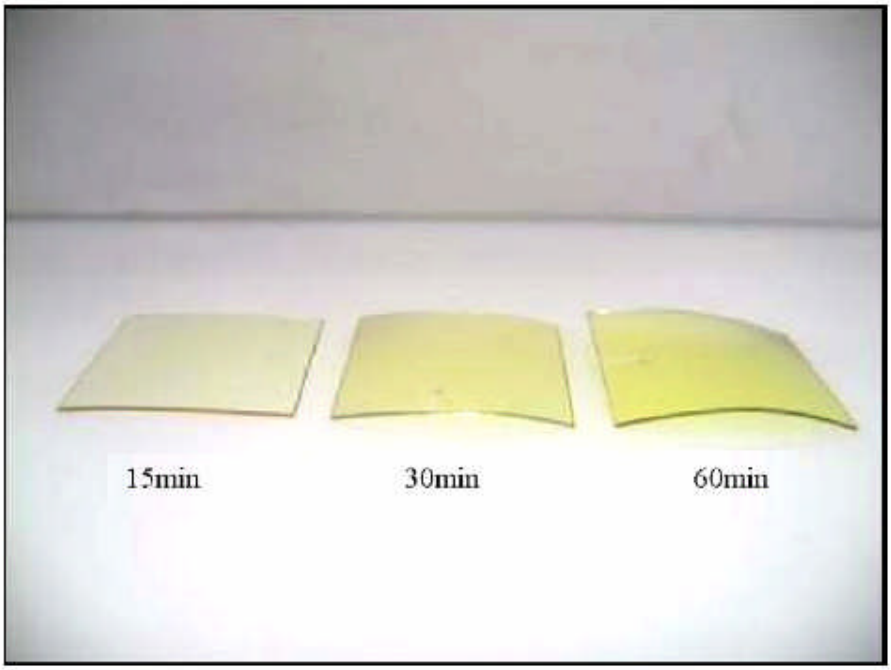

Figure 3-21: Comparable view of the substrate flexural condition depending on the deposition time (Lin et al., 2007)

3.4.2.2. Electrical properties

In most case, it is necessary to reduce the process temperature because of the poor thermal properties of the polymer substrates, thus the conductivity of the ITO thin films reduces. Indeed as it was explained in part 3-3-2-1, the grain size gets smaller with lower working temperatures leading to less carrier mobility. This results in higher resistivities generally.

Figure 3-22 shows the difference of electrical properties between glass and polymer substrates. Guillén & Herrero determined sheet resistivities and subsequently ITO specific resistivity. In this way, Figure 3-23 shows that PET is more sensitive than glass to film thickness.

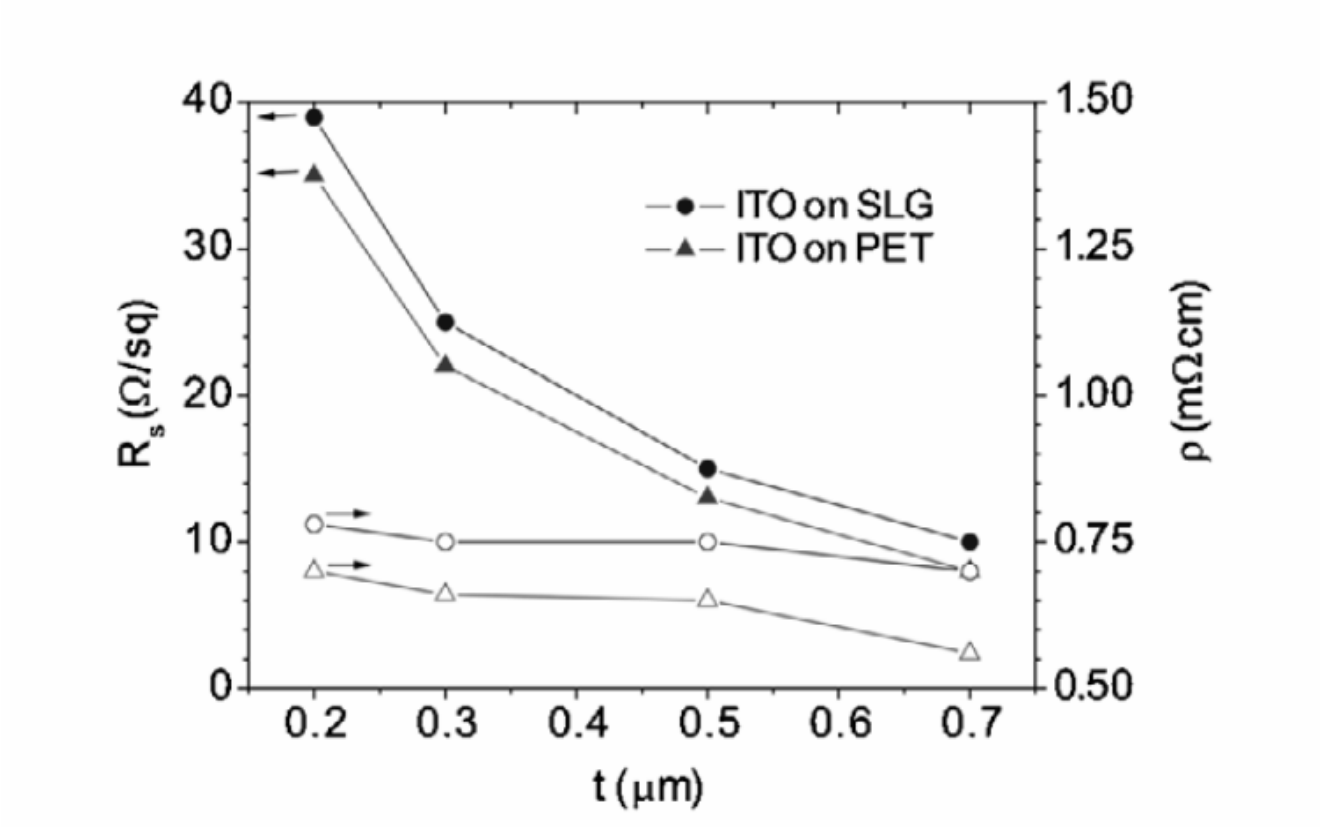

Figure 3-22: Evolution of the sheet resistance, Rs, and specific resistivity, ρ, as a function of the ITO film thickness, t, deposited on soda lime glass and PET substrates. (Guillén & Herrero, 2008)

In order to palliate this tendency, it is possible to increase the film thickness or to increase the deposition power. This supports the findings with ITO on glass where it was reported in part 3-3-2-3 that an increase of the thickness causes a decrease of the resistivity. In addition, it was observed by Lee et al. in 2007 that as the sputtering power increases, the carrier concentration increases, leading to better electrical properties. Figure 3-20 illustrates this fact.

3.4.2.3. Optical properties

For both polymer and glass substrates, the transmissivity appears similar depending on sputtering conditions. In 2007, Lin et al. found that the average optical transmittance for thin ITO films deposited on PES reached 80%. In 2008, Guillén & Herrero observed that the transmittance of ITO films in the range of 400 – 800nm was around 90% regardless of the substrate types. Guillén & Herrero have summarised these results in a graph shown in Figure 3-23 . However, this Figure shows that the transmittance in ITO near infra red is very sensitive to thickness and decreases with an increase in thickness on both PET and glass in a similar way. The behaviour is independent of the substrate.

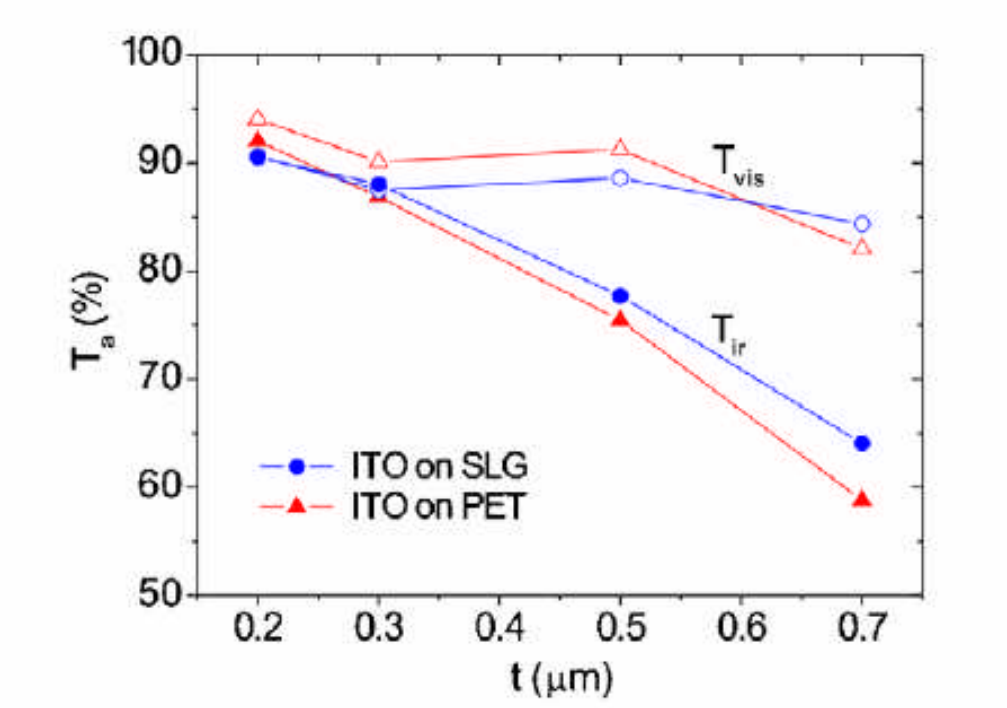

Figure 3-23: Average transmittance in the visible, Tvis (400-800nm), and near infrared, Tir (800-1500 nm), of ITO films deposited on soda lime glass and PET substrates. (Guillén & Herrero, 2008)

3.4.2.4. Microstructure of the ITO films

If nothing else is changed, the microstructure of the ITO films deposited on polymer depends highly on the polymer substrates itself. In fact, Yang et al. observed in 2007 that a film deposited on glass substrates showed more crystallinity that one deposited on PC and COC. They wrote that " *Polycarbonate and cyclo-olefin copolymers substrates have lower surface energy for the molecular structure of the long chain form, so it is difficult for an ITO membrane to grow in preferred orientations*." The amorphous structure of the film can be seen in figure 3-24 . Actually, close examination of trace (a) for the PC shows the start of some crystalline behaviour under the deposition conditions used.

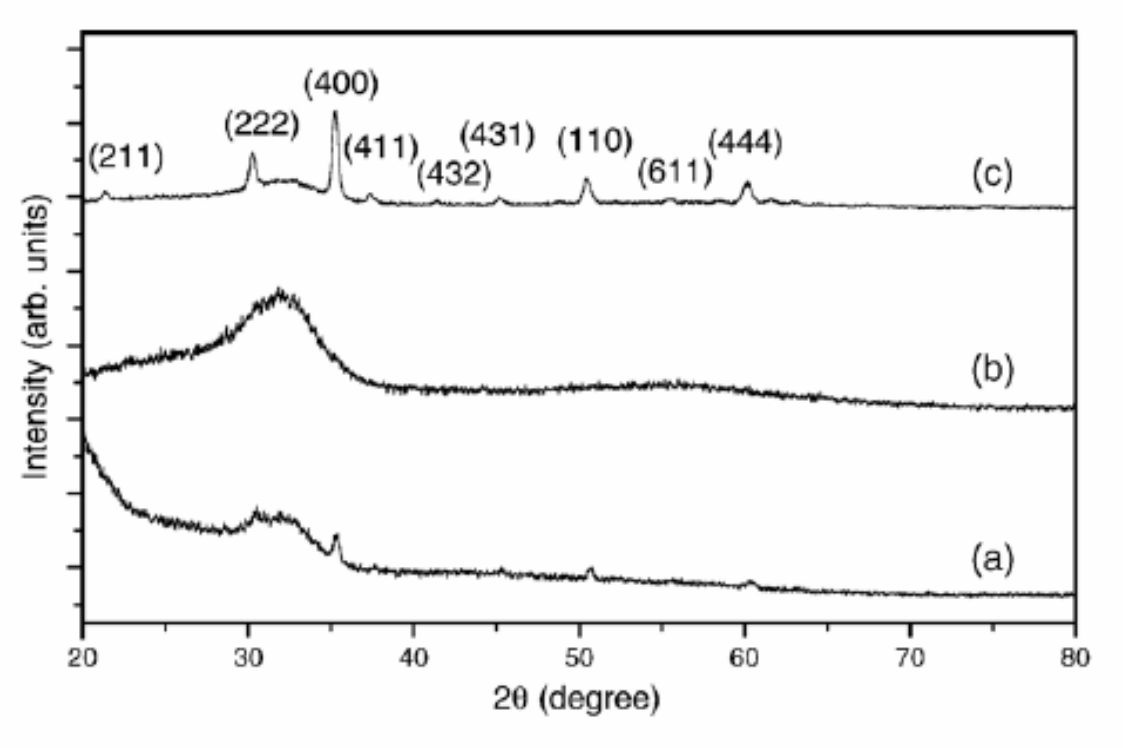

Figure 3-24: XRD diffraction pattern for ITO films deposition on (a) PC (b) COC and (c) glass substrates deposition power at 100W. (Yang et al.,2007)

Other studies made on PES led to different results. In 2007, Y.C Lin et al. produced ITO thin films having (222) and (400) crystal plane preferred orientation at 100 W as shown in Figure 3-25. A crystalline microstructure with different orientation has also been observed with over 700nm of ITO when PET substrates where used as shown in Figure 3-26 (Guillén & Herrero, 2008).

Thus literature reports crystalline ITO can be deposited on polymer substrates particularly for PET, PES and COC. As with deposition of ITO onto glass the particular sputtering parameters used are critical.

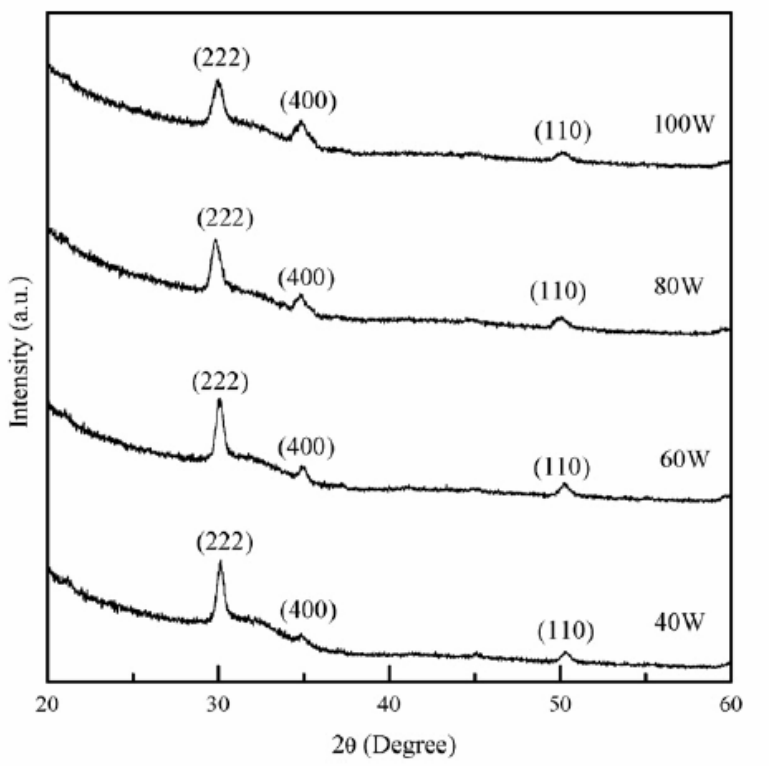

Figure 3-25: Diffractograms corresponding to ITO thin films deposited at various power on PES substrates. (Lin et al., 2007)

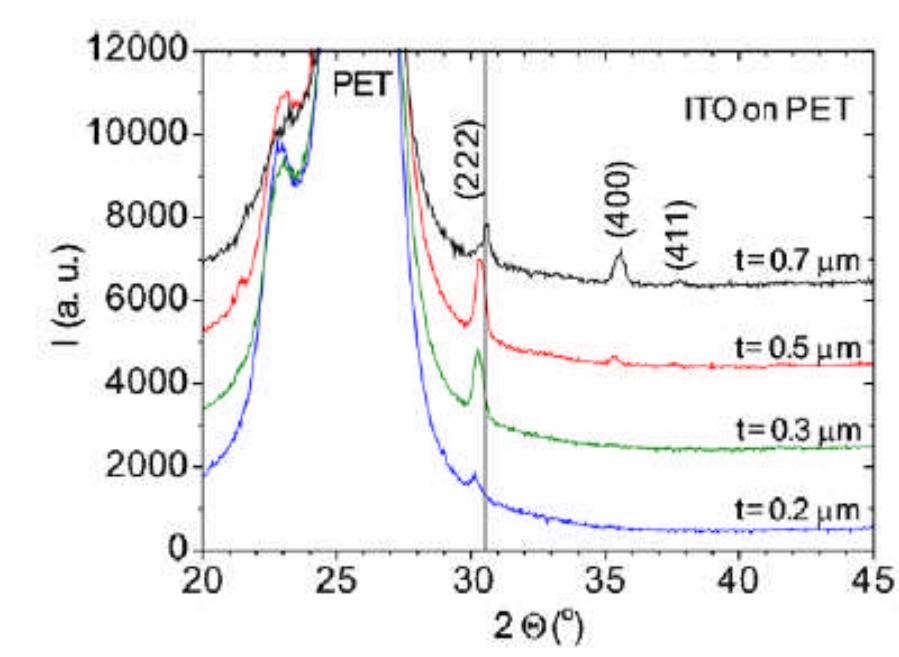

Figure 3-26: Diffractograms corresponding to ITO thin films deposited with various thicknesses on PET substrates. (Guillén & Herrero, 2008)

3.5. Values found in literature

In general, for ITO films deposited on glass (films showing the best electrical properties), the resistivity values have not been found below 2 x 10^{-4} Ωcm. All the figures shown in part 3-3-2 representing the evolution of ITO film resistivities regardless of the sputtering parameter, do not go under the value of 2 x 10^{-4} Ωcm. The corresponding optical transmittances are of the order of 90%.

The aim of this work is to achieve lower resistivities with a remaining high transparency and to concentrate on factors that are suitable for low temperature deposition.

In the following chapter, the experimental programme used to deposit ITO onto glass and polymer as a function of sputtering parameters is reported.

4. Experiments

4.1. Deposition of ITO on glass substrates

4.1.1. Sputtering process

ITO thin films have been prepared by pulsed dc magnetron sputtering from an oxide ceramic target with 10.2 x 20.3 cm² area. The substrates were standard soda lime glass slides with 2.5 x 7.5 cm area which were cleaned using isopropanol before being introduced into the chamber. These substrates were placed in equivalent position for each experiment. Four slides were stuck on a vertical frame using Kapton tape. Their disposition is showed in Figure 4-1. High purity argon and oxygen were introduced through independent mass flow controller after the vacuum chamber was evacuated below 5.10^{-5} Torr. Before beginning deposition, the target was pre-sputtered for 10 minutes. The frame where the samples are located, is moved in front of the target to allow ITO deposition on glass, without heating.

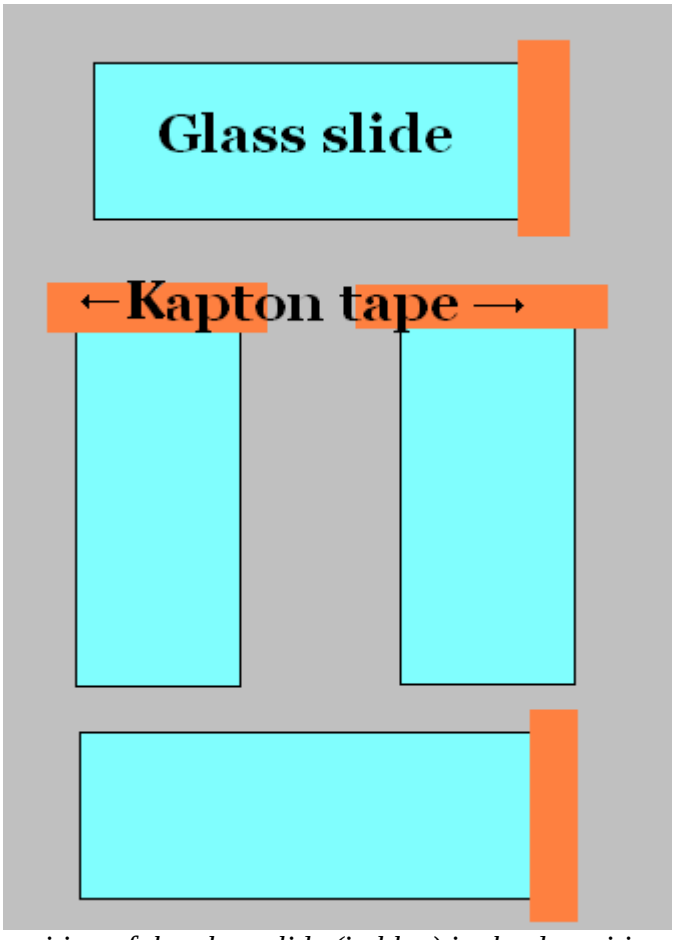

Figure 4-1: Disposition of the glass slide (in blue) in the deposition chamber

The sputtering parameters were changed, one after the other in order to see their influence on the ITO film properties (Electrical properties, optical properties and crystallinity). The best experimental parameters were then kept for further depositions. The different set of experiments and their values are gathered in the Table 4-1. It is important to indicate the sputtering power densities employed during the experiments. For the different powers applied they were respectively of 0.48 W/cm^2, 0.72 W/cm^2, 0.96 W/cm^2 , 1.44 W/cm^2 and 1.69 W/cm^2 . Finally, in order to see the influence of the gas inlets' position, some depositions have been done with one of them closed.

Parameter checked	Features
Influence of the thickness	200 nm - 500 nm - 1000nm
Influence of the chamber pressure	5 mtorr - 10 mtorr
Influence of the rotation	Yes - No
Influence of the oxygen amount	1% - 5% - 10% - 12% - 15% - 17% - 20%
Influence of the sputtering power	100 W - 150 W - 200 W - 300 W - 350 W

Table 4-1: Sputtering parameters checked during the deposition on glass

4.1.2. Film measurements and analysis

The thicknesses of the films were obtained using a Taylor- Hobson Talysurf 10.The crystal structure of the films was observed by X-Ray Diffraction (XRD) technique, using a Kα1 emission line of copper (λ = 1.540 56 Å) in a Siemens D5005. The crystallites size of the film has been calculated using the Scherrer formula :

$$d_0 = \frac{0.94\,\lambda}{\beta\,(2\theta)\cos\theta}$$

Where d_0 is the crystallite size, λ is the wavelength, β is the full width at half maximum*(*FWHM), θ is the angle of diffraction.

The film sheet resistance was obtained with silver paint (Agar scientific ltd. Cambridge) and an ohmmeter (Megger BM 100). The sheet resistances of two areas were measured (see Figure 4-2). In order to calculate the resistivity of the samples, the following equation as been used :

$$R = \frac{\rho}{t}\frac{L}{W}$$

Where R is the sheet resistance, ρ is the resistivity, t is the film thickness, L the length of the area measured and W the width of the area measured. For a square, L/W = 1.

Optical measurement of the films was done with a spectrophotometer (Perkin-V/VIS Spectrophotometer). For the latter, a bare soda lime glass slide was used as a reference.

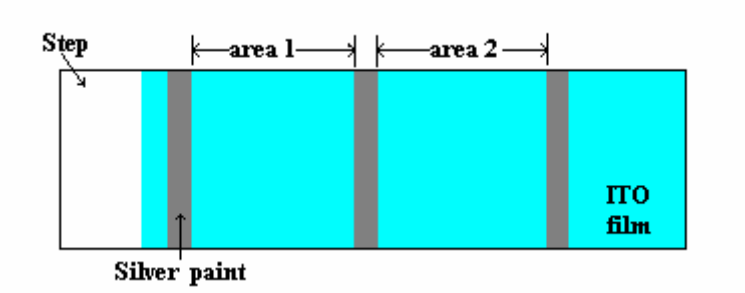

Figure 4-2: Resistivity measurement of the ITO coated glass substrates.

4.1.3. Annealing

Some of the ITO coated glass substrates were baked at 370°C in a furnace (Gallenkamp Box Furnace size 1) for one hour. Other tries were done on other samples at 150°C for 48 hours. Their electrical , optical properties and their crystallinity were then measured the same way as described above. The results obtained were compared to non-heated samples.

4.2. Deposition of ITO on polymer substrates

4.2.1. Sputtering process

The ITO thin films have been prepared by pulsed dc magnetron sputtering like for the glass substrate samples. The substrates were cut from a few microns thick PET film. The samples were 2.5 x 7.5 cm. Before being installed in the deposition chamber, the PET substrates were cleaned with isopropanol. Their disposition was the same as for the glass samples (figure 4-1). High purity argon and oxygen were introduced through independent mass flow controller after the vacuum chamber was evacuated below 5.10^{-5} Torr. Before beginning deposition, the target was pre-sputtered for 10 minutes. The frame where the samples were located, was moved in front of the target to allow ITO deposition on glass, without heating.

The experiments on the polymer substrates were launched with the best parameters found with the tests done on glass. They are shown in table 4-2.

Parameter	Value
thickness	500 nm – 1000 nm
chamber pressure	10 mtorr
rotation	Yes - No
oxygen amount	10 % 02
Sputtering power	100 W

Table 4-2: Sputtering parameters used for the deposition of ITO on PET

4.2.2. Film measurement and analysis

Several techniques were used to try to measure the film thickness : Tylasurf (Taylor-Hobson Talysurf 10) , Dektak and AFM (Digital Instruments). The crystal structure of the films were observed by XRD, using a Kα1 emission line of cobalt (λ = 1.788 97 Å) in a PW 1720 Philips X'pert instrument. Squares measuring 2.5 x 2.5 cm were cut from the coated films in order to be put in the XRD machine. The film sheet resistance was obtained with silver paint and an ohmmeter. Optical measurements of the films were done with a spectrophotometer. The ITO coated PET samples were held between two glass slides in order to be kept flat. The same operation was done for the reference bare PET film.

4.2.3. Annealing

Some of the ITO coated PET substrates were baked at 150°C for 48 hours. Their electrical , optical properties and their crystallinity were then measured the same way as described above. The results obtained were compared to non-heated samples.

4.3. EDS analysis

Some ITO films deposited on glass slides were analysed using the XL30 ESEM energy dispersive spectrometer (*EDS*) in order to compare their compositions. A piece of the ITO target and two 3 microns thick films on glass slides were analysed. The EDS first focused on the surface of the three samples, then on two different locations of the cross sections (middle of the film, bottom of the film). Those areas have been chosen in order to visualise the different composition depending on the thickness of the film. The amounts of carbon, indium and tin were looked at.

5. Results

5.1. Deposition of ITO on glass substrates

The following chapter presents the results obtained for the ITO films deposited on glass. The state of the electrical and optical properties is described for each sputtering parameter changed. The crystallinity of the samples is also shown.

5.1.1. Influence of the film thickness

The dependence of film resistivity on glass substrate as a function of the film thickness is illustrated in Figure 5-1. They became conductive for a thickness of 400 nm. The 200 nm ITO thin films showed a sheet resistance higher than 200 MΩ/square and were therefore considered as not conductive. From 400 nm to 800 nm, the resistivity decreased gradually to 78 Ωcm. (all the results of the resistivities calculations can be found in Appendix A)

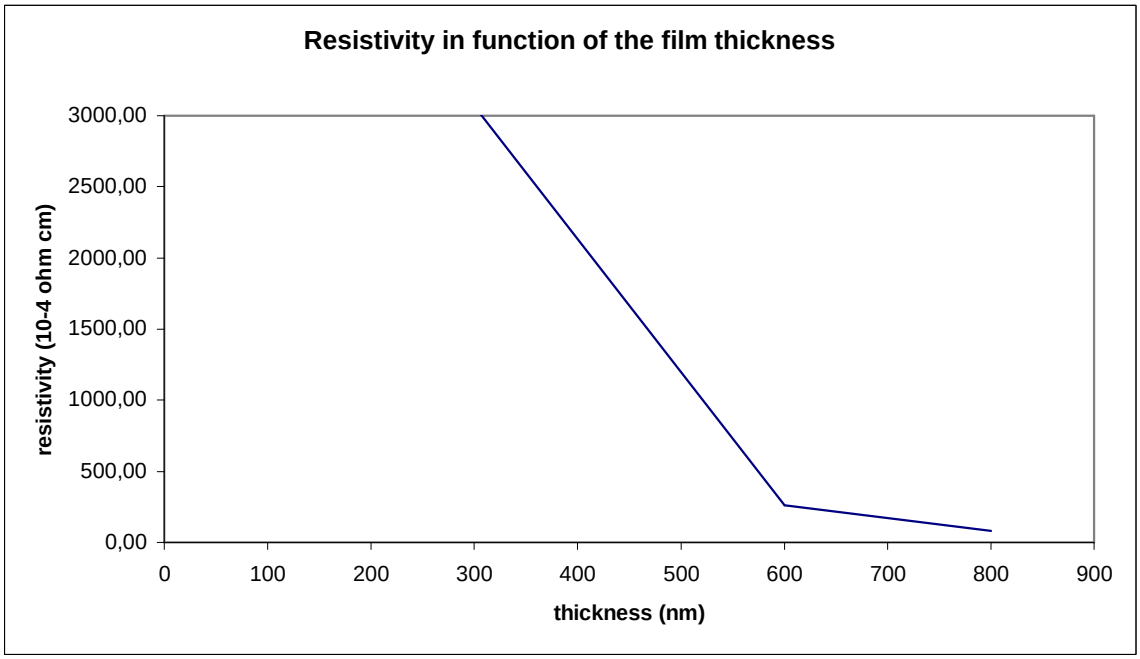

Figure 5-1: Resistivity of ITO thin films coated on glass substrates in function of the thickness

The optical transmittance of the ITO films with various thicknesses is shown in Figure 5-2. No important difference can be observed between the different samples. The transmittance stays around 90% in the visible (very transparent coatings). The absorption of light in the ultra-violet is an indication of the film's conductivity. The results obtain with the

spectrophotometer corroborate the resistivities calculations. Indeed the 200 nm sample's spectrum shows that it is not conductive. It is interesting to notice that the reflexion effect caused by the film and the glass slide is linked to the coating's thickness. The frequency and the amplitude of the interferences are higher for thick films.

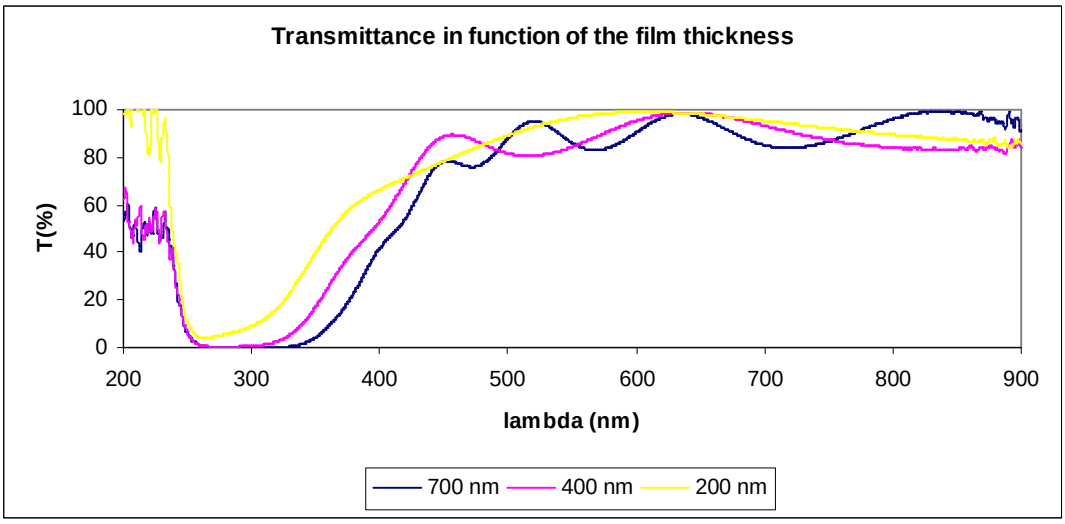

Figure 5-2: Transmittance of ITO thin films coated on glass substrates in function of the thickness

From the diffractogram shown in Figure 5-4, the ITO film produced have [2,2,2] crystal plane preferred orientation. When the thickness increases from 400 nm to above, additional diffraction peaks appear (plane [4,1,1]), indicating the formation of crystallites with other orientations. Guillén & Herrero also obtained those peaks with the same range of thicknesses. However, their diffractograms showed [4,0,0] crystal planes for thick films. All further calculations and studies will focuses on those three plane ([2,2,2],[4,0,0],[4,1,1]). The crystallite sizes have been calculated and are shown in the following graph (Figure 5-3).

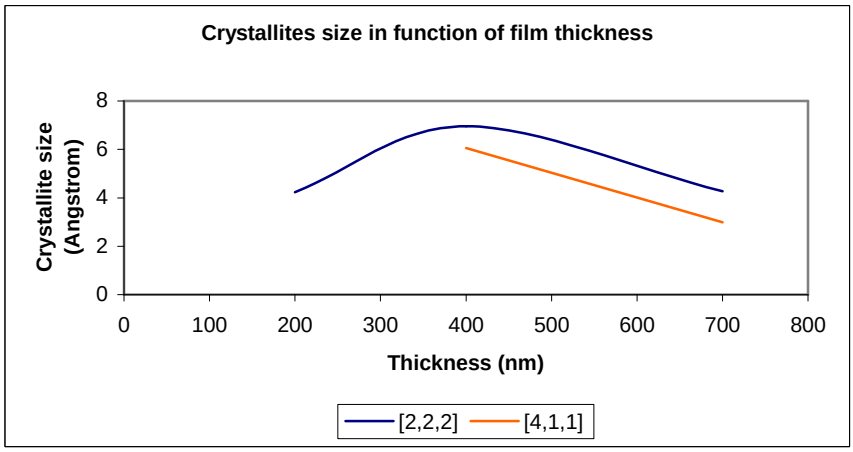

Figure 5-3: Crystallite size of different planes in function of the film thickness

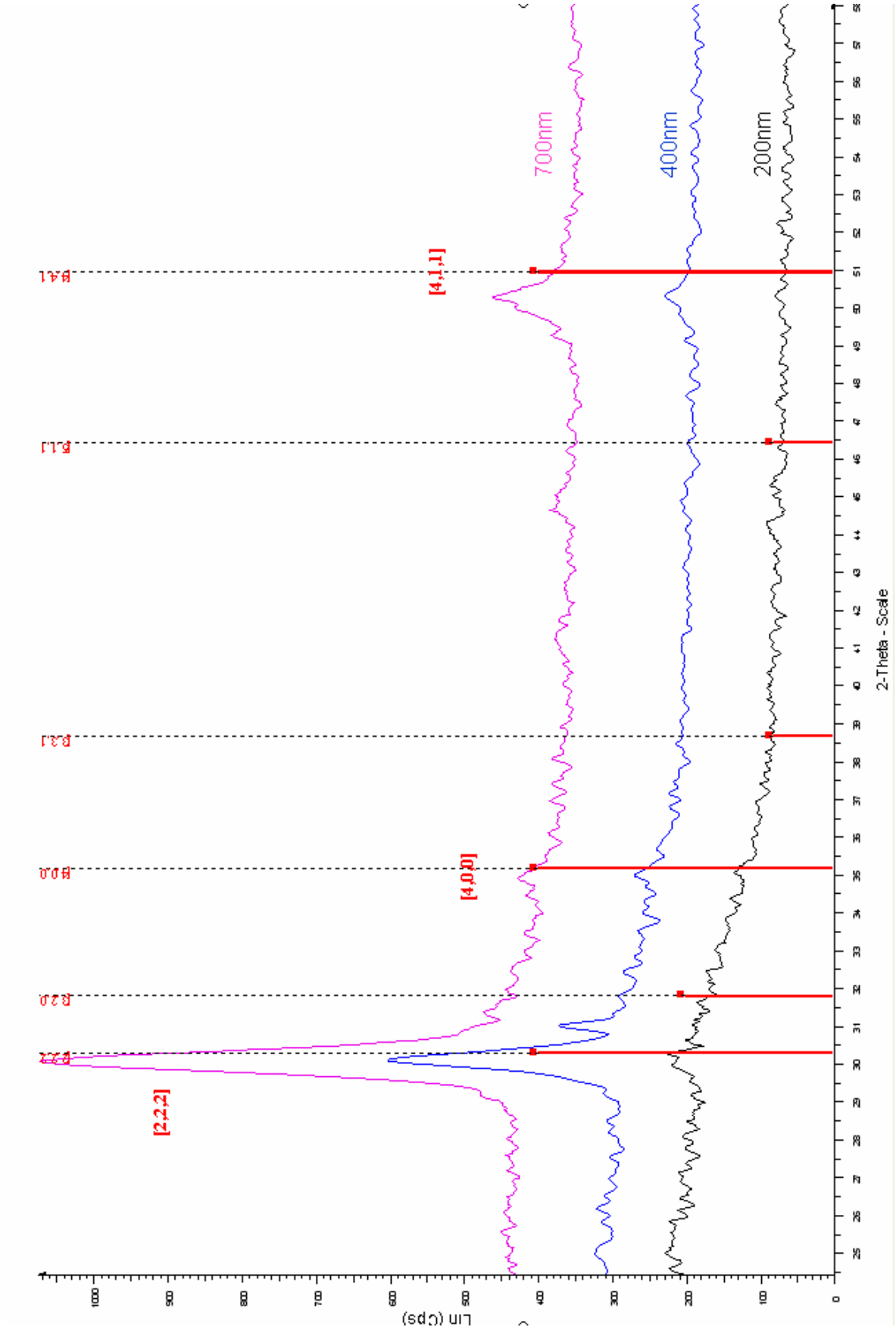

Figure 5-4: Diffractograms corresponding to ITO thin films with various thicknesses.

5.1.2. Influence of the chamber pressure

Figure 5-5 shows the evolution of resistivity in function of the chamber pressure. The film thickness measured is 700 nm. For a pressure of 5 mtorr, the resistivity was of $76x10^{-4}$ Ωcm whereas with a pressure of 10 mtorr, the resistivity reaches $162x10^{-4}$ Ωcm. From these results, it can be said that decreasing the chamber pressure enhances the electric properties of ITO films.

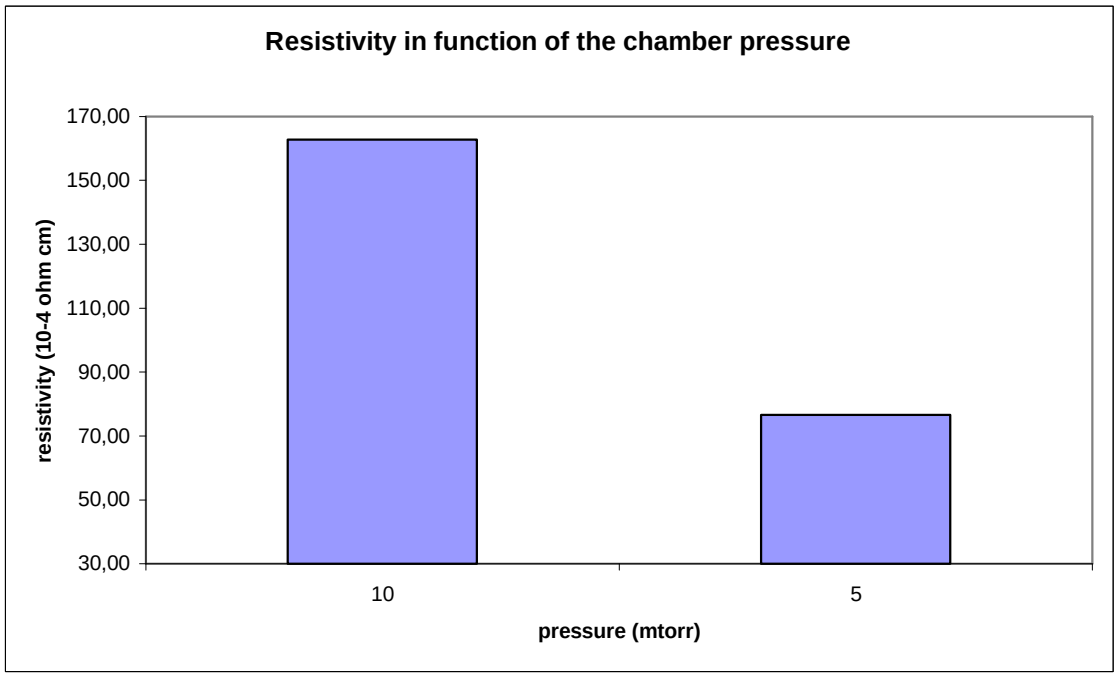

Figure 5-5: Resistivity of ITO thin films coated on glass substrates in function of the chamber pressure

The comparison of the optical transmittance spectra of the samples shows that the sputtering pressure has a great influence (Figure 5-6). It is seen that the average transmittance of the films in the range 400-800 nm is over 90% regardless of the pressure. However, as the chamber pressure increase, the transmittance of the ITO films increase slightly. This difference can be clearly seen after 550 nm.

As the results concerning the optical and the electrical properties are contradictory, it is needed to make a compromise between 10 mtorr and 5 mtorr to continue the experiments. Former tests will show that it is possible to keep a pressure of 10 mtorr.

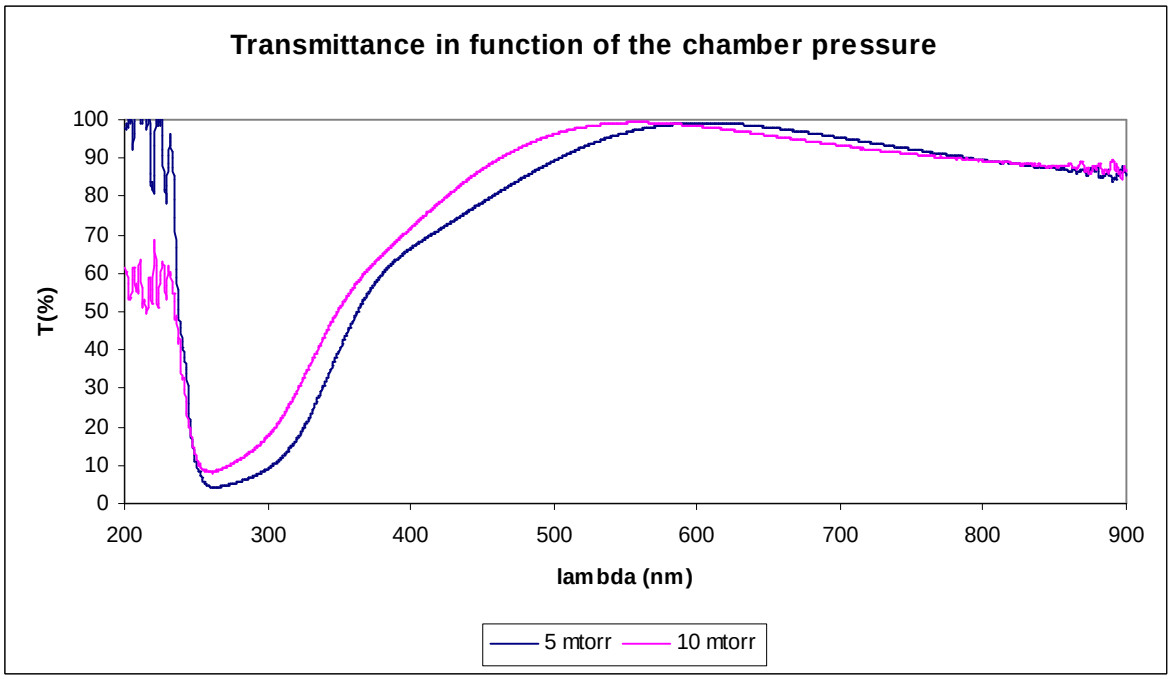

Figure 5-6: Transmittance of ITO thin films coated on glass substrates in function of the chamber pressure

X-ray diffraction patterns of ITO films deposited with different pressures are shown in Figure 5-8. Both of the samples are crystalline. However, the film deposited at 10 mtorr has got crystallites growing preferentially in the [4,1,1] plane whereas the one deposited at 5 mtorr grows in the [2,2,2] plane. The sputtering pressure influences the growth direction of the film. The crystallite sizes have been calculated and are shown in the following graph (Figure 5-7) (all the results of the resistivities calculations can be found in Appendix B).

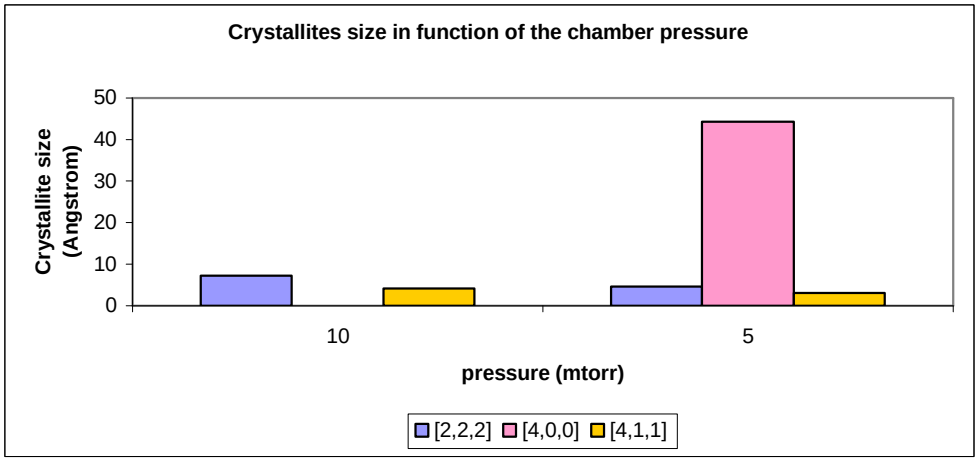

Figure 5-7: Crystallite size of different planes in function of the chamber pressure

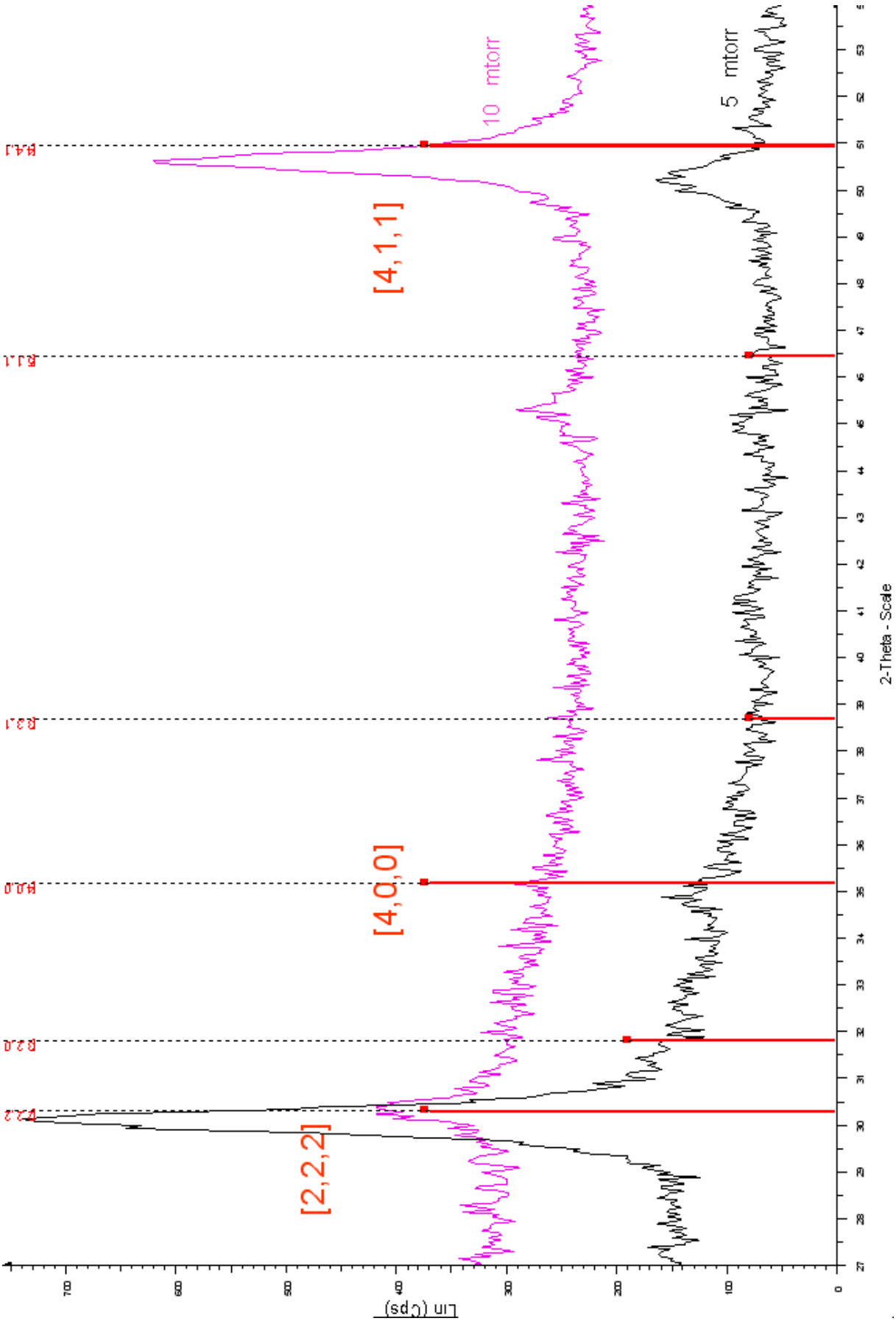

Figure 5-8: Diffractograms corresponding to ITO thin films deposited on glass with various chamber pressure.

5.1.3. Influence of the rotation

Samples of 500 nm thick were deposited with a chamber pressure of 10 mtorr, 20% O_2 and a power of 200W. For some of them, the process was done with the frame rotating. The others were staying still in front of the target. The resistivities are shown in Figure 5-9. From this chart, it can be said that the rotating increases the resistivity of the film. Indeed, values jump from $148x10^{-4}$ Ωcm to $701x10^{-4}$ Ωcm.

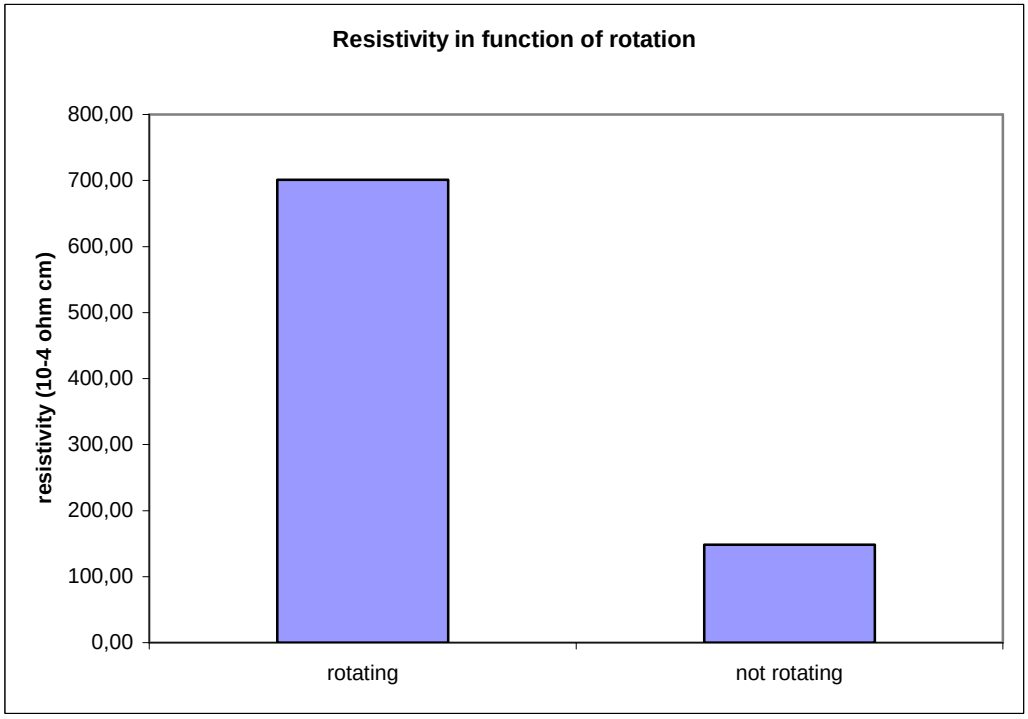

Figure 5-9: Resistivity of ITO thin films coated on glass substrates in function of the rotation

The transmittance of samples deposited without rotation (in blue) and with rotation (in orange) is described in Figure 5-10. The four samples placed in the chamber were analysed each time in order to see the influence of the location of the glass slide (see figure 4-1). The average of transmissivity for the films deposited without rotation is around 80% while it is of 70 % for the ones deposited with rotation. Yet, the scattering between the samples of each set of experiment is lower for a rotating process. Thus, the films obtained are more homogenous after a rotating deposition. The sudden loss of transmissivity is due to the change of stoichiometry of the films. This phenomenon is discussed in part 5.3.

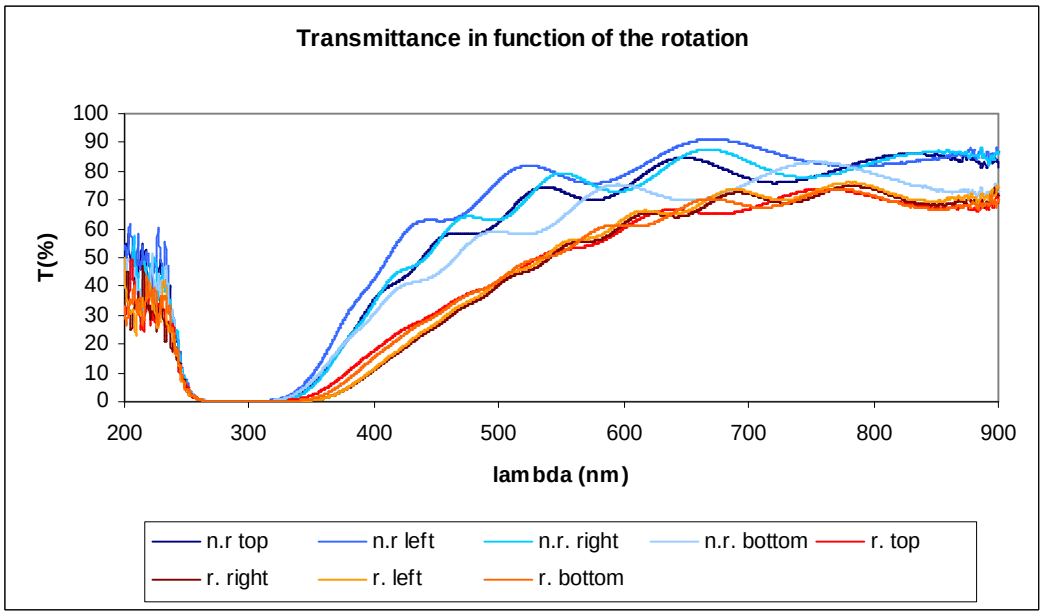

Figure 5-10: Transmittance of ITO thin films coated on glass substrates in function of the rotation (n.r = non rotating; r= rotating)

Figure 5-12 represents the X-ray diffraction pattern of samples deposited with or without rotation. It can be seen that the crystallites grew with different orientation depending on the way the ITO was deposited. [2,2,2], [4,0,0], [0,3,1] and [4,1,1] planes are present for samples deposited without rotation. A preferential crystallite growth in the [4,0,0] plane can be deduced from the huge peak seen on the "rotating" diffractogram. The frame's spin has the effect of allowing only one crystallite growth direction.

However, even if the rotated samples have a preferred growing pattern, the size of their crystallites (38.9 Å for the [4,0,0] plane) stays under the one of non-rotated glass slides (45.7 Å for the [4,0,0] plane) (Figure 5-11).

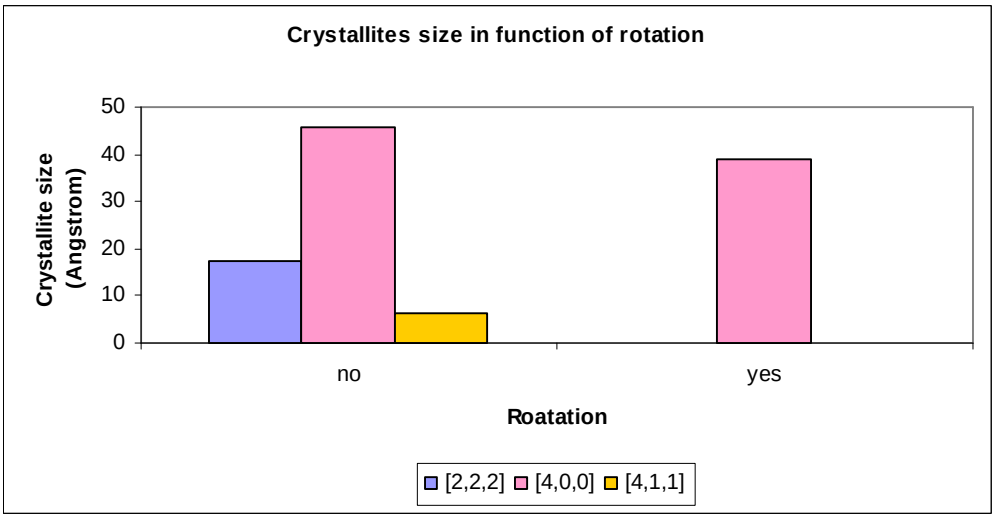

Figure 5-11: Crystallite size of different planes in function of the rotation

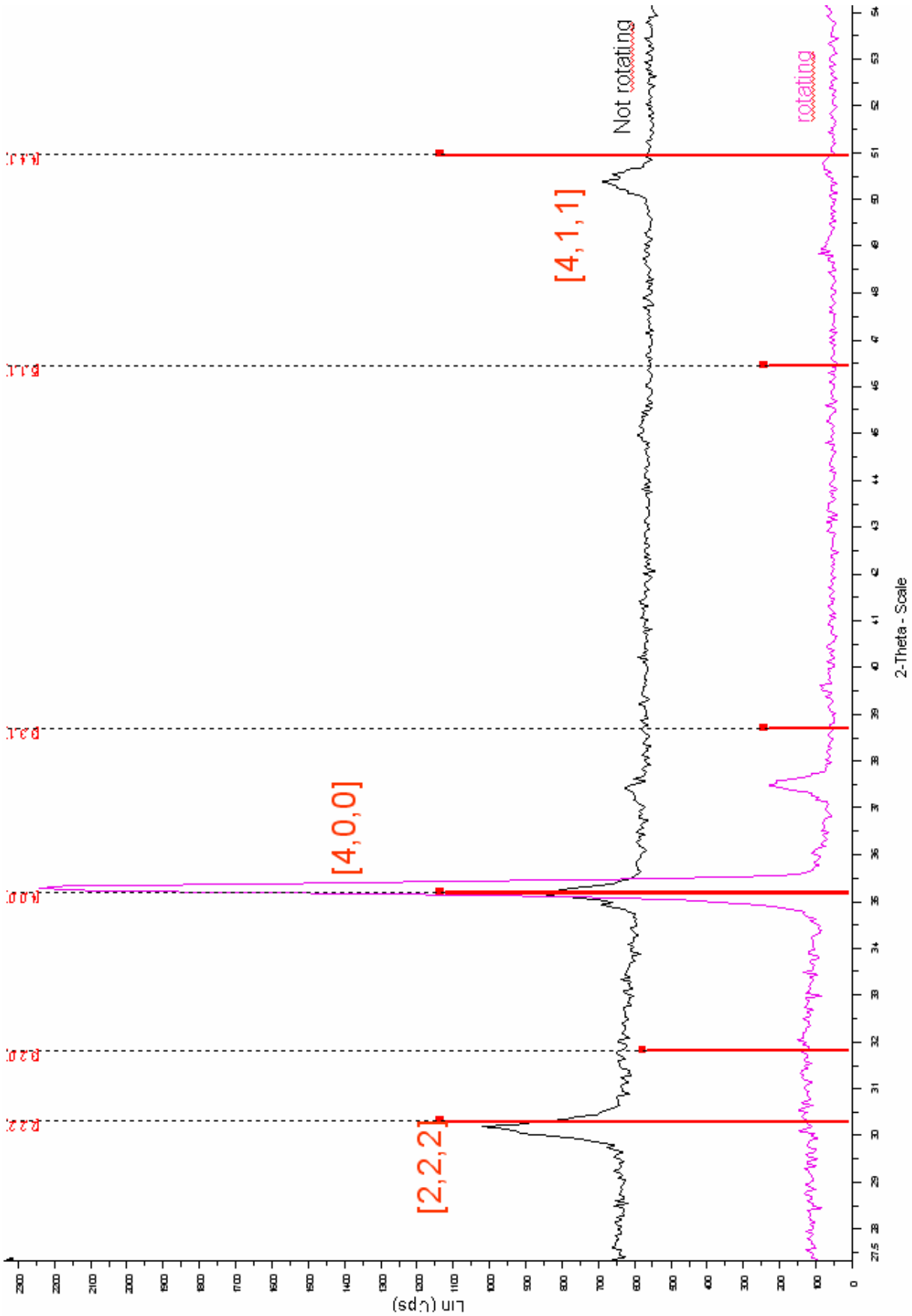

Figure 5-12: Diffractograms corresponding to ITO thin films deposited on glass with or without rotation.

5.1.4. Influence of the oxygen amount

Resistivities of ITO films deposited at various amount of oxygen amount in the argon sputtering gas are plotted in Figure 5-13. The ITO film resistivity increases exponentially with increasing oxygen amount (except for the sample deposited with 15% of O_2). The sample deposited with 20% O_2 has got a resistivity of $78x10^{-4}$ Ωcm while the one deposited with 17% O_2 falls to $3.6x10^{-4}$ Ωcm. The raise of resistivity at 15% may be an experimental error. After 10% oxygen the resistivities stabilize and increase slightly after 5%.

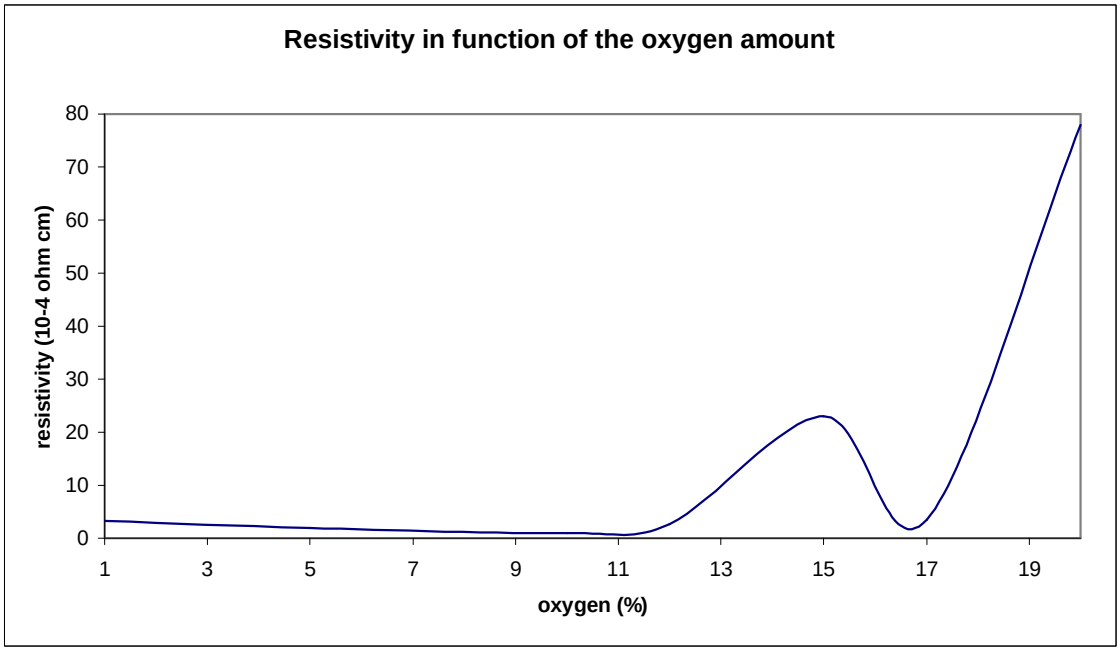

Figure 5-13: Resistivity of ITO thin films coated on glass substrates in function of the oxygen amount

Because of a substoichiometric deposition of indium oxides (see part 5.3) the samples turned from transparent to brown. This phenomenon was amplified with the diminution of the oxygen amount. That's why the spectrogram showed in Figure 5-14 is not very relevant. Nevertheless, the transmissivity stays high for high amounts of oxygen and reduces below 17% O_2. It goes from an average of 90% to an average of 70% in the range of 400-800nm.

While the decrease of the oxygen amount enhances the electrical properties of the ITO films, it depletes the optical ones. For this project, the best amount of oxygen is 10%.

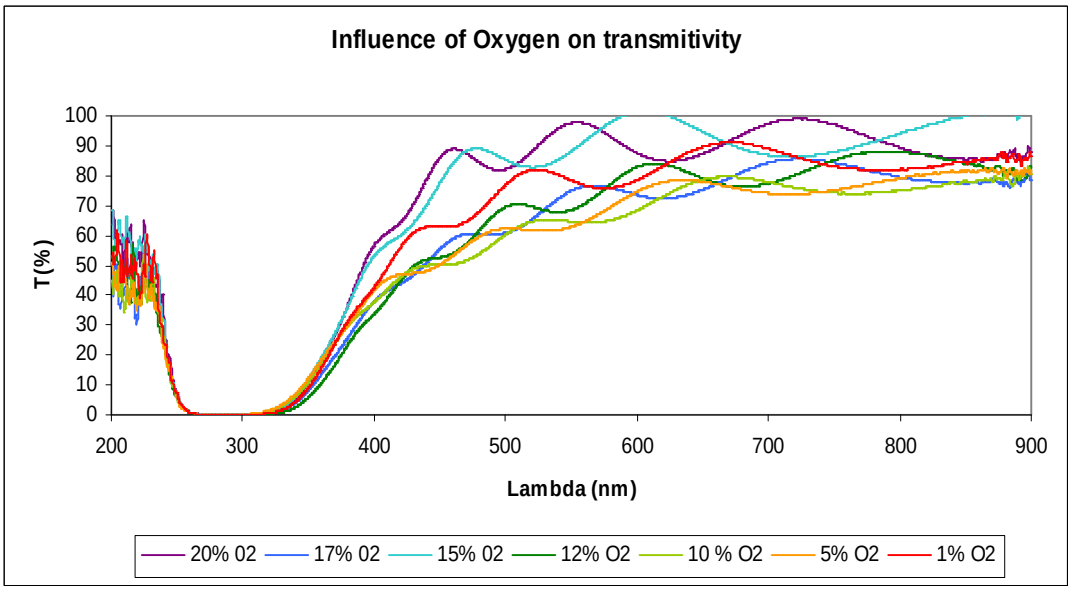

Figure 5-14: Transmittance of ITO thin films coated on glass substrates in function of the oxygen amount

Figure 5-16 represents the X-ray diffraction pattern of the samples deposited with different oxygen amounts. It can be seen that the crystallites grew with the same orientation regardless on the way the ITO was deposited. [2,2,2], [4,0,0], [0,3,1] and [4,1,1] planes are present for all the samples, except for the one deposited with 20% O_2 which has not got the [4,0,0] and [0,3,1] planes.

Looking at the size of the crystallites in Figure 5-15, it is noticed that the one growing in the [4,0,0] direction is higher than the others. The lowest sizes for the three planes were obtained for an amount of 10% which is the same value of the lowest resistivity.

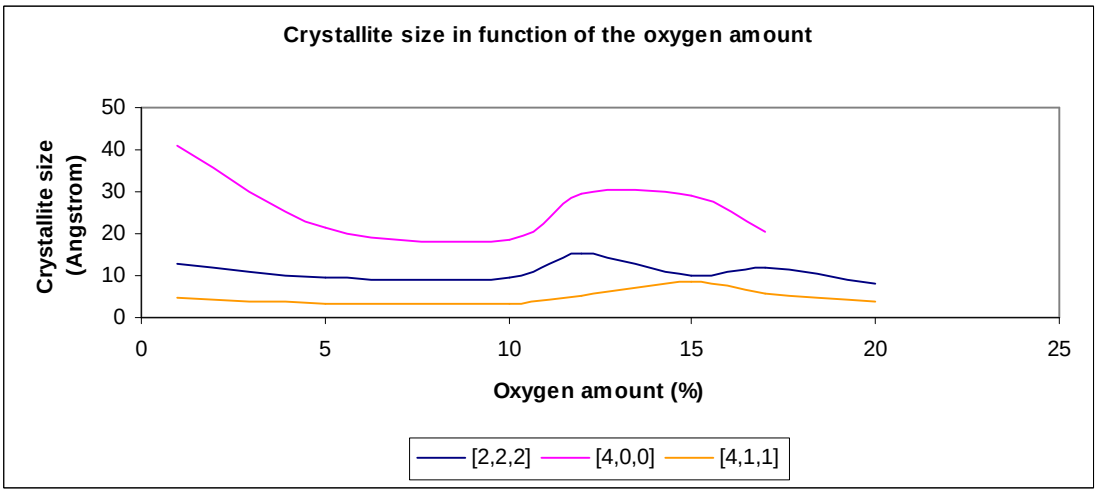

Figure 5-15: Crystallite sizes corresponding to ITO thin films deposited on glass with various oxygen amounts.

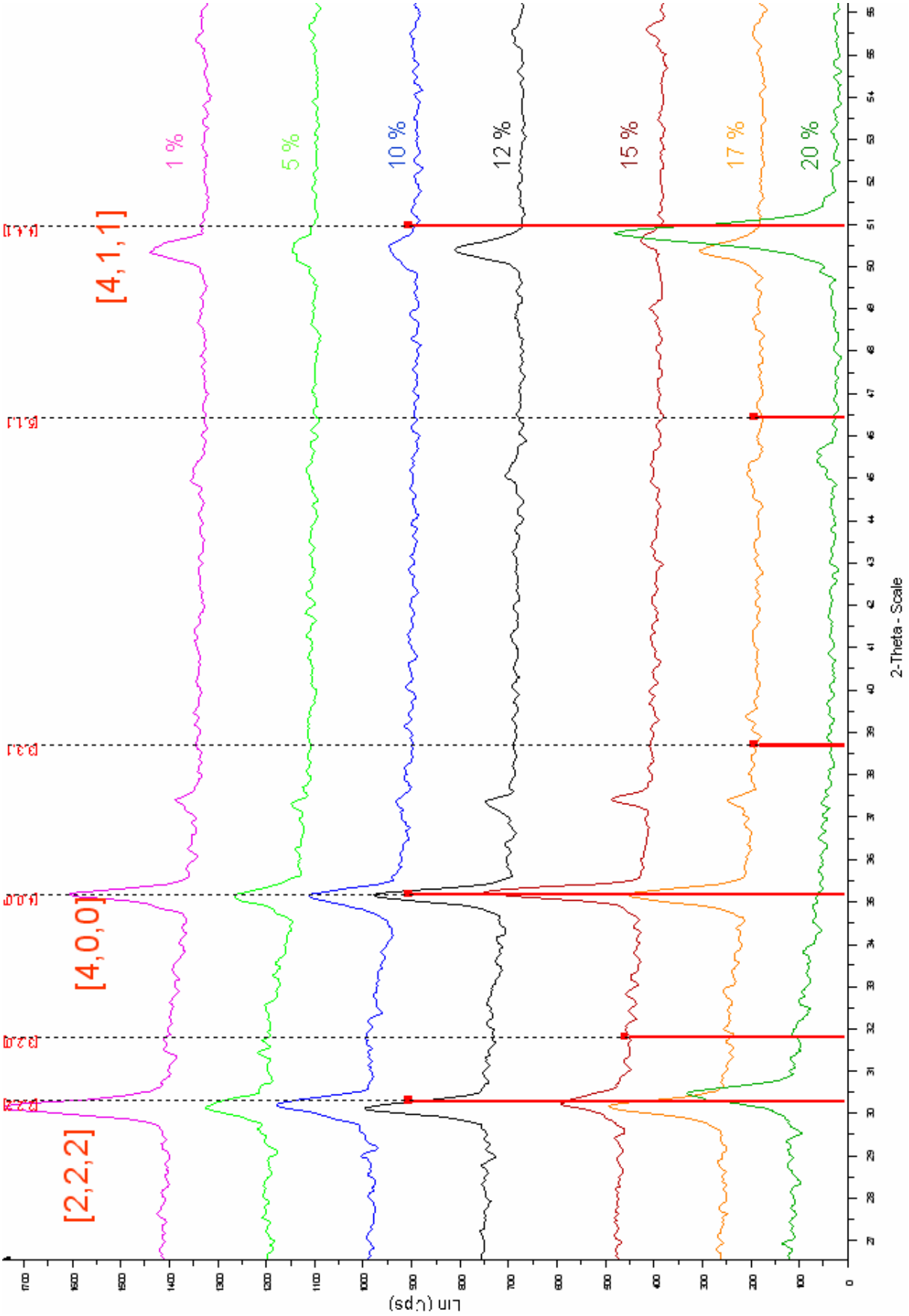

Figure 5-16: Diffractograms corresponding to ITO thin films deposited on glass with various oxygen amounts.

5.1.5. Influence of the sputtering power

The dependence of film resistivity on the glass substrate as a function of the sputtering power is illustrated in Figure 5-17. From 100W to 200W, the resistivity increases with increasing sputtering power. It rises from $1.8x10^{-4}$ Ωcm to $3.2x10^{-4}$ Ωcm. Then for values above 200W, the resistivities stabilise around $3x10^{-4}$ Ωcm.

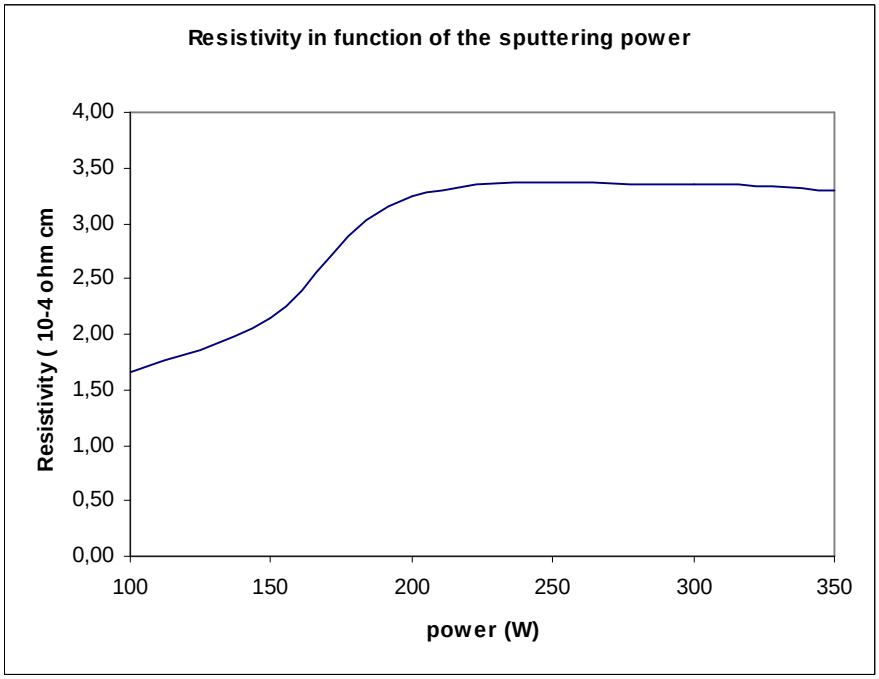

Figure 5-17: Resistivity of ITO thin films coated on glass substrates in function of the sputtering power

From Figure 5-18, it can be seen that the increase of the sputtering power has a beneficial effect on the transmissivity. Indeed for higher values, the mean of transmittance is around 80% percent whereas it goes down to 65% for samples deposited at 150 W. Here again, the loss of transparency of the sample due to the change of the film's colour distorting slightly the results. However, if the spectrum obtained at 100W is considered as an experimental error (since it doesn't follow the general tendency), it can be said that the increase of the power increases greatly the transmittance of the films.

Yet, because of the brownish aspect of the films, optical properties turn out to be less critical than the electrical ones for the choice of the best sputtering parameters. Therefore, following experiments will be held with a sputtering power of 100W.

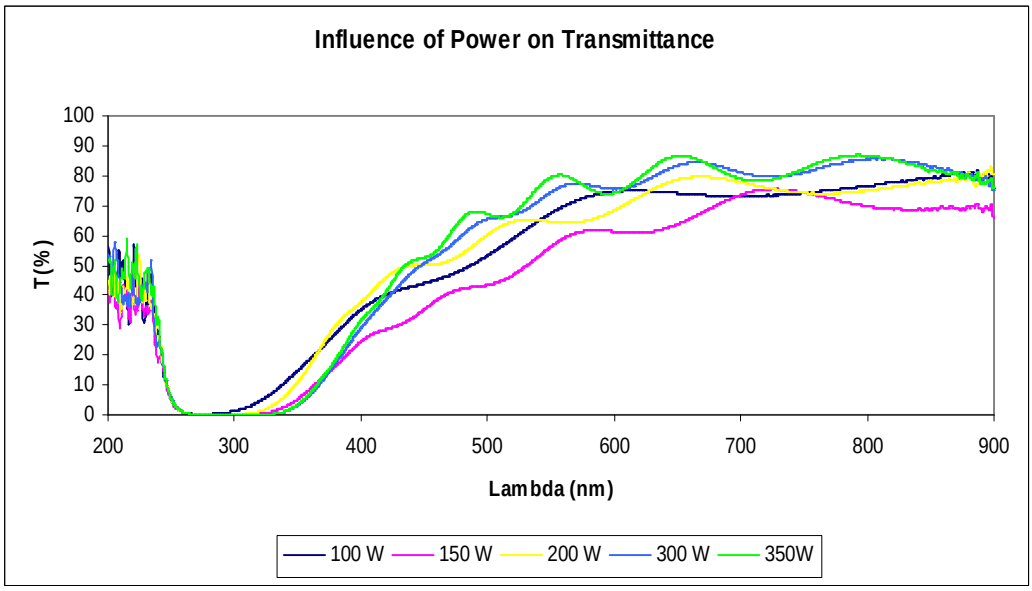

Figure 5-18: Transmittance of ITO thin films coated on glass substrates in function of the sputtering power

From the diffractogram shown in Figure 5-20, the diminution of the sputtering power causes the production of amorphous ITO films. Indeed on the samples deposited at 100W and 150W, no diffraction peak can be observed. However, from 200 W to 350W the films show a high orientation of the crystallite in the [2,2,2], [4,0,0] and [4,1,1] planes. The crystallite size as a function of the sputtering power has been plotted in Figure 5-19. Apart from the [4,1,1] plane, the crystallite sizes tend to rise when the power is lowered. For the [2,2,2] plane, they measure from 17 to 8 Å and for the [4,0,0] plane, they go from 27 to 18 Å.

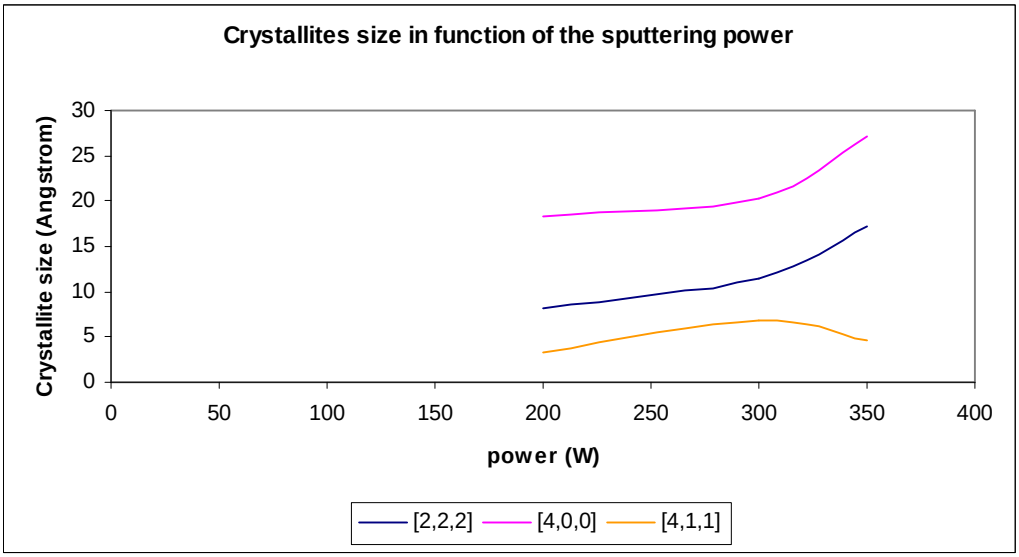

Figure 5-19: Crystallite sizes of ITO thin films coated on glass substrates in function of the sputtering power

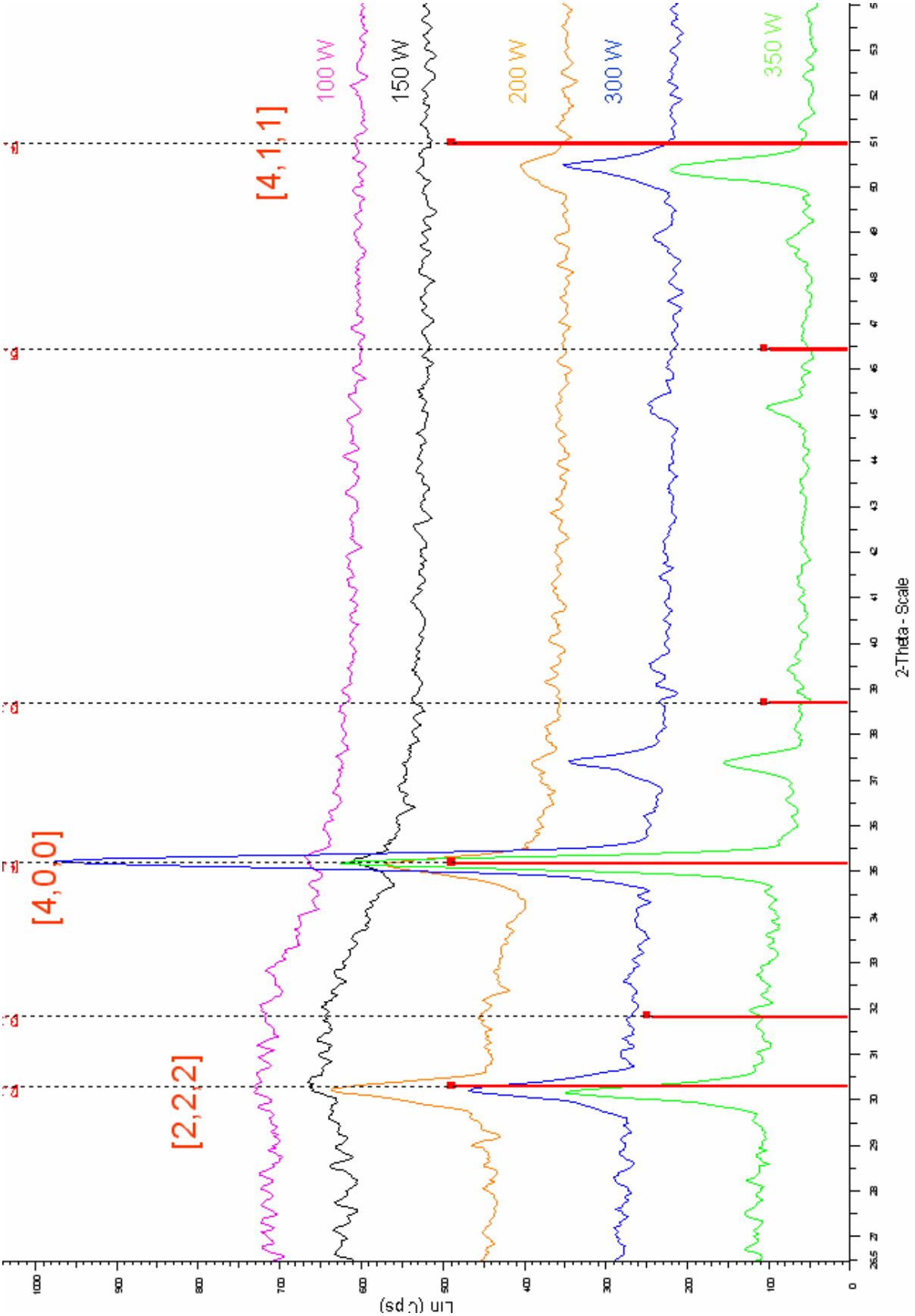

Figure 5-20: Diffractograms corresponding to ITO thin films deposited on glass with various sputtering power

5.1.6. The influence of the gas inlets

The measurement of the resistivities of a set of ITO coated glass slides deposited with a different gas flow path, shown that it has no influence on the electrical properties. Indeed, no tendencies can be found by looking at the features gathered in Tables 5-1 and 5-2. Each time the resistivities of two samples stuck at the same place in the deposition chamber has been compared. The thicknesses of the samples are all around 500 nm.

sample (10% O2 - 200W)	Resistivity (ohm cm x10-4)		sample (10% O2 - 200W)
	2 gas inlets	1 gas inlet	
68 (left)	0,265	0,36	72 (left)
69 (right)	0,29	0,285	73 (right)

Table 5-1: Resistivities corresponding to ITO thin films deposited with a power of 200W on glass with various gas flow path.

sample (10% O2 - 350W)	Resistivity (ohm cm x10-4)		sample (10% O2 - 350W)
	2 gas inlets	1 gas inlet	
76 (left)	0,34	0,21	84 (left)
77 (right)	0,21	0,00002	85 (right)

Table 5-2: Resistivities corresponding to ITO thin films deposited with a power of 350W on glass with various gas flow path.

5.1.7. Influence of the annealing

The influence of annealing on the electrical and optical properties of ITO films deposited on glass substrates are reported in this part. A first set of samples was baked at 370°C for 1 hour and another one at 150°C for 48 hours. The temperature of 150°C was chosen because it is the higher working temperature limit of PET. The behaviour of the ITO films in this condition will be helpful for the study of films on plastic substrates.

5.1.7.1. Results for substrates baked at 370°C

The aspect of two ITO films deposited on glass before and after annealing is shown in Figure 5-21.

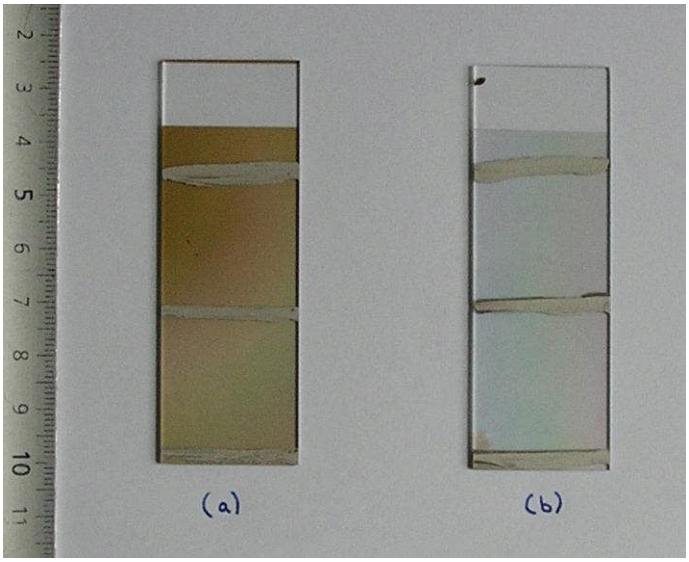

Figure 5-21: ITO films deposited on glass before (a) and after(b) annealing at 370°C

The resistivity's evolution of ITO coated glass samples after being baked at 370°C for 1 hour is shown in Figure 5-22. The x-axis corresponds to the denomination of glass samples (the corresponding deposition parameters can be seen in Appendix A). Those samples are an overall representation of all the films obtained with the different parameters. It is observed that annealing decreases greatly the resistivities of the samples. The films that were not conductive before annealing (resistivity above 200×10^{-4} MΩcm) became highly conductive. Their resistivities dropped to 7×10^{-4} Ωcm and even to 0.75×10^{-4} Ωcm for one of them. The other samples showed an amelioration of their electrical properties. For samples deposited with lower amount of oxygen and at lower sputtering power (Samples 37 – 40 – 87 – 88) the resistivities obtained are below 2×10^{-4} Ωcm.

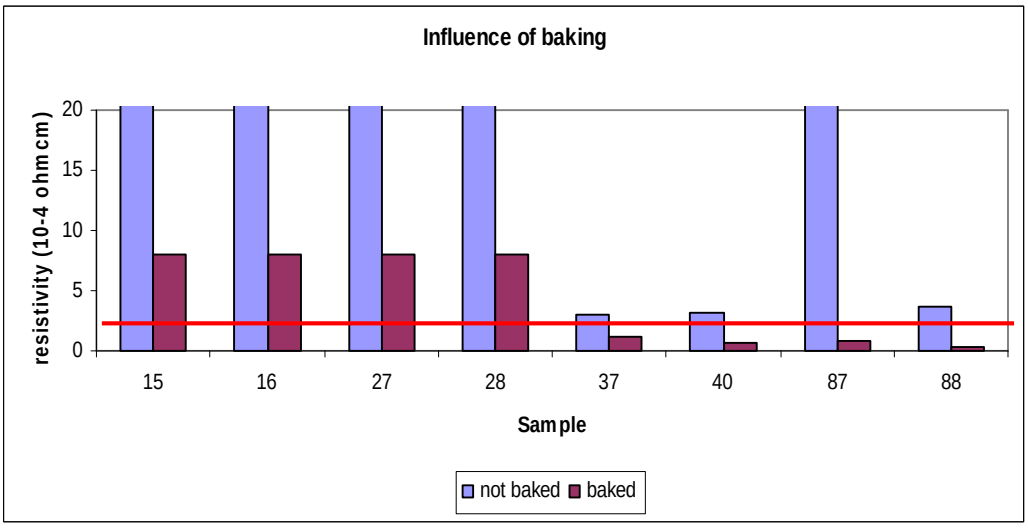

Figure 5-22: Resistivity of ITO thin films coated on glass substrates before and after annealing at 370°C

Figure 5-23 presents the transmittance of two baked and non-baked transparent ITO films on glass substrates. Annealing does not seem to have a great effect for these samples. Their transparency is not enhanced or reduced. The average transmittance stays rather high (around 90 % for sample 2) .

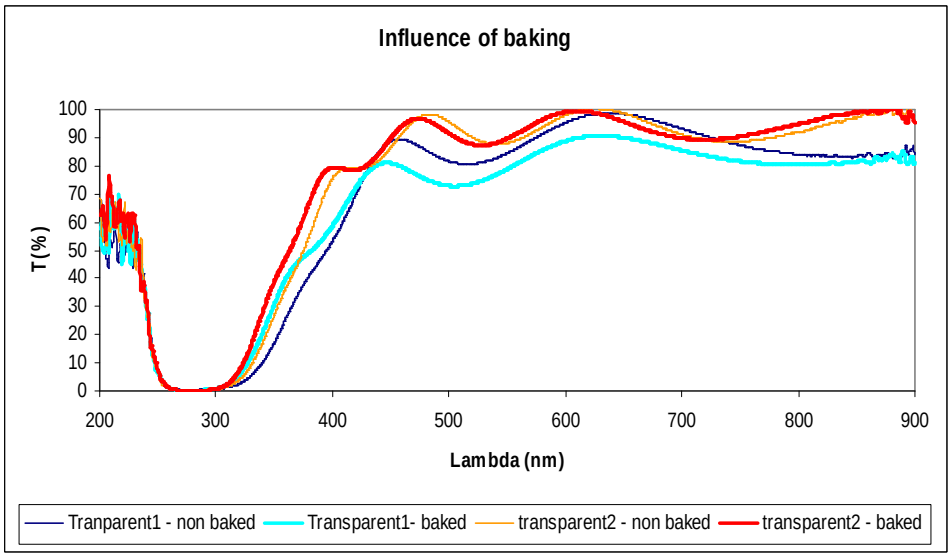

Figure 5-23: Transmittance of ITO thin films (transparent) coated on glass substrates before and after annealing at 370°C

On the other hand, the transmittance of brown ITO coatings (see part 5.3 for more details) on baked glass substrates is highly improved. Figure 5-24 shows clearly this tendency. The baked samples represented by bold spectrum, have an average transmittance of 90% while it is below 80% when they are not annealed.

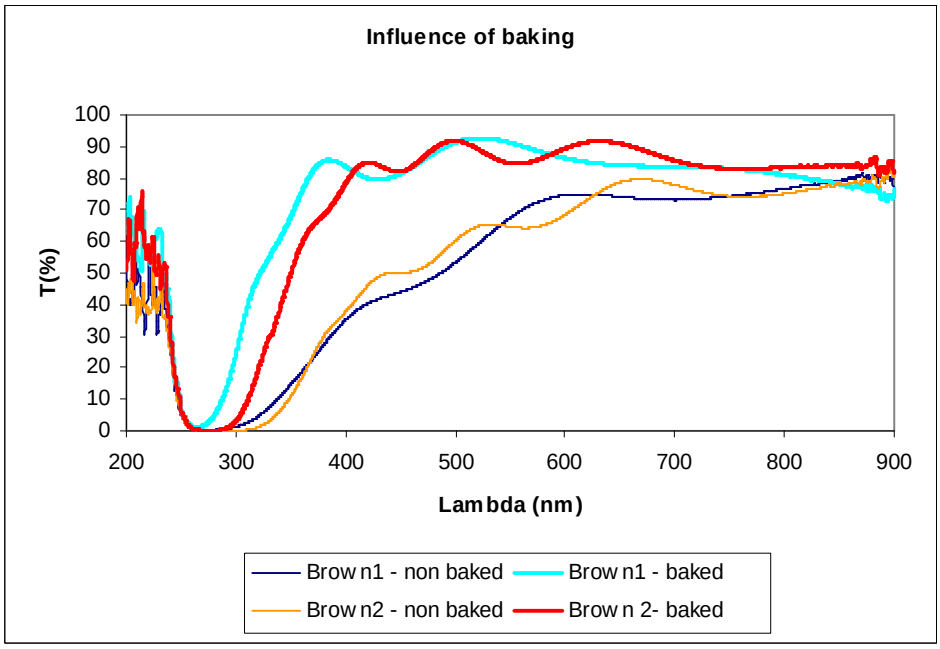

Figure 5-24: : Transmittance of ITO thin films (brownish) coated on glass substrates before and after annealing at 370°C

The observation of the crystallinity of annealed and non-annealed samples by X-ray diffraction tells that baking improves the crystallinity of the film. Indeed, from figure 5-25, the not baked sample is amorphous whereas the baked one is polycrystalline. The crystallites grow preferentially in the [2,2,2], [4,0,0] and [4,1,1] planes.

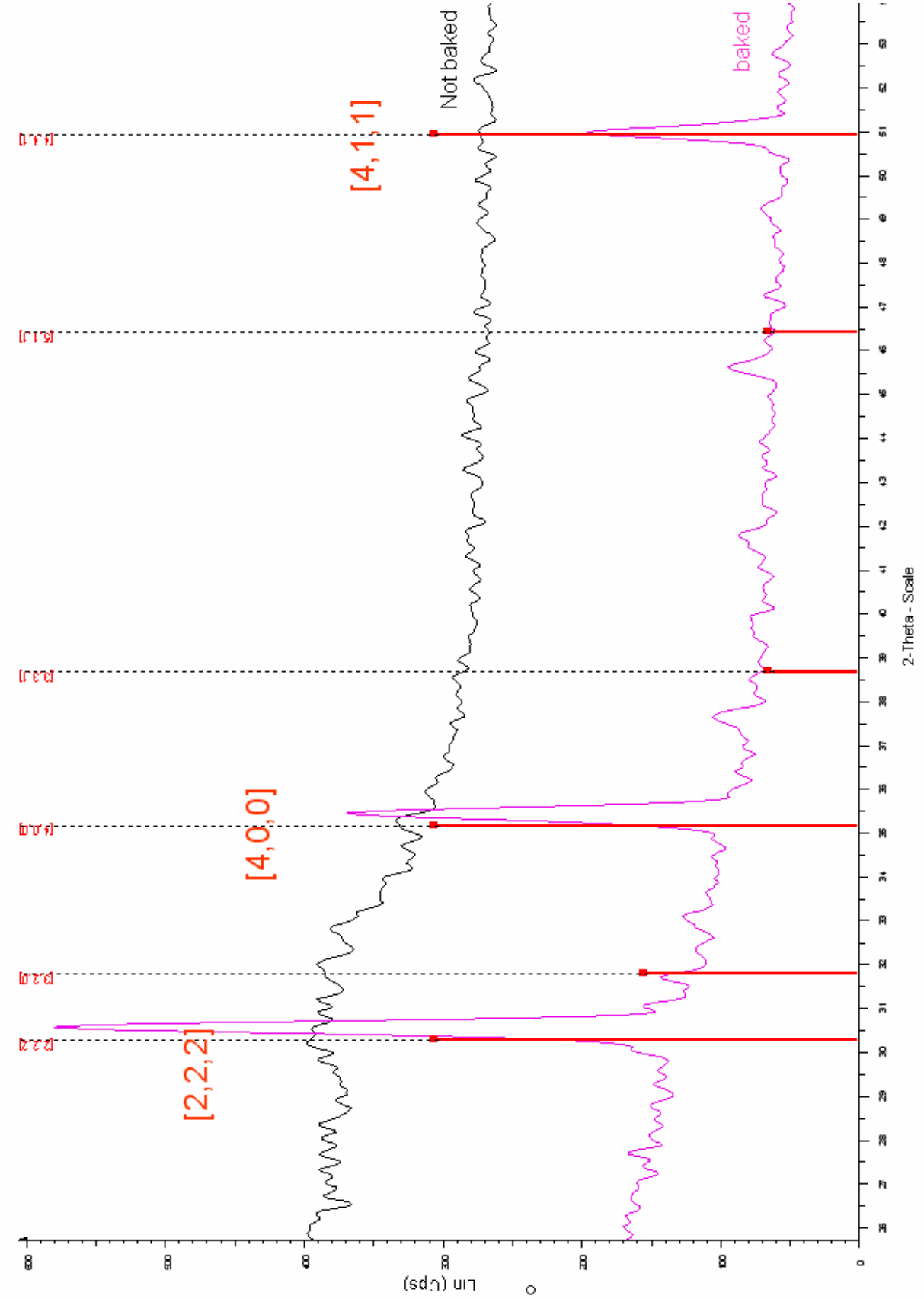

Figure 5-25: : X-Ray Diffractograms of ITO thin films coated on glass substrates before and after annealing at 370°C

5.1.7.2. Results for substrates baked at 150°C

The resistivity's evolution of ITO coated glass samples after being baked at 150°C for 48 hours is shown in Figure 5-26, It is interesting to notice that before this experiment, other samples were baked at 100°C. The films properties remained unchanged and therefore, the results are not presented in this report. In the chart, the x-axis corresponds to the denomination of glass samples. Those samples were deposited with the best parameters found from the former experiments. It is observed that annealing decreases greatly the resistivities of the samples. The resistivities obtained are below $2x10^{-4}$ Ωcm.

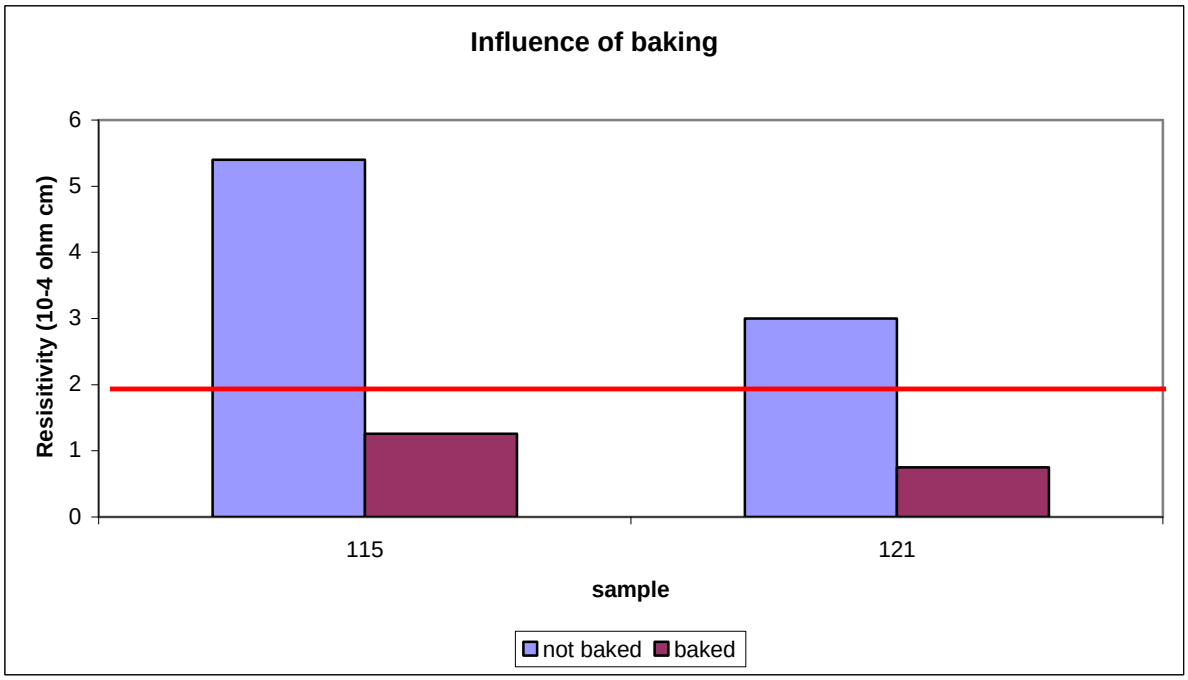

Figure 5-26: : Resistivity of ITO thin films coated on glass substrates before and after annealing at 150°C.

The spectra shown in figure 5-27 proves that at 150°C, annealing as a beneficial effect on the transmissivity of the ITO thin films. Indeed, the non-baked sample's transmittance hardly reaches an average of 70% in the visible while the baked sample is transparent (average of 85% in the visible).

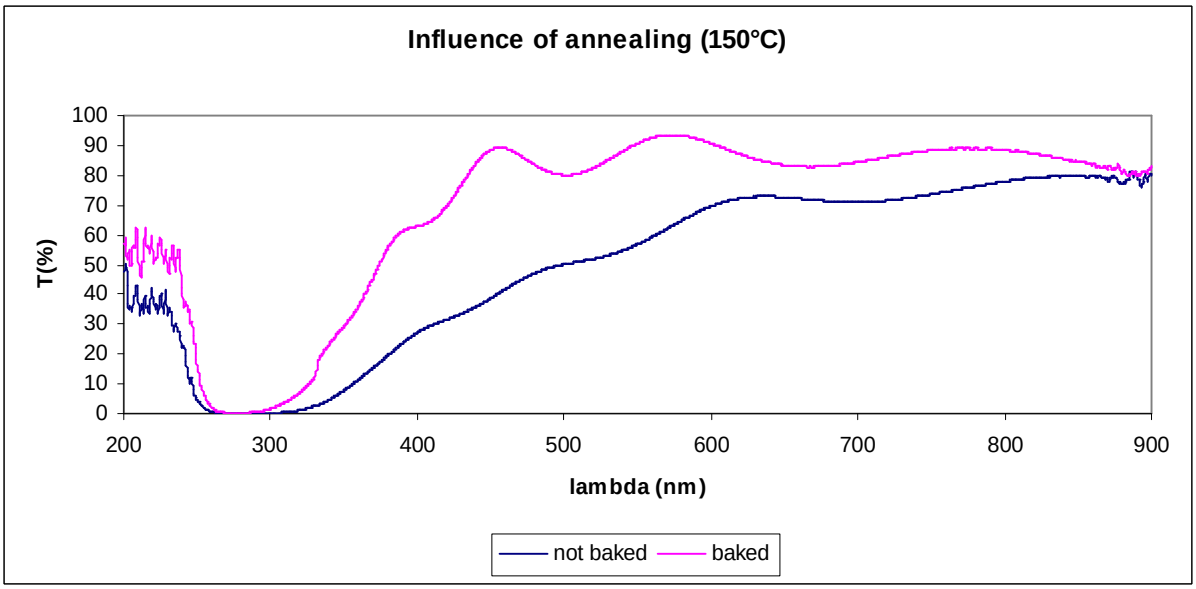

Figure 5-27: : Transmittance of ITO thin films coated on glass substrates before and after annealing at 150°C.

The observation of the crystallinity of annealed and non-annealed samples by X-ray diffraction tells that baking improves the crystallinity of the film. Indeed like for samples baked at 370°C the not baked samples are amorphous whereas the baked ones are polycrystalline (figure 5-28). The crystallites grow preferentially in the [2,2,2], [4,0,0] and [4,1,1] planes. Figure 5-29 represents the comparison of 370°C baked samples and 150°C ones in terms of crystallites sizes. From this figure, the annealing has the effect of reducing the crystallites sizes for most of the planes. The increase of the annealing temperature refines the crystals size.

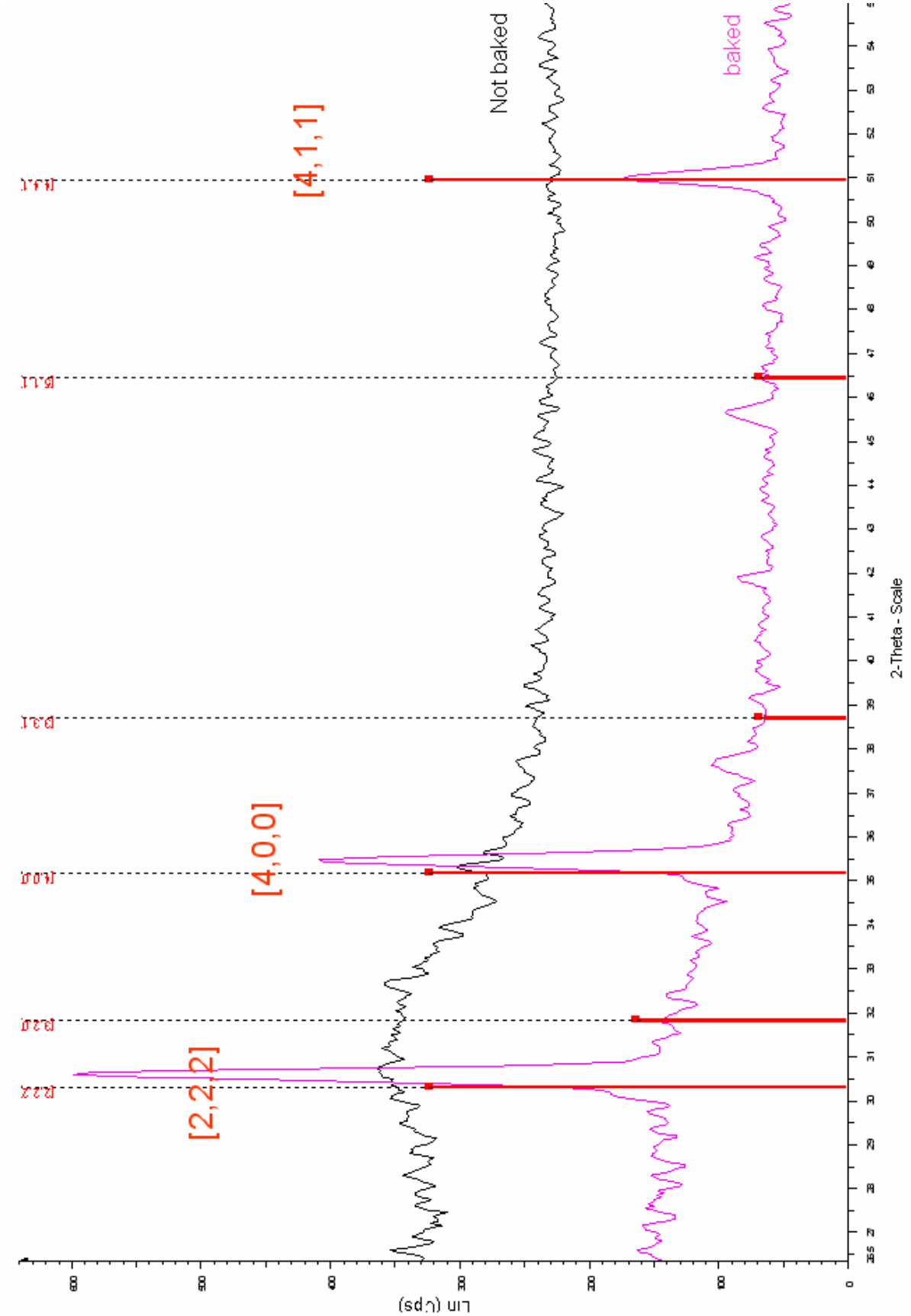

Figure 5-28: : X-Ray diffraction pattern of ITO thin films coated on glass substrates before and after annealing at 150°C.

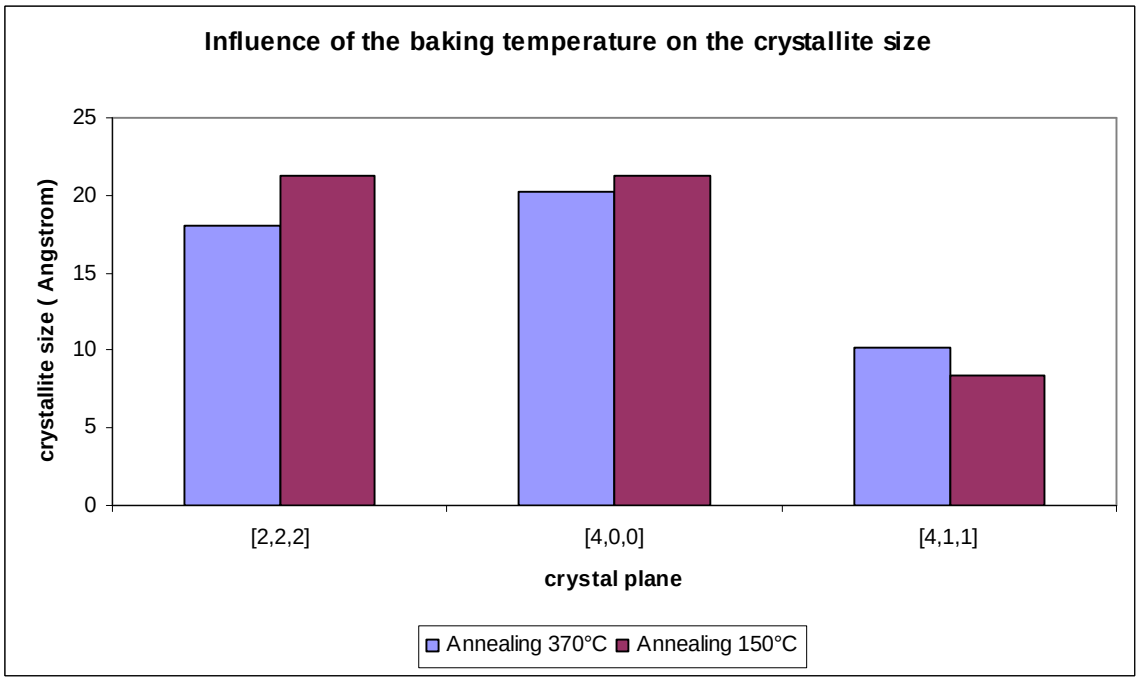

Figure 5-29: : Crystallite sizes of ITO thin films coated on glass substrates before and after annealing at 370°C and 150°C.

5.1.8. Summary

Table 5-3 summarises the general influences of the sputtering parameters on the electrical and optical properties of ITO films coated on glass substrates .

Influence of :	on resistivity	Features (10-4 ohmcm)
thickness increase	decrease	from non-conductive film to 63
chamber pressure increase	increase	from 75 to 165
rotation	increase	from 63 to non-conductive
oxygen amount increase	decrease	from 63 to 2
sputtering power increase	increase	from 1 to 3

Influence of :	on transmittance	Features (T%)
thickness increase	no big influence	above 90
chamber pressure increase	increase	above 90 - (shift)
rotation	decrease	from 80 to 70
oxygen amount increase	increase	from 70 to 95
sputtering power increase	increase	from 70 to 85

Table 5-3: Influence of the sputtering parameters studied on the electrical and optical properties.

Regarding those results, some compromises between the enhancement of the electrical properties and the optical properties have been made. The best parameters have

been selected in order to be applied during the deposition of ITO on the flexible substrates. They are gathered in Table 5-4.

Parameter	Value
thickness	500 nm
chamber pressure	10 mtorr
rotation	yes
oxygen amount	10 % 02
sputtering power	100 W

Table 5-4: Best sputtering parameters kept for the deposition of ITO on glass substrates.

5.2. Deposition of ITO on polymer substrates

5.2.1. Influence of the substrates

Figure 5-30 shows ITO thin films coated on glass and PET.

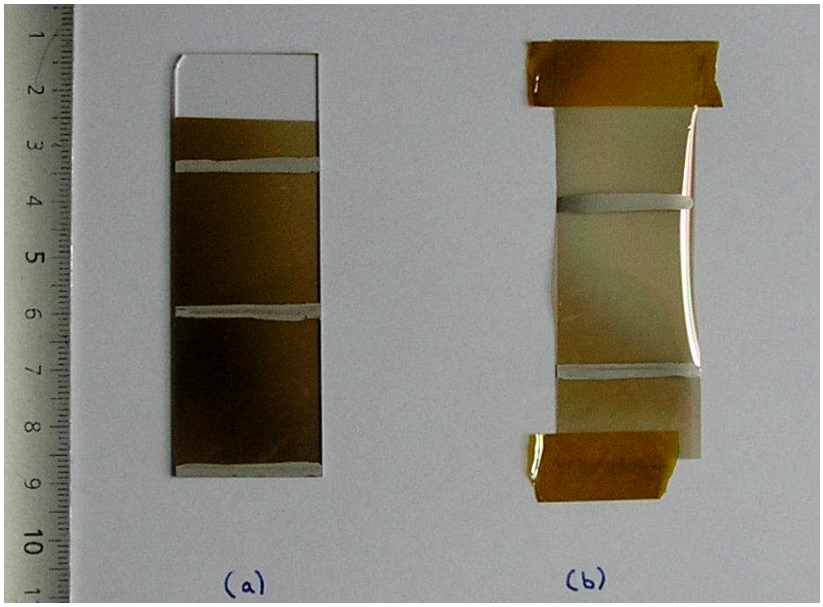

Figure 5-30: ITO films deposited on glass (a) and PET (b)

The attempts to get the film thickness with the tylasurf, the Dektak and the AFM were unsuccessful because of the softness and the roughness of PET. The residual stresses caused

by the difference in coefficient of thermal expansion of ITO and of PET substrates made the analyses very difficult.

The mean resistivity of the ITO films coated on PET substrates is compared to the one of films coated on glass substrates in Table 5-5. The resistivity on plastic substrates is 1.6 times higher than on glass. PET substrates diminished the electrical properties of the ITO films.

	Sheet resistance (x10-4 Ωcm) (PET)	Sheet resistance (x10-4 Ωcm) (Glass)
500nm 100W 10%02 1x10-2 torr	4.2	2.6

Table 5-5: Resistivity of ITO thin films coated on polymer and glass substrates

Contrary results are found for the transmittance of the films. Indeed the spectra in Figure 5-31 Show that the film are more transparent when coated on the PET substrates. The average transmittance in the range of 400-800nm goes from 75% on the glass to 85% on the polymer.

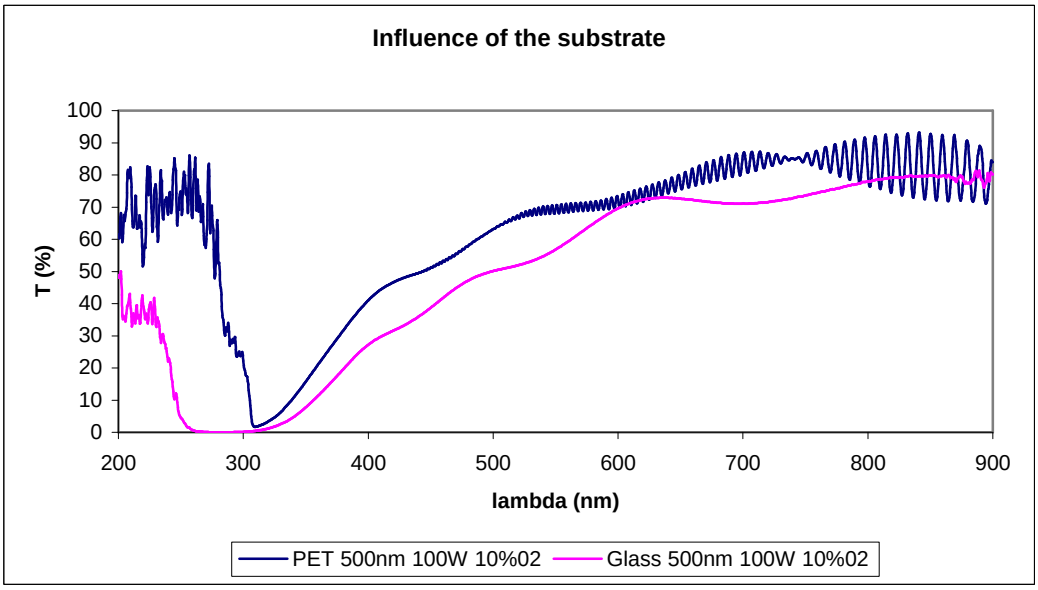

Figure 5-31: Transmittance of ITO thin films coated on polymer and glass substrates

Figure 5-32 shows the X-ray diffraction pattern of two samples deposited with an amount of 10% O_2 and a sputtering power of 100W on glass and PET substrates. The huge

peak appearing for low theta values correspond to the PET substrate. Otherwise, it can be said that the PET substrates does not really improve the crystallisation of the ITO. The crystallites seem to grow with other orientations. Indeed, instead of a [4,0,0] peak like on the glass substrates, the films deposited on the polymer show [3,3,1] peak. The [4,0,0] peak is much smaller.

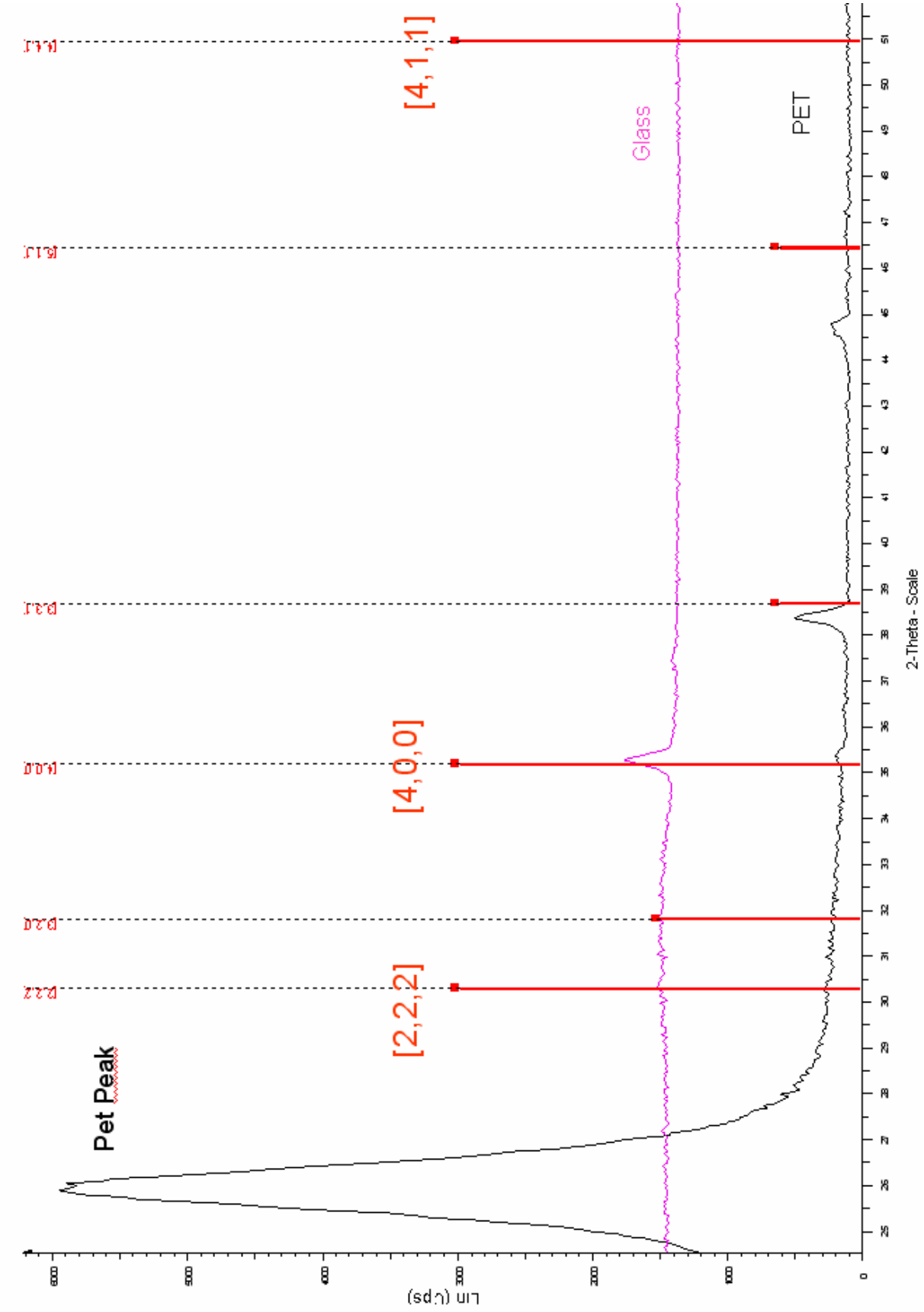

Figure 5-32: X-Ray diffraction pattern of ITO thin films coated on glass and polymer substrates.

5.2.2. Influence of the annealing

Figure 5-33 shows to samples of ITO films deposited on PET before an after annealing.

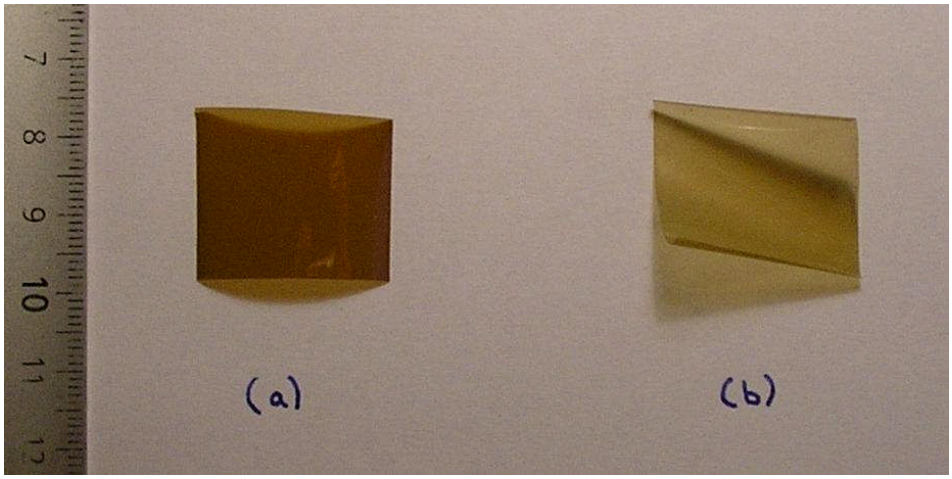

Figure 5-33: ITO films deposited on PET before (a) and after(b) annealing at 150°C

The resistivity's evolution of ITO coated glass samples after being baked at 150°C for 48 hours is shown in Figure 5-34. Those samples were deposited with the best parameters found from the former experiments. It is observed that annealing decreases greatly the resistivities of the samples. The resistivities obtained are below $2x10^{-4}$ Ωcm (20 Ω/square).

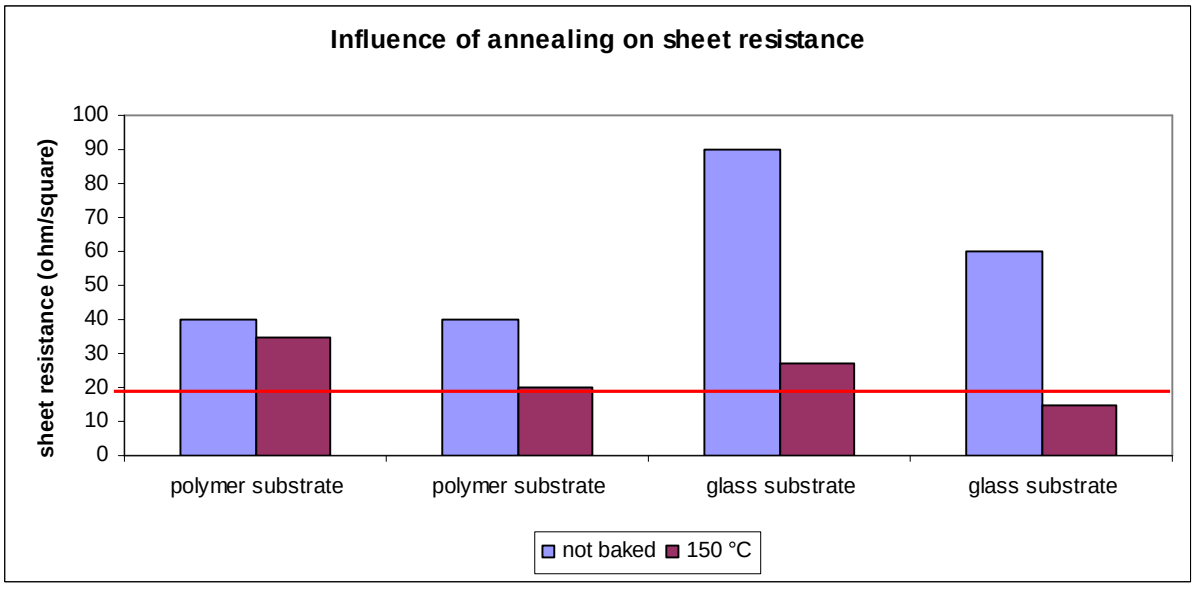

Figure 5-34: Sheet resistance of ITO thin films coated on PET substrates before and after annealing

The spectra shown in Figure 5-35 proves that at 150°C, the annealing has not a beneficial effect on the transmissivity of the ITO thin films in the visible. Indeed, the baked

sample transmittance hardly reaches an average of 60% while the not baked sample has got a transmissivity of 85%. However, in the ultra-violet, the not baked sample turns out to be more light absorbent than the other one.

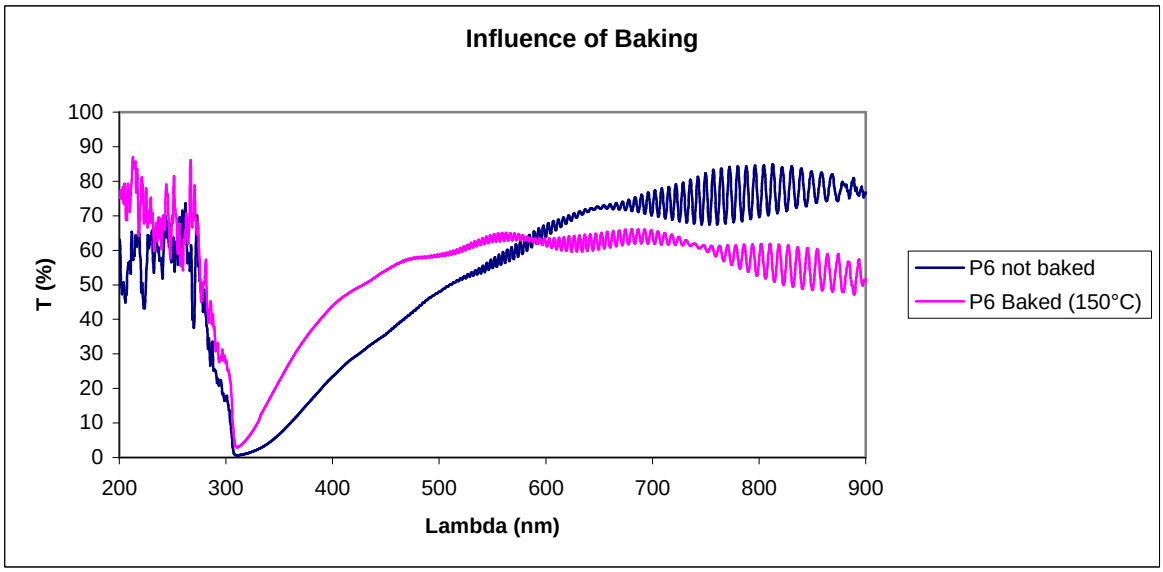

Figure 5-35: Resistivity of ITO thin films coated on PET substrates before and after annealing

The X-ray diffraction reveals that the annealing enhances the crystallography of the ITO deposited on the polymer substrates. Indeed, it can be seen on Figure 5-36 that the number of diffraction peak and their size raise greatly after the samples have been baked. The crystallites orientated in the [4, 0, 0] plane grew a lot compared to the other ones. The absence of [2, 2, 2] peak on both diffractograms reveals that no crystallites grow on this plane on the PET substrates.

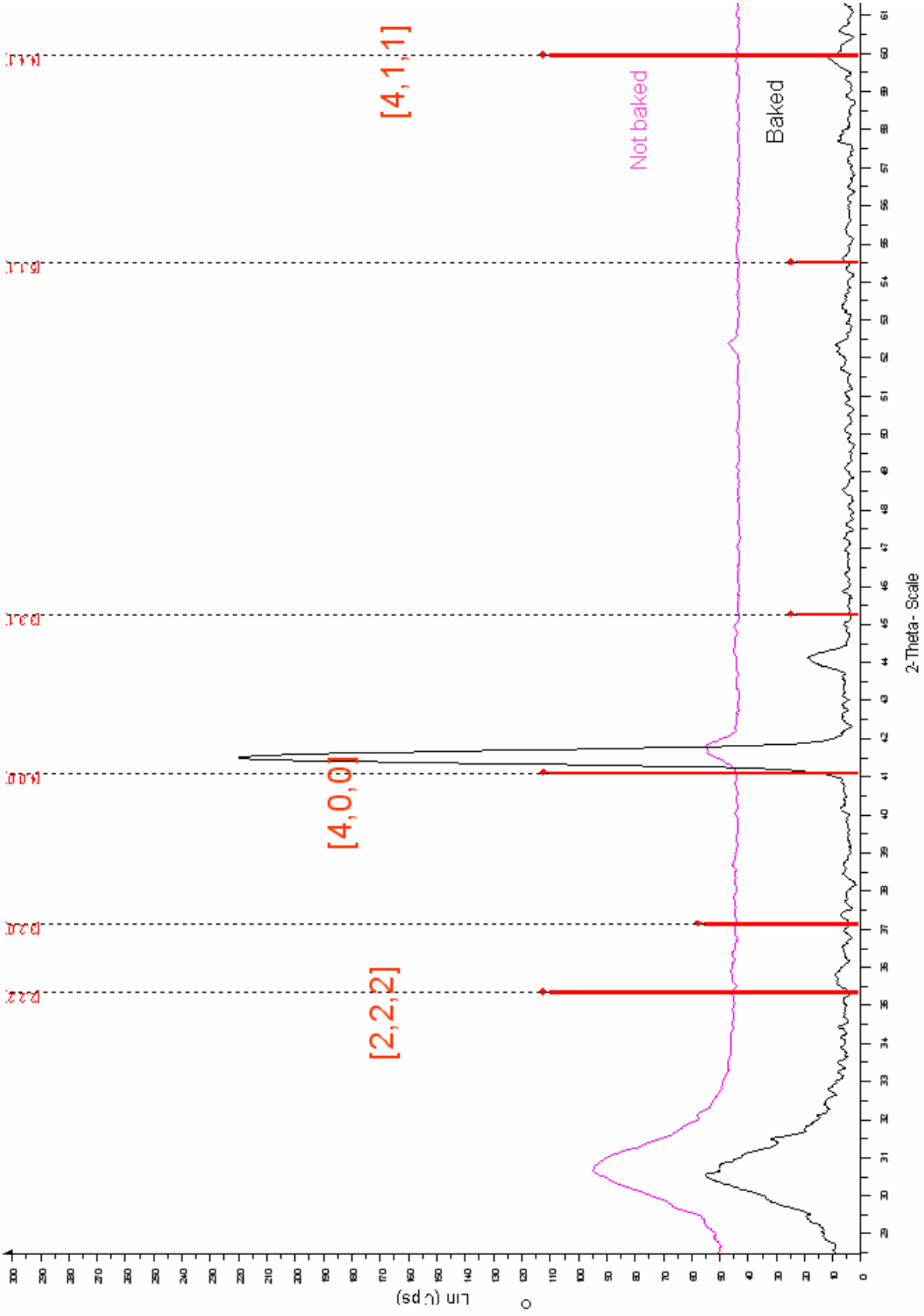

Figure 5-36: X-Ray diffraction pattern of ITO thin films coated on glass substrates before and after annealing at 150°C

5.3. Energy Dispersive Spectrometry analysis

The first ITO films coated on glass substrates appeared to get excellent optical properties. Indeed, they were transparent with an average transmissivity of 95%. However, without any precursory signs, the films produced became brown. Their optical transmissivity greatly diminished. After looking at the sputtering ITO target because of a cooling issue, it was noticed that all its length was cracked.

Knowing this, two hypothesises explaining this phenomenon were made:

- The brown colour is caused by a carbon pollution of the ITO films due to the crack in the target.
- The colour is due to a change in the ITO composition.

A piece of the target, a transparent film and a brown film coated on glass have been analysed under energy dispersive spectrometry in order to indentify the cause of this phenomenon. The results are detailed in the following part. (All the detailed samples' compositions can be found in a Appendix C)

5.3.1. EDS Analysis of the target

Figure 5-37 is a picture obtained under a scattered electron microscope of the target and the location of the elemental analysis. On the spectrum showed in Figure 5-38, it can be seen that the target is mostly composed of indium, tin and oxygen. The composition is detailed in Table 5-6.

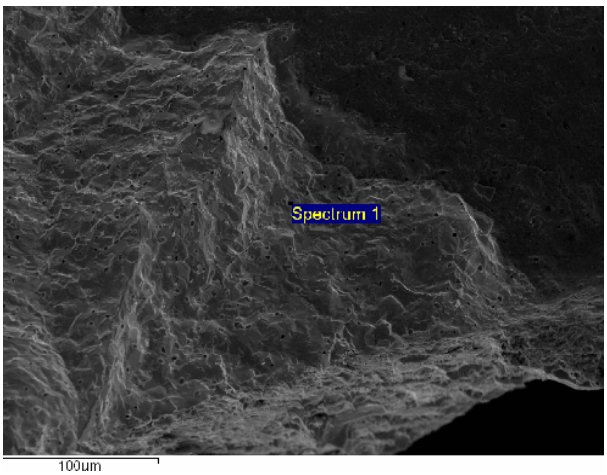

Figure 5-37: Observation under scattered electron microscopy of the target's surface

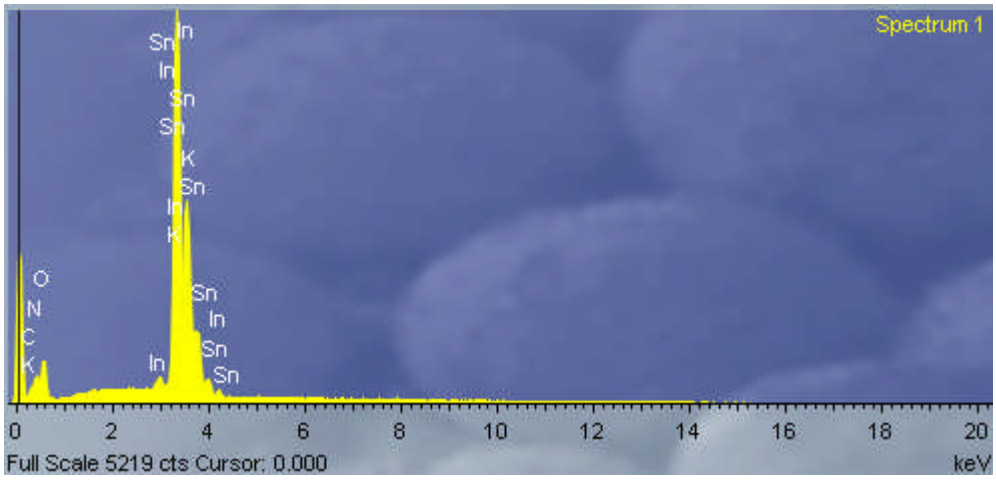

Figure 5-38: EDS spectrum of the target's surface

Spectrum	In stats.	C	N	O	K	In	Sn	Total
Spectrum 1	Yes	1,32	4,92	22,33	1,17	63,11	7,15	100

Table 5-6: Elemental composition of the ITO target (in weight %)

5.3.2. Analysis of the transparent sample

The different areas analysed with the EDS are shown in Figure 5-39. Those three areas have been selected in order to see the evolution of the composition depending on the thickness of the film and to identify any contamination of the coating.

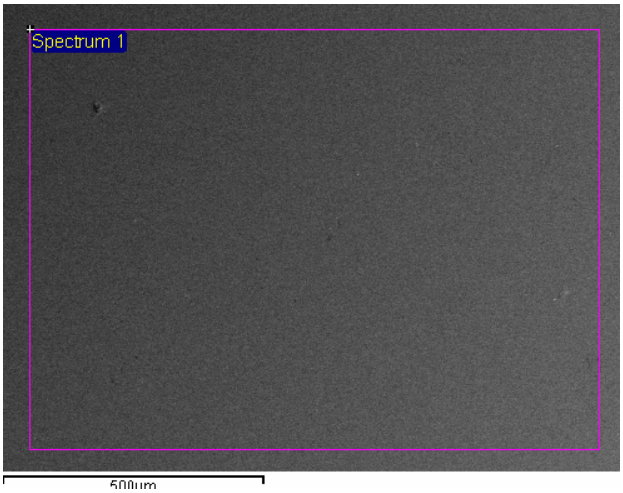

(a)

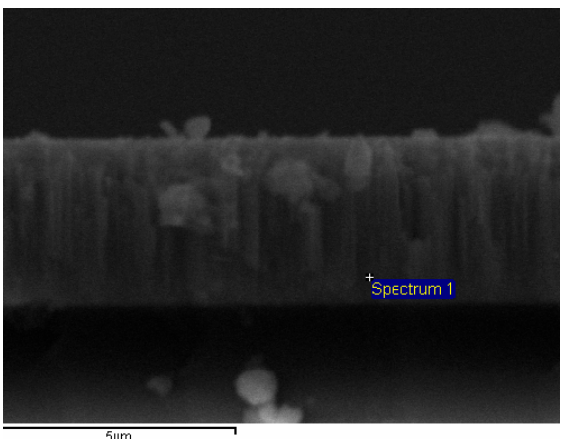

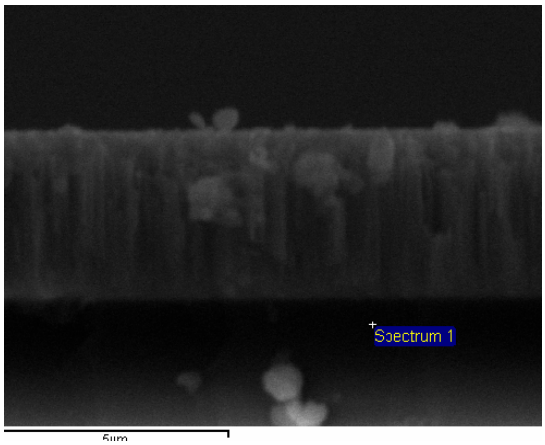

(b) (c)

Figure 5-39: Observation under scattered electron microscopy of the transparent coating's (a) surface (b) ITO layer(middle) (c) ITO layer(bottom).

The three different spectra obtained are in figure 5-40. The more the analysis is done in depth, the more elements are present in the film. These elements come mostly from the glass substrates. The composition weights are gathered in Table 5-7. It is noticed that the amount of indium oxides and tin oxides reduces when the analyse goes deeper is the ITO layer.

(a)

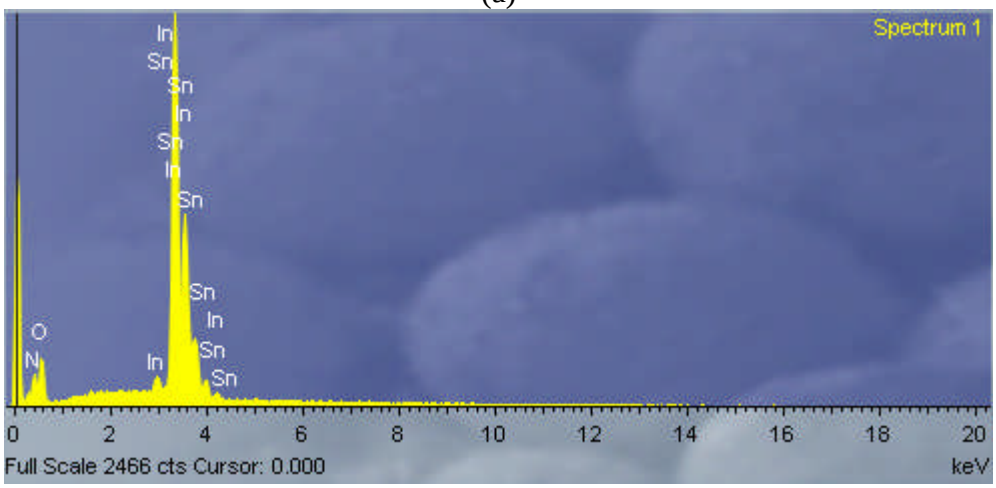

(b)

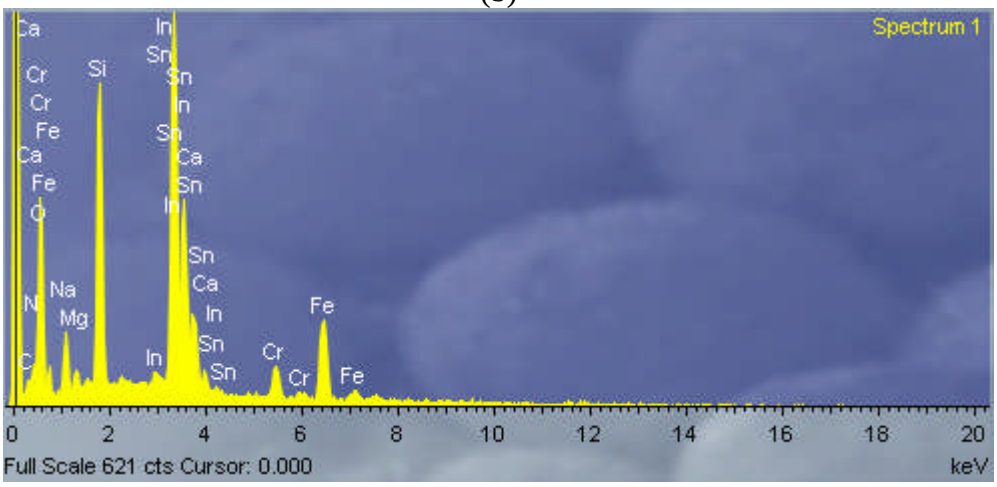

(c)

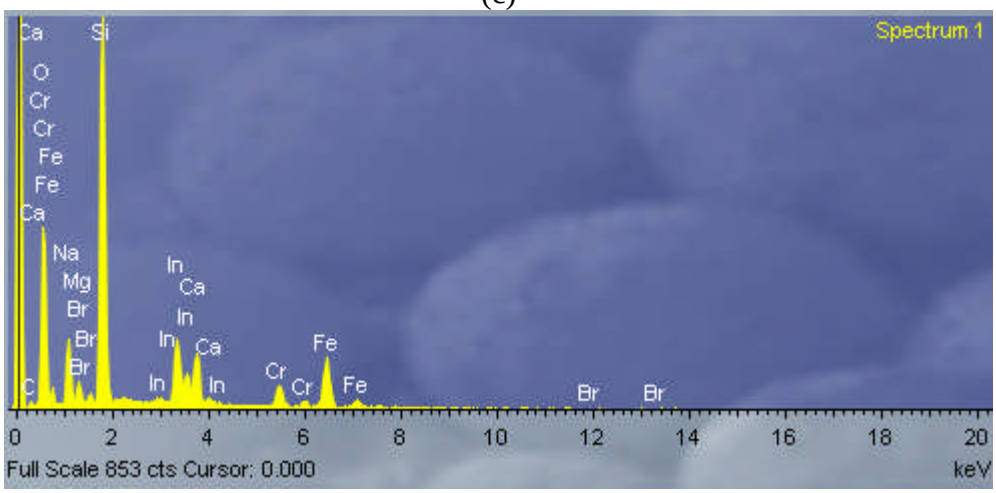

Figure 5-40: : EDS spectrum of the transparent coating's (a) surface (b) ITO layer(middle) (c) ITO layer(bottom).

Spectrum	In stats.	C	O	In	Sn	Other (K,Na,Si,Ca,Fe…)
Surface		-	23,79	62,75	6,67	6,79
ITO layer (middle)		1,76	35,78	34,32	2,53	25,61
ITO layer (bottom)		2,27	40,14	11,61	-	45,98

Table 5-7: Elemental composition of the transparent 3µm thick ITO film coated on glass (in weight %)

5.3.3. Analysis of the brown sample

The brown sample's composition has been studied in the areas shown in Figure 5-41. The spectra obtained are gathered in Figure 5-42.

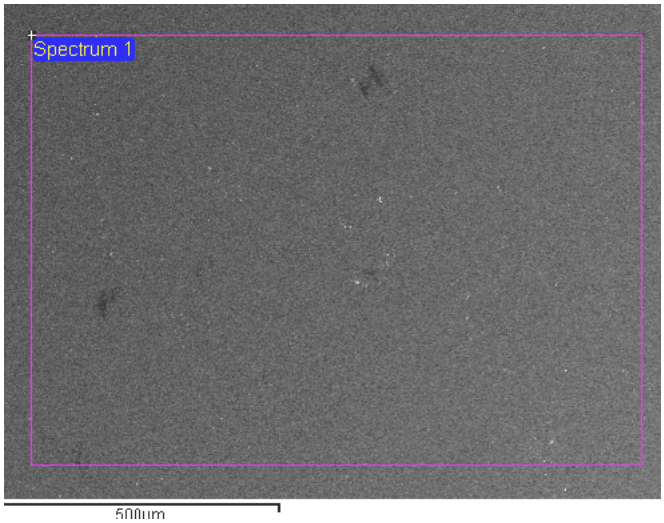

(a)

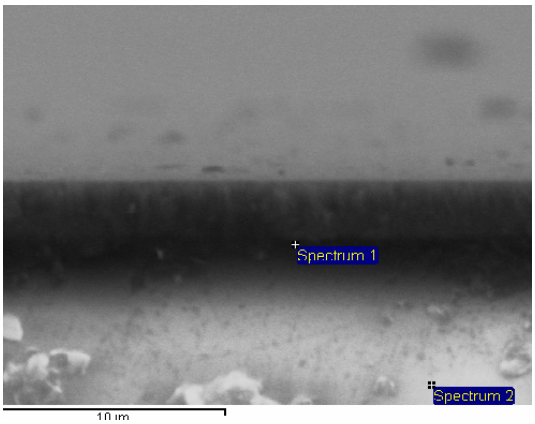

(b)

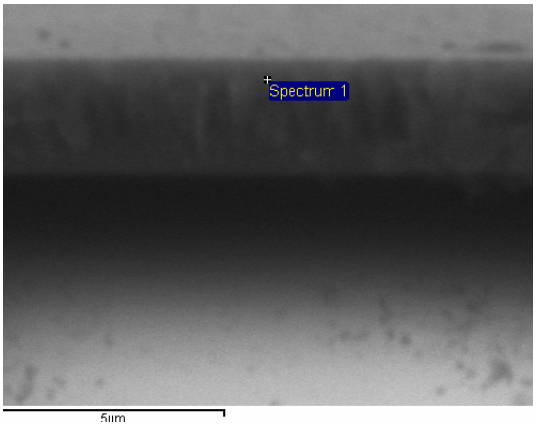

(c)

Figure 5-41: Observation under scattered electron microscopy of the brown coating's (a) surface (b) ITO layer(middle) (c) ITO layer(bottom).

(a)

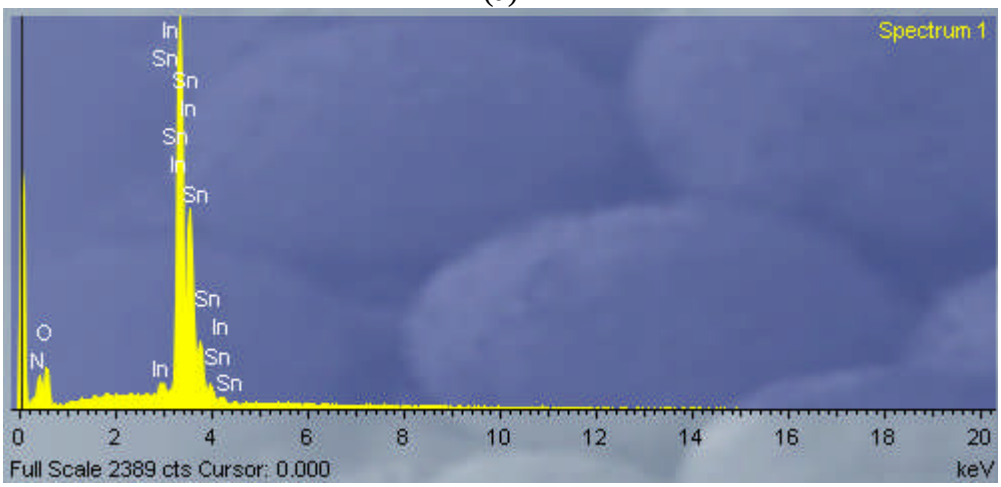

(b)

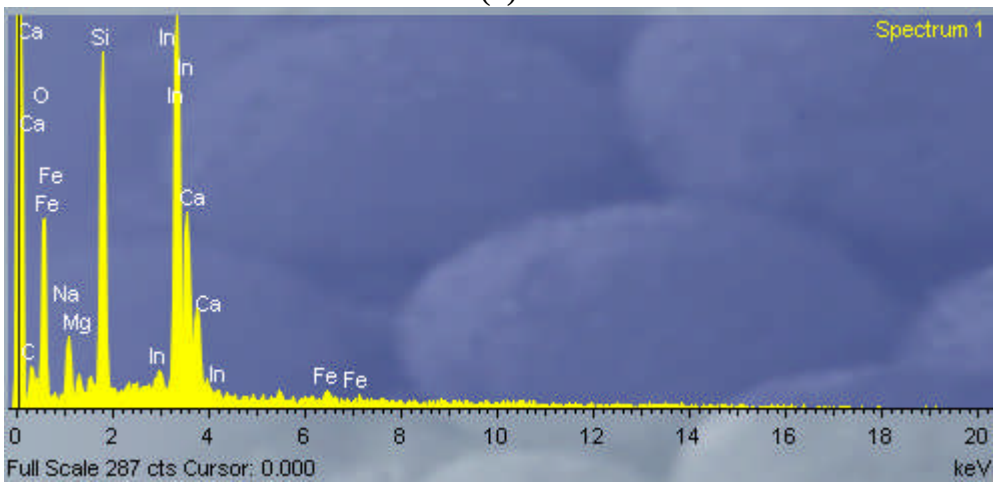

(c)

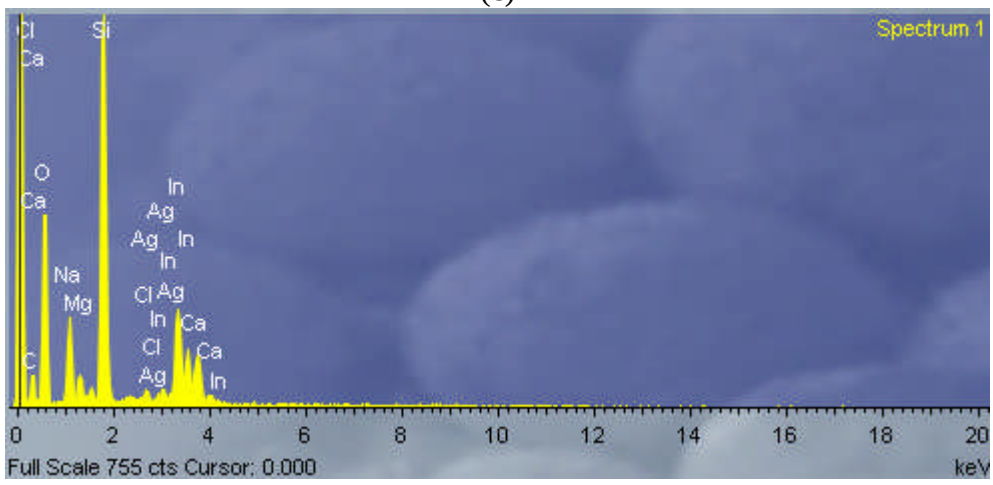

Figure 5-42: : EDS spectrum of the brown coating's (a) surface (b) ITO layer(middle) (c) ITO layer(bottom).

The composition of the samples is gathered in Table 5-8. It is noticed that the amount of indium oxides reduces when the analyse goes deeper is the ITO layer. Apart on the surface, no tin is present in the coating according to the table. A huge amount of carbons is observed at the bottom of the ITO layer.

Spectrum	In stats.	C	O	In	Sn	Other (K,Na,Si,Ca,Fe…)
Surface		-	22,45	68,12	5,09	4,34
ITO layer (middle)		2,58	43,29	30,78	-	23,35
ITO layer (bottom)		12,7	45,62	13,85	-	27,83

Table 5-8: Elemental composition of the brown 3µm thick ITO film coated on glass (in weight %) Comparison of the three samples

The amount of carbons, indium and tin atoms is compared for the three sorts of samples in Table 5-9.

C%	ITO Target	Transparent sample	Brown Sample
Surface	**1,32**	-	-
ITO layer (middle)	-	**1,76**	2,58
ITO layer (bottom)	-	2,27	**12,7**
In%	**ITO Target**	**Transparent sample**	**Brown Sample**
Surface	**63,11**	**62,75**	**69,12**
ITO layer (middle)	-	34,32	30,78
ITO layer (bottom)	-	11,61	13,85
Sn%	**ITO Target**	**Transparent sample**	**Brown Sample**
Surface	**7,15**	**6,67**	**5,09**
ITO layer (middle)	-	2,53	-
ITO layer (bottom)	-	-	-

Table 5-9: Elemental composition of the ITO target (in weight %)

The features for the transparent samples stay always close from the ones of the ITO target, regardless of the area checked. The carbon amount is around 1.5%, the indium amount around 63 % and the tin amount around 6.7%. Those values are considered as references to look at the composition of the brown film.

The amount of carbon present in the bottom part of the ITO layer is much higher for the brown sample than for the transparent one. It comes to 12.7 % instead of 1.5%.

Looking at the indium, here again, the amount is higher than for good coatings. It rises at 69.12%.

On the contrary, the amount of tin depletes to 5.09% which is too low compared to the other samples.

For these observations, it can be said that the two hypotheses can be true. The brown coatings suffer from a pollution of carbon on the part of the coating and more indium oxide is present in the film.

6. Discussion

6.1. Deposition of ITO on glass substrates

6.1.1. Film structure and properties

The effects of the different sputtering parameters on the resistivity are compared to the crystallites size in Table 6-1:

	Effect on resistivity	Crystallite size		
		[2,2,2]	[4,0,0]	[4,1,1]
Increasing thickness	Decrease	Max. at 400nm	-	Decrease
Increasing pressure	Increase	Decrease	Increase	Decrease
Rotation	Decrease	Decrease	Increase	Decrease
Increasing oxygen amount	Increase	Min. at 10%	Min. at 10%	Min. at 10%
Increasing power	Increase	Increase	Increase	Increase
Annealing	Decrease	Increase	Increase	Decrease

Table 6-1: Correlation between the parameters' effects on the electrical properties and the crystallites sizes

Majority of the results obtained on the films microstructure showed that they were preferentially growing in the <1, 1, 1> direction. (See parts 5.1.1, 5.1.3, 5.1.4, 5.1.5) It has been showed by Qiao & al. in 2004 that when the grains grow more along the <1, 1, 1> axis than along the <1, 0, 0>, it means that more interstitial oxygen atoms are included in the ITO structure.

Considering the crystallographic composition of the indium tin oxide, a large amount of oxygen in the lattice leads to great distortion. Yet, Guillén & Herrero have proved in 2008 that this tensile lattice distortion was directly linked to the carrier concentration of the films. Indeed, a decrease of the distortion leads to an increase of the carrier concentration and vice-versa. It is also important to notice that these interstitial oxygen atoms can combine with Sn^{4+} ions which removes electrons from the whole system and leads to the reduction of the carrier concentration.

Thus, the diminution of the <2, 2, 2> peaks going with a raise of the <4, 0, 0> one, corresponding to the decrease of the oxygen amount in the lattice and therefore to less distortion, leads to an increase of the carrier concentration. The electrical properties are therefore enhanced since greater carrier concentration lowers the resistivity of the coating.

The preferred [4, 0, 0] growing orientation observed when the samples were rotated can be explained by the spinning movement of the sample which does not allow the particles to deposit in all directions.

Concerning the influence of the increasing oxygen amount, the increase of the resistivity can be explained by the reduction of the oxygen vacancies of ITO leading to the depletion of the carrier concentration.

It can be seen from the optical spectra shown in part 5, that the loss of transmissivity of the ITO thin films is accompanied by a blue shift of the band gap. This phenomenon occurs generally when the films observed under XRD are less crystalline regardless of the sputtering parameters studied. Tan et al. found in 2005 similar results for zinc oxide coatings. They concluded that the absorption edge blue shift was caused by the poor crystallinity of the films grown at low temperature. They explained that as the fraction of amorphous ZnO phase increased in the films, the extended localization in the conduction and the valence bands increased. This caused the absorption of the photons by the amorphous phase and hence the shift of the absorption edge. Those results can be extended to ITO for this project.

6.1.2. Annealing and film properties

The annealing made the resistivity decrease a lot (part 5.1.7). This can be explained by the increase of the grain size, due to the heat contribution, illustrated by the raise of the crystallites' size in the [2,2,2] and [4,0,0] direction. Indeed, the smaller the size of the ITO crystallite, the higher the resistivity.

The higher the annealing temperature, the better the electrical property enhancement. However, to obtain the same enhancement properties at lower temperature, the time of annealing needs to be longer. That is why the samples were baked for 48 hours instead of 1 hour when the temperature was 150°C.

The enhancement of the optical properties of the ITO films can be attributed to the increase of structural homogeneity and crystallinity.

6.2. Deposition of ITO on polymer substrates

It can be assumed that good quality films were deposited on the PET substrates as the sputtering power was lowered to 100W. This power is high enough for an efficient nucleation and growth to occur and low enough though to avoid the damage of the organic substrate.

The rise of the resistivities of the films deposited on PET can be explained by their microstructure. Indeed the strength of the [2, 2, 2] crystal plane orientation is non existent for the ITO coated polymer samples. This means that the thin film's structure is impaired. It causes a carrier scattering near the grain boundaries and therefore reduces the conductivity. The polymer roughness is another reason of the less intense diffraction peaks.

Yang et al. found in 2007 the same results on PC substrates and proved that over a thickness of 450 nm (this project's ITO coated PET films are 500 nm thick), the resistivity of the films rapidly increased. This is explained by the accumulation of heat as the ITO deposits on the substrate, resulting in a slight deformation of the polymer. This leads to a diminution of the carrier concentration.

The enhancement of the electrical and optical properties of the ITO films after annealing can be explained the same way as for the one deposited on glass.

6.3. EDS analysis of non transparent samples

The hypothesis of the carbon contamination will be considered first. It appears that a high amount of this element is only observed at the bottom of the ITO layer. Looking closely to the spectrum, it is seen that the carbon comes out with a lot of other elements (Table 6-2).

Spectrum	In stats.	C	O	Na	Mg	Al
Spectrum 1	Yes	12,7	45,62	5,91	1,49	

Si	Cl	K	Ca	Ag	In	Total
16,38	0,55		2,32	1,18	13,85	100

Table 6-2: *Detailed composition of the bottom ITO layer of the brown coated glass sample*

Those elements may have nothing to do with the coating itself. Their emission radiations are very close to each other (2.622 KV for the chlorine, 2.98 KV for the silver

which is very close to the 3.287 KV of the indium). The high amount of carbon may be an error. Moreover, a carbon contamination should have been present in all the coating. This means that this hypothesis is not the explanation of the ITO films' loss of transparency.

The majority of the spectra have shown that a little amount of nitrogen was present in the target and in the ITO coated samples. It may come from the sintering process occurring during the manufacture of the target. A nitrogen atmosphere could have been used because no reaction is expected with indium and tin oxides. The nitrogen is trapped in the matrix.

Let's now consider the change of stoichiometry.

It is very difficult to obtain a material's stoichiometry by analysing an EDS spectrum. Some phenomena caused by the interaction between elements and X-ray radiations can distort the results. The spectra obtained also depend on the area selected on the sample.

However, in order to illustrate the change in stoichiometry, the ratios of SnO_2 and In_2O_3 of the samples have been compared. The calculations showed that the same proportions of SnO_2 and In_2O_3 are obtained for the target and the transparent coating. The ratio is 1 SnO_2 for 4.5 In_2O_3. The ratio of the brown coating is 1 SnO_2 for 7 In_2O_3. The loss of transparency is caused by the raise of the indium oxides ratio.

This affects a lot the optical properties of the coatings. Yet, the electrical properties stay unchanged. After annealing, the indium oxides ratio goes back to normal which enhances the transmissivity of the films.

6.4. ITO deposition optimisation

In order to obtain optimised ITO films on glass substrates, it is reckoned to set the following parameters:

- Rotating deposition
- Reduce sputtering power to 100W
- Sputtering gas : Ar + 10% O2
- Post-baking over 300°C

If annealing needs to be avoided as it add a step in the manufacture of the thin films, it is advised to do the following actions:

- increase substrate temperature,
- decrease the oxygen amount in the Argon gas,
- have a film thickness under 500 nm to keep good optical properties.

On the other hand, in order to obtain optimised ITO films on polymer substrates, it is reckoned to set the following parameters:

- Rotating deposition
- Reduce sputtering power to 100W
- Sputtering gas : Ar + 10% O2 (or less)
- Post-baking at 150°C

6.5. Limitations

The main limitation of the results obtained within the framework of this project is the amount of tests done for each parameters tested. More depositions should be done to check the repeatability of the measured resistivities and transmissivities.

As the thicknesses of the ITO films were difficult to obtain with all the means available in site, they were calculated in function of the growth rate of the films. An exact measurement of this thickness may bring some minor fluctuations in the calculated features.

7. Conclusion

Indium tin oxide films have been deposited by magnetron sputtering without intentional heating on glass and PET. The coatings deposited on glass have shown good electrical properties with resistivities under $1x10^{-4}$ Ωcm. The optical properties remained good with a transmittance above 90% in the visible. The objectives of obtaining resistivities below $2x10^{-4}$ Ωcm and high transmittance were fulfilled. Good quality ITO films were also deposited on PET without any pealing. They were showing a good conductivity and transparency.

The study of the film microstructure revealed that the films' electrical and optical properties were influenced greatly by the size of the crystallites and their growth direction.

Finally, the brown coatings phenomenon was elucidated. The EDS analysis revealed the increase of the indium oxides amount in the films.

However, these high quality films were obtained after annealing. Further experiments enhancing the ITO films' properties avoiding the baking step, like the deposition with an off-set angle, should be done.

8. Further Work

- Enhance the electrical properties of ITO thin films on polymer substrates without post-baking by depositing them with an off-set angle or with a substrate temperature around 100°C.

- Run experiments on a larger amount of samples to check repeatability.

- Find an efficient way to measure thickness of ITO thin films on polymer substrates.

- Measure roughness of sample. Indeed the cell efficiency is dependant on light scattering enhanced by rough coatings.

- Deposit ITO on other substrates.

References

Anthpoulos T.D. & Shafai T.S. (2003), "Influence of oxygen doping on the electrical and photovoltaic properties of Schottky type solar cells based on α-nickel phthalocyanine", *Thin Solid Films*, Vol. 441, pp. 207-213.

Beaurain A. Luxembourg D., Dufour C., Koncar V., Capoen B., Bouazaoui M. (2007), "Effects of annealing temperature and heat-treatment duration on electrical properties of sol–gel derived indium-tin-oxide thin films", *Thin Solid Films*, Vol. 516, pp. 4102-4106.

Berginski M., Hüpkes J., Reetz W., Rech B., Wuttig M. (2007), "Recent development on surface-textured ZnO:Al films prepared by sputtering for thin-film solar cell application", *Thin Solid Films*, Vol. 516,pp. 5836-5841

Beyer W., Hüpkes J., Stiebig H. (2007), "Transparent conducting oxide films for thin film silicon photovoltaics", *Thin Solid Films*, Vol. 516, pp. 174-154.

Boehme M. & Charton C. (2005), "Properties of ITO on PET in dependence on the coating conditions and thermal processing", *Surface & Coatings Technology*, Vol. 200, pp. 932-935.

Calnan S., Hüpkes J., Rech B. Siekmann H., Tiwari A.N. (2007), "High deposition rate aluminium-doped zinc oxide films with highly efficient light trapping for silicon thin film solar cells", *Thin Solid Films*, Vol. 516, pp.1242-1248.

Calnan S., Upadhyaya H..M., Dann S.E., Thwaites M.J., Tiwari A.N. (2007),"Effects of target bias voltage on indium tin oxide films deposited by high target utilisation sputtering", *Thin Solid Films*, Vol. 515, pp. 8500-8504.

Calnan S., Upadhyaya H.M., Thwaites M.J., Tiwari A.N. (2007), "Properties of indium tin oxide films deposited using High Target Utilisation Sputtering", *Thin Solid Films*, Vol. 515, pp. 6045-6050

Chang C.Y & Sze S.M. (1996), "ULSI technology", *New York : McGraw-Hill*

Cho S.H., Park J.H., Lee S.C., Cho W.S., Lee J.H.,Yon H.H., Song P.K. (2007), "Effects of O2 addition on microstructure and electrical property for ITO films deposited with several kinds of ITO targets", *Journal of Physics and Chemistry of Solids*, Vol. 69, pp. 1334-1337.

Danson N., Safi I., Hall G.W., Howson R.P. (1997), "Techniques for the sputtering of optimum indium-tin oxide films on to room-temperature substrates", *Surface & Coatings Technology*, Vol. 99. pp. 147-160.

Duta A. (2006), "TiO_2 thin layers with controlled morphology of ETA (extremely thin absorber) solar cells", *Thin Solid Films*, Vol. 511-512, pp. 195-198.

Ederth J. (2003), "Electrical Transport in Nanoparticle Thin Films of Gold and Indium Tin Oxide", doctoral degree dissertation, Uppsala University, pp. 4 -6

Elfallal I., Rilkington R.D., Hill A.E. (1993) "Formation of a statistical thermodynamic model for the electron concentration in heavily doped metal oxide semiconductors applied to the tin-doped indium oxide system", Vol. 223, pp. 303-310

Guillén C. & Herrero J. (2008), "Influence of the film thickness on the structure, optical and electrical of ITO coatings deposited by sputtering at room temperature on glass and plastic substrates", *Semiconductor Science and Technology*, Vol. 23, pp. 1-5.

Gupta L., Mansingh A., Srivastava P.K. (1989), "Band Gap Narrowing and the Band Structure of Tin Doped Indium Oxide Films", *Thin Solid Films*, Vol. 176, pp. 33 -44

Hollingum J. (2001), "Space technology comes down to earth", *Sensor Review*, Vol. 21, pp. 112-117.

Jung Y.S, Lee D.W., Jeon D.Y. (2003), "Influence of DC magnetron sputtering parameters on the properties of amorphous indium zinc oxide thin film" ,*Thin Solid Films*, Vol. 445, pp. 63–71

Jung Y.S., Seo J.Y., Lee D.W., Jeon D.Y. (2004), "Influence of dc magnetron sputtering parameters on surface morphology of indium tin oxide thin films" , *Applied Surface Science*, Vol. 221, pp. 136–142.

Kim D. & Kim S. (2003), "AFM observation of ITO thin films deposited on polycarbonate substrates by sputter type negative metal ion source", *Surface and Coatings Technology*, Vol. 176, pp. 23–29.

Kim D.H., Park M.R., Lee G.-H. (2006), "Preparation of high quality ITO films on a plastic substrate using RF magnetron sputtering", *Surface & Coatings Technology*, Vol. 201, pp. 927-931.

Lee J. , Jung H., Lim D., Yang K., Song W., Yi J. (2004), "Effects of bias voltage on the properties of ITO films prepared on polymer substrates", *Thin Solid Films*, Vol. 480-481, pp. 157-161.

Lee J., Lee D., Lim D., Yang K. (2007), "Structural, electrical and optical properties of ZNO:Al films deposited on flexible organic substrates for solar cell applications", *Thin Solid Films*, Vol. 515, pp. 6094-6098,.

Lin Y.C., Li J.Y., Yen W.T. (2007), "Low temperature ITO thin film deposition on PES substrate using pulse magnetron sputtering", *Applied Surface Science*, Vol. 254, pp. 3262-3268.

Luque A. & Hegedus S. (2005), Handbook of Photovoltaic Science and Engineering, John Wiley and Sons.

Mientus R. & Ellmer K. (2001), "Reactive magnetron sputtering of tin-doped indium oxide ITO: influence of argon pressure and plasma excitation mode", *Surface and Coatings Technology*, Vol. 142-144, pp.748- 754.

Narita T., Iida T., Ogawa S., Mizuno K., So J., Kondo A., Yoshida N., Itoh T., Nomomura S., Tanaka Y. (2007), "Ion beam modification of $Ti0_2$ films prepared by Cat-CVD for solar cell", *Thin Solid Films*, Vol. 516, pp. 810-813.

Park Y.R, Kim E.K, Jung D., Park T.S., Kim Y.S. (2008), "Growth of transparent conducting nano-structured In doped ZnO thin films by pulsed DC magnetron sputtering", *Applied Surface Science*, Vol. 254, pp. 2250–2254.

Plà J., Tamasi M., Rizzoli R., Losurdo M., Centurioni E.,Summonte C., Rubinelli F. (2002), "Optimization of ITO layers for applications in a-Si/c-Si heterojunction solar cells", *Thin Solid Films*, Vol. 425, pp. 185-192.

Pulker H.K, Huber D. (2008), "ITO Films produced by reactive low-voltage ion plating" available at www.thinfilmproducts.umicore.com

Qiao Z., Latz R., Mergela D. (2004), "Thickness dependence of In2O3:Sn film growth", *Thin Solid Films*, Vol. 466, pp. 250-258

Robbie K., Sit J.C., Brett M.J. (1998), "Advanced techniques for glancing angle deposition", *Journal of Vacuum Technology*, Vol. 16, pp. 1115-1118.

Ruske F., Jacobs C., Sittinger V., Szyszka B., Werner W. (2007), "Large area ZnO:Al films with tailored light scattering properties for photovoltaic applications", *Thin Solid Films*, Vol. 515, pp. 8695-8698.

Solarbuzz (2008), Solar Cell Technology available at http://www.solarbuzz.com/technologies.htm

Stowell M., Müller J., Ruske M., Lutz M., Linz T. (2007), "RF-superimposed DC and pulsed DC sputtering for deposition of transparent conductive oxides" , *Thin Solid Films*, Vol. 515, pp. 7654–7657.

Tan S. T., Chen B. J., Sun X.W., Fan W.J., Kwok H.S., Zhang and S. J. Chu S.J. (2005), "Blueshift of optical band gap in ZnO thin films grown by metal-organic chemical-vapor deposition", *Journal of Applied Physics*, Vol. 98.

Tangram Technology ltd. (2003), polymer data files available at http://www.tangram.co.uk/index.htm

Tohsophon T., Hüpkes J., Siekmann H., Schultheis M., Sirikulrat N. (2007), "High rate direct current magnetron sputtered and texture etched zinc oxide films for silicon thin film solar cells", *Thin Solid Films*, Vol. 516,pp. 4628-4632

U.S. Department of Energy (2007), solar energy technologies program available at http://www1.eere.energy.gov/solar/animations.html

Wang L.M., Chen Y.J., Liao J.W. (2008), "Characteristics of indium–tin oxide thin films grown on flexible plastic substrates at room temperature" , *Journal of Physics and Chemistry of Solids*, Vol. 69, pp. 527–530.

Xie Z., Henry B.M., Kirov K.R., Smith H.E., Barkhouse A. Grovenor C.R.M., Assender H.E., Briggs G.A.D., Webster G.R., Burn P.L. Kano M., Tsukahara Y. (2006), "Study of changing of the microstructure of titania layers on composite solar cell performance", *Thin Solid Films*, Vol. 511-512, pp. 523-528.

Yang C.-H., Lee S.-C., Lin T.-C., Chen S.-C. (2007), "Electrical and optical properties of indium tin oxide films prepared on plastic substrates by radio frequency magnetron sputtering", *Thin Solid Films*, Vol. 516, pp.1984-1991.

Zebaza Kana M. G., Centurioni E., Iencinella D., Summonte C. (2005), "Influence of the sputtering system's vacuum level on the properties of indium tin oxide films", *Thin Solid Films*, Vol. 500, pp. 203-208

APPENDIX A : SAMPLES' RESISVITIES

Sample	Thickness	Sheet Resist. (Ohm/square)	Resistivity (ohm cm x10-4)	parameter checked
2	450	2100	94,50	thickness : 500nm
	450	1400	63,00	thickness : 500nm
3	600	3300	198,00	thickness : 1000nm
	600	5400	324,00	thickness : 1000nm
4	800	2200	176,00	thickness : 1000nm
	800	1600	128,00	thickness : 1000nm
5	800	920	73,60	thickness : 1000nm
	800	970	77,60	thickness : 1000nm
6	650		0,00	thickness : 1000nm
	650	5300	344,50	thickness : 1000nm
7	200	200000	4000,00	thickness : 200nm
	200	200000	4000,00	thickness : 200nm
8	200	200000	4000,00	thickness : 200nm
	200	200000	4000,00	thickness : 200nm
9	200	200000	4000,00	thickness : 200nm
	200	200000	4000,00	thickness : 200nm
10	200	200000	4000,00	thickness : 200nm
	200	200000	4000,00	thickness : 200nm
11	800	450	36,00	chamber pressure : 5 mtorr
	800	2000	160,00	chamber pressure : 5 mtorr
12	700	1600	112,00	chamber pressure : 5 mtorr
	700	1700	119,00	chamber pressure : 5 mtorr
13	800	1100	88,00	chamber pressure : 5 mtorr
	800	700	56,00	chamber pressure : 5 mtorr
14	600	300	18,00	chamber pressure : 5 mtorr
	600	400	24,00	chamber pressure : 50 mtorr
15	400	200000	8000,00	chamber pressure : 50 mtorr
	400	200000	8000,00	chamber pressure : 5 mtorr
16	450	100000	4500,00	chamber pressure : 5 mtorr
	450	30000	1350,00	chamber pressure : 5 mtorr
17	400	50000	2000,00	chamber pressure : 5 mtorr
	400	75000	3000,00	chamber pressure : 5 mtorr
18	450	200000	9000,00	chamber pressure : 5 mtorr
	450	200000	9000,00	chamber pressure : 5 mtorr
19	200	200000	4000,00	chamber pressure : 5 mtorr
	200	200000	4000,00	chamber pressure : 5 mtorr
20	200	200000	4000,00	chamber pressure : 5 mtorr
	200	200000	4000,00	chamber pressure : 5 mtorr
21	200	200000	4000,00	chamber pressure : 5 mtorr
	200	200000	4000,00	chamber pressure : 5 mtorr
22	200	200000	4000,00	chamber pressure : 5 mtorr
	200	150000	3000,00	chamber pressure : 5 mtorr
23	200	200000	4000,00	rotation
	200	200000	4000,00	rotation
24	200	200000	4000,00	rotation
	200	200000	4000,00	rotation

25	200	200000	4000,00	rotation
	200	200000	4000,00	rotation
26	200	200000	4000,00	rotation
	200	200000	4000,00	rotation
27	500	50000	2500,00	rotation
	500	50000	2500,00	rotation
28	500	40000	2000,00	rotation
	500	50000	2500,00	rotation
29	500	200000	10000,00	rotation
	500	200000	10000,00	rotation
30	500	20000	1000,00	rotation
	500	20000	1000,00	rotation
31	900	10000	900,00	rotation
	900	7000	630,00	rotation
32	1200	4000	480,00	rotation
	1200	5000	600,00	rotation
33	1200	5000	600,00	rotation
	1200	5000	600,00	rotation
34	1000	10000	1000,00	rotation
	1000	8000	800,00	rotation
35	1000	25	2,50	oxygen amount : 10%
	1000	50	5,00	oxygen amount : 10%
36	1000	12	1,20	oxygen amount : 10%
	1000	15	1,50	oxygen amount : 10%
37	1300	12	1,56	oxygen amount : 10%
	1300	11	1,43	oxygen amount : 10%
38	1100	20	2,20	oxygen amount : 10%
	1100	12	1,32	oxygen amount : 10%
39	600	32	1,92	oxygen amount : 10%
	600	70	4,20	oxygen amount : 10%
40	500	60	3,00	oxygen amount : 10%
	500	70	3,50	oxygen amount : 10%
41	650	15	0,98	oxygen amount : 10%
	650	15	0,98	oxygen amount : 10%
42	500	30	1,50	oxygen amount : 10%
	500	45	2,25	oxygen amount : 10%
43	600	50	3,00	oxygen amount : 5%
	600	100	6,00	oxygen amount : 5%
44	500	35	1,75	oxygen amount : 5%
	500	40	2,00	oxygen amount : 5%
45	500	40	2,00	oxygen amount : 5%
	500	45	2,25	oxygen amount : 5%
46	400	30	1,20	oxygen amount : 5%
	400	45	1,80	oxygen amount : 5%
47	600	30	1,80	oxygen amount : 1%
	600	30	1,80	oxygen amount : 1%
48	500	60	3,00	oxygen amount : 1%
	500	70	3,50	oxygen amount : 1%
49	650	35	2,28	oxygen amount : 1%
	650	33	2,15	oxygen amount : 1%
50	600	41	2,46	oxygen amount : 1%
	600	35	2,10	oxygen amount : 1%

59	400	1800	72,00	oxygen amount : 15%
	400	1200	48,00	oxygen amount : 15%
60	400	550	22,00	oxygen amount : 15%
	400	600	24,00	oxygen amount : 15%
61	400	1000	40,00	oxygen amount : 15%
	400	600	24,00	oxygen amount : 15%
62	350	1700	59,50	oxygen amount : 15%
	350	1200	42,00	oxygen amount : 15%
63	400	100	4,00	oxygen amount : 17%
	400	200	8,00	oxygen amount : 17%
64	500	60	3,00	oxygen amount : 17%
	500	80	4,00	oxygen amount : 17%
65	600	45	2,70	oxygen amount : 17%
	600	48	2,88	oxygen amount : 17%
66	500	40	2,00	oxygen amount : 17%
	500	60	3,00	oxygen amount : 17%
67	400	100	4,00	oxygen amount : 12%
	400	150	6,00	oxygen amount : 12%
68	500	50	2,50	oxygen amount : 12%
	500	55	2,75	oxygen amount : 12%
69	550	45	2,48	oxygen amount : 12%
	550	60	3,30	oxygen amount : 12%
70	500	70	3,50	oxygen amount : 12%
	500	60	3,00	oxygen amount : 12%
71	400	100	4,00	oxygen amount : 12% (1gas inlet only)
	400	80	3,20	oxygen amount : 12% (1gas inlet only)
72	550	70	3,85	oxygen amount : 12% (1gas inlet only)
	550	60	3,30	oxygen amount : 12% (1gas inlet only)
73	600	50	3,00	oxygen amount : 12% (1gas inlet only)
	600	45	2,70	oxygen amount : 12% (1gas inlet only)
74	500	50	2,50	oxygen amount : 12% (1gas inlet only)
	500	50	2,50	sputtering power : 300 W
75	600	70	4,20	sputtering power : 300 W
	600	65	3,90	sputtering power : 300 W
76	650	43	2,80	sputtering power : 300 W
	650	60	3,90	sputtering power : 300 W
77	650	23	1,50	sputtering power : 300 W
	650	25	1,63	sputtering power : 300 W
78	650	40	2,60	sputtering power : 300 W
	650	65	4,23	sputtering power : 300 W
79	600	80	4,80	sputtering power : 350 W
	600	85	5,10	sputtering power : 350 W
80	750	33	2,48	sputtering power : 350 W
	750	55	4,13	sputtering power : 350 W
81	600	35	2,10	sputtering power : 350 W
	600	35	2,10	sputtering power : 350 W
82	650	30	1,95	sputtering power : 350 W
	650	45	2,93	sputtering power : 350 W (1gas inlet only)
83	600	50	3,00	sputtering power : 350 W (1gas inlet only)
	600	200000	12000,00	sputtering power : 350 W (1gas inlet only)

84	600	37	2,22	sputtering power : 350 W (1gas inlet only)
	600	35	2,10	sputtering power : 350 W (1gas inlet only)
85	650	22	1,43	sputtering power : 350 W (1gas inlet only)
	650	35	2,28	sputtering power : 350 W (1gas inlet only)
86	650	37	2,41	sputtering power : 350 W (1gas inlet only)
	650	50	3,25	sputtering power : 350 W (1gas inlet only)
87	400	50	2,00	sputtering power : 100 W
	400	200000	8000,00	sputtering power : 100 W
88	200	100	2,00	sputtering power : 100 W
	200	80	1,60	sputtering power : 100 W
89	350	45	1,58	sputtering power : 100 W
	350	50	1,75	sputtering power : 100 W
90	350	50	1,75	sputtering power : 100 W
	350	70	2,45	sputtering power : 100 W
91	350	70	2,45	sputtering power : 150 W
	350	200000	7000,00	sputtering power : 150 W
92	350	60	2,10	sputtering power : 150 W
	350	60	2,10	sputtering power : 150 W
93	450	35	1,58	sputtering power : 150 W
	450	60	2,70	sputtering power : 150 W
94	500	80	4,00	sputtering power : 150 W
	500	80	4,00	sputtering power : 150 W
95	200	125	2,50	sputtering power : 100 W (1 gas inlet only)
	200	200000	4000,00	sputtering power : 100 W (1 gas inlet only)
96	250	90	2,25	sputtering power : 100 W (1 gas inlet only)
	250	85	2,13	sputtering power : 100 W (1 gas inlet only)
97	500	7	0,35	sputtering power : 100 W (1 gas inlet only)
	500	70	3,50	sputtering power : 100 W (1 gas inlet only)
98	200	55	1,10	sputtering power : 100 W (1 gas inlet only)
	200	65	1,30	sputtering power : 100 W (1 gas inlet only)
115	600	70	4,20	12% 02 + 100W
	600	110	6,60	12% 02 + 100W
116	500	75	3,75	12% 02 + 100W
	500	80	4,00	12% 02 + 100W
117	800	30	2,40	12% 02 + 100W
	800	30	2,40	12% 02 + 100W
118	700	55	3,85	12% 02 + 100W
	700	90	6,30	12% 02 + 100W
119	500	50	2,50	12% 02 + 100W
	500	45	2,25	12% 02 + 100W
120	650	30	1,95	12% 02 + 100W
	650	36	2,34	12% 02 + 100W

121	500	70	3,50	10% 02+ 100W
	500	50	2,50	10% 02+ 100W
122	500	40	2,00	10% 02+ 100W
	500	80	4,00	10% 02+ 100W
15 baked	400	200	8,00	baked 350°C
	400	200	8,00	baked 350°C
16 baked	400	200	8,00	baked 350°C
	400	200	8,00	baked 350°C
27 baked	400	200	8,00	baked 350°C
	400	200	8,00	baked 350°C
28 baked	400	200	8,00	baked 350°C
	400	200	8,00	baked 350°C
39 baked	600	20	1,20	baked 350°C
	600	22	1,32	baked 350°C
40 baked	500	13	0,65	baked 350°C
	500	15	0,75	baked 350°C
87 baked	400	20	0,80	baked 350°C
	400	20	0,80	baked 350°C
88 baked	200	15	0,30	baked 350°C
	200	17	0,34	baked 350°C
115 baked	600	27	1,62	baked 150°C
	600	15	0,90	baked 150°C
121 baked	500	15	0,75	baked 150°C
	500	15	0,75	baked 150°C
116 baked	500	20	1,00	baked 150°C

APPENDIX B: CRYSTALLITE SIZE CALCULATION

Sample	Peak	FWHM (°)	Instrument Broadening (degree)	2theta (degree)	D(crystallite size) (Angstrom)	parameter's value
Thickness						
12	[2,2,2]	0,657	0,243	30,0741	4,275917552	700
16	[2,2,2]	0,498	0,243	30,071	6,950637621	400
20	[2,2,2]	0,632	0,243	30,278	4,230907437	200
12	[4,1,1]	0,637	0,172	50,316	2,982757909	700
16	[4,1,1]	0,401	0,172	50,331	6,058010072	400
20	[4,1,1]	-	0,172	-	-	200
pressure						
3	[2,2,2]	0,471	0,243	30,261	7,258238017	10
11	[2,2,2]	0,607	0,243	30,261	4,546368868	5
3	[4,0,0]	-	0,172	-	-	10
11	[4,0,0]	0,287	0,172	35,109	44,2844856	5
3	[4,1,1]	0,519	0,172	50,7	4,091986939	10
11	[4,1,1]	0,616	0,172	50,224	3,123509678	5
rotation						
48	[2,2,2]	0,342	0,243	30,121	17,55913494	no
52	[2,2,2]	-	0,243	-	-	yes
48	[4,0,0]	0,272	0,172	35,174	45,70271048	no
52	[4,0,0]	0,272	0,172	35,285	38,97266967	yes
48	[4,1,1]	0,391	0,172	50,388	6,343130889	no
52	[4,1,1]	-	0,172	-	-	yes
oxygen						
48	[2,2,2]	0,378	0,243	30,092	13,02083668	1
44	[2,2,2]	0,42	0,243	30,153	9,705033698	5
40	[2,2,2]	0,425	0,243	30,157	9,424645167	10
68	[2,2,2]	0,358	0,243	30,104	15,21446855	12
60	[2,2,2]	0,408	0,243	30,235	10,1161024	15
64	[2,2,2]	0,387	0,243	30,123	12,06278931	17
28	[2,2,2]	0,44	0,243	30,406	8,04197495	20
48	[4,0,0]	0,294	0,172	35,117	41,16200161	1
44	[4,0,0]	0,42	0,172	35,087	21,36709589	5
40	[4,0,0]	0,456	0,172	35,083	18,7973006	10
68	[4,0,0]	0,339	0,172	35,123	29,75979659	12
60	[4,0,0]	0,323	0,172	35,196	29,25766336	15
64	[4,0,0]	0,39	0,172	35,196	20,26562921	17
28	[4,0,0]	-	0,172	-	-	20
48	[4,1,1]	0,465	0,172	50,378	4,739717171	1
44	[4,1,1]	0,591	0,172	50,396	3,316223585	5
40	[4,1,1]	0,609	0,172	50,382	3,178252515	10
68	[4,1,1]	0,439	0,172	50,407	5,206061134	12
60	[4,1,1]	0,339	0,172	50,656	8,4634617	15
64	[4,1,1]	0,419	0,172	50,406	5,627405822	17
28	[4,1,1]	0,527	0,172	50,778	4,037594074	20
power						
88	[2,2,2]	-	0,243	-	-	100

92	[2,2,2]	-	0,243	-	-	150
40	[2,2,2]	0,455	0,243	30,145	8,12662642	200
76	[2,2,2]	0,393	0,243	30,174	11,36529083	300
80	[2,2,2]	0,344	0,243	30,127	17,17254851	350
88	[4,0,0]	-	0,172	-	-	100
92	[4,0,0]	-	0,172	-	-	150
40	[4,0,0]	0,465	0,172	35,083	18,21990911	200
76	[4,0,0]	0,393	0,172	35,189	20,20459024	300
80	[4,0,0]	0,344	0,172	35,16	27,16934167	350
88	[4,1,1]	-	0,172	-	-	100
92	[4,1,1]	-	0,172	-	-	150
40	[4,1,1]	0,599	0,172	50,37	3,251605299	200
76	[4,1,1]	0,375	0,172	50,459	6,862344778	300
80	[4,1,1]	0,475	0,172	50,409	4,587846684	350
Annealing 370°C						
88b	[2,2,2]	0,328	0,243	30,541	18,00806872	370
88b	[4,0,0]	0,334	0,172	35,43	20,25604893	370
88b	[4,1,1]	0,319	0,172	51,009	10,12380283	370
Annealing 150°C						
121b	[2,2,2]	0,315	0,243	30,543	21,24959807	150
121b	[4,0,0]	0,326	0,172	35,43	21,30831121	150
121b	[4,1,1]	0,351	0,172	51,021	8,333605903	150

APPENDIX C: EDS ANALYSIS – DETAILLED COMPOSITIONS

ITO target:

Spectrum	In stats.	C	N	O	K	In	Sn	Total
Spectrum 1	**Yes**	**1,32**	**4,92**	**22,33**	**1,17**	**63,11**	**7,15**	**100**

Transparent ITO film on glass (surface):

Spectrum	In stats.	N	O	K	In	Sn	Total
Spectrum 1	Yes	5,27	23,79	1,52	62,75	6,67	100

Transparent ITO film on glass (ITO layer):

Spectrum	In stats.	C	N	O	Na	Mg
Spectrum 1	Yes	1,76	0	35,78	3,52	0,88

Si	Ca	Cr	Fe	In	Sn	Total
9,17	0,77	2,43	8,83	34,32	2,53	100

Transparent ITO film on glass (bottom):

Spectrum	In stats.	C	O	Na	Mg	Si
Spectrum 1	Yes	**2,27**	**40,14**	**6,68**	**1,35**	**21,01**

Ca	Cr	Fe	Br	In	Total
3,27	**2,91**	**9,73**	**1,03**	**11,61**	**100**

Brown ITO film on glass (surface):

Spectrum	In stats.	N	O	In	Sn	Total
Spectrum 1	Yes	4,34	22,45	68,12	5,09	100

Brown ITO film on glass (ITO layer):

Spectrum	In stats.	C	O	Na	Mg	Si	Ca	In	Total
Spectrum 1	Yes	2,58	43,29	5,44	1,06	14,68	2,17	30,78	100

Brown ITO film on glass (bottom):

Spectrum	In stats.	C	O	Na	Mg	Al
Spectrum 1	Yes	12,7	45,62	5,91	1,49	

Si	Cl	K	Ca	Ag	In	Total
16,38	0,55		2,32	1,18	13,85	100